

ELT - MICADO

MICADO SCAO Science Cases

Doc. No.: ELT-PLA-MCD-56305-0013

Issue: 001

Date: 16.09.2019

Author(s): E. Tolstoy.....

Name

Date

Signature



R. Davies.....

Name

Date

Signature



WP Manager: E. Tolstoy

Name

Date

Signature

Proj. Responsible: R. Davies 17.09.2019

Name

Date

Signature

CHANGE RECORD

ISSUE	DATE	SECTION/PARAGRAPH AFFECTED	REASON/INITIATION DOCUMENTS/REMARKS
version 0	09/19	All	submitted for STC/ESC

TABLE OF CONTENTS

1	Scope.....	4
2	MICADO SCAO-mode overview.....	4
3	Revisiting the MICADO science cases for SCAO-mode only.....	5
3.1	Dynamics of Dense Stellar Systems	6
3.2	Resolved Stellar Populations	14
3.3	Galaxy Evolution: detailed properties of distant galaxies	31
3.4	Exoplanets and planet formation	37
3.5	The Solar System.....	45
3.6	Black-holes in Galaxies	58
3.7	The Centre of the Milky Way.....	63
3.8	Resolving Individual Stellar photospheres	75

1 Scope

The aim of this document is to highlight important science themes that will benefit from the MICADO imaging and spectroscopy in SCAO mode. This is effectively an Appendix to the Science Case document ELT-PLA-MCD-56305-0006-1, where key MICADO science themes and potential science cases were initially presented. Here we focus on the science cases that will benefit most from SCAO, as a means to emphasize the importance SCAO-mode plays in the MICADO science case. We thus show that MICADO can operate very successfully in stand-alone SCAO mode, and SCAO will continue to be used when an MCAO system is also present. This document is a compilation of contributions. The cases have been supported by new simulations to show their feasibility using the PSFs provided by the SCAO team. We show that MICADO in SCAO stand-alone mode will provide an excellent show case for the capabilities of high resolution imaging and spectroscopy with the ELT.

2 MICADO SCAO-mode overview

The SCAO-mode can provide excellent AO performance, better than MCAO, but over a smaller field of view, and with a much less uniform PSF over the field (see Figure 1). In addition, SCAO-mode also requires a bright guide star ($V \leq 15\text{-}16\text{mag}$) within 15-20arcsec of the field of interest, and the exact properties of the available star and distance from the field has a very large impact on the correction. The fainter the guide star, and the further away it is the worse the AO performance. The effect of the guide star magnitude and distance on the performance can be estimated from Figure 1, which is taken from the “SCAO Analysis Report of AO Performance” (document ELT-SPE-MCD-56304-0020), Figure 65. The SCAO PSF is expected to maintain a diffraction limited core over a large fraction of the MICADO field of view, even at very low strehl ratio, see Figure 2, but the sensitivity obviously declines with the decreasing strehl.

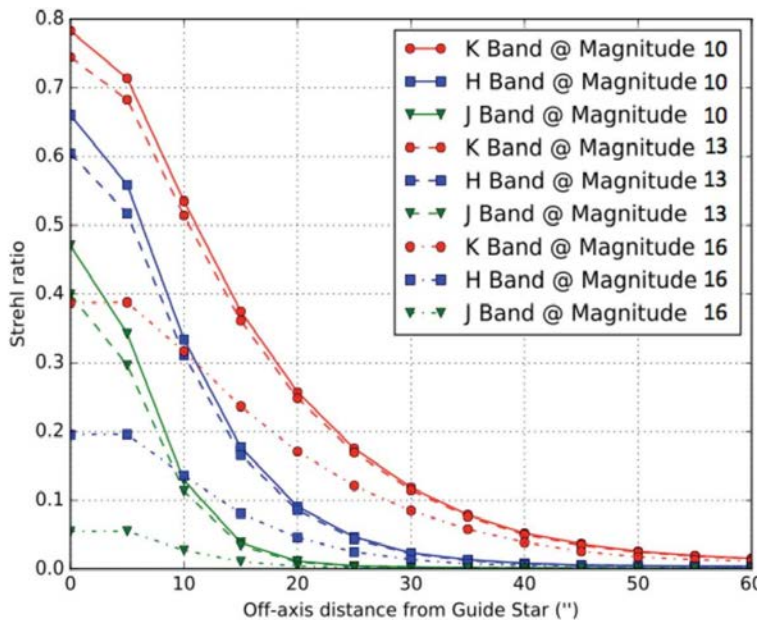


Figure 1: Off-axis SCAO performance in J, H, and K under average seeing conditions for 3 guide star magnitudes ($V=10, 13, 16$), showing the effect of moving off-axis on the strehl ratio.

The primary use of SCAO was originally envisaged to support a multi-purpose high strehl imager. The science case has always included exo-planets, solar system objects, stellar physics, AGN and of course the Galactic centre. The strehl for on-axis targets with reasonably bright guide stars will always be significantly better than MCAO can provide. We believe that improvements in photometry software combined with developments in PSF-R will also allow us to make use of SCAO images in other

scientific areas as well, such as deep imaging of crowded fields, in nearby stellar systems and compact objects, such as black holes in the centres of galaxies, both near and far.

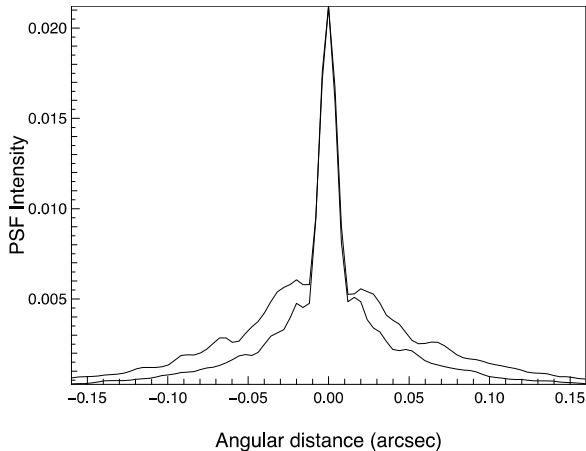


Figure 2: X- and Y-axis cuts through the K SCAO PSF at 60 arcsec off-axis, where the Strehl ratio is a mere 2%.

In summary, the main differences between SCAO and MCAO modes, from the point of view of an astronomer wishing to make scientifically useful observations, are the size of the field of view; the stability of the PSF correction over the field of view; the demanding guide star requirement with a tight relation to the strehl (and thus sensitivity). The diffraction limited angular resolution provided by ELT remains the same, and indeed the top strehl of the SCAO system is much higher than MCAO can ever provide. But this is only available for targets with bright on axis guide star. This is perfectly suited for exo-planet studies, many solar system studies and also looking at the central regions of compact galaxies and globular clusters. It can also be used for a number serendipitous cases where a bright guide star falls close to an object of interest.

3 Revisiting the MICADO science cases for SCAO-mode only

Envisaging a period when MICADO, with only a SCAO-mode, is on the telescope and needs to be available for an undetermined period of time (perhaps as much as 1-2 years) before the full MAORY system arrives and is commissioned, we quantitatively investigate the top level science areas that can benefit from this situation. We use the original MICADO PDR science case (ELT-PLA-MCD-56305-0006-1) and re-emphasize the power of SCAO-mode and what it can contribute to all the science areas covered. We focus on how the SCAO capabilities will provide important break-through scientific results in the early years of MICADO operation. The individual science cases are not repeated from the original science case document, the additional information is provided as an addition to the detailed descriptions provided there, and thus **these two documents should be considered together**. This document is a compilation of contributions which have been attached to a general overview statement for each science area covered in the original PDR science case.

3.1 Dynamics of Dense Stellar Systems

Coordinator: Davide Massari (NOVA/Groningen)

Contributors: S. Dreizler, N. Neumayer, E. Tolstoy, A. Marasco, R. Davies

This science area contains numerous cases where the SCAO mode is a good fit to the science goals. Galactic globular clusters contain numerous bright guide stars, and the search for dense objects, or other kinematic anomalies can be carried out within a very small region on the sky. More distant extended objects, such as dwarf galaxies, and potentially galaxies beyond the Local Group will most likely need to wait for MCAO. This is partly because of the required field of view, and partly because of the guide star requirements. There are a few exceptions here and there which will be able to provide an initial first look at a few more distant stellar systems.

This kind of work has been carried out with current AO instrumentation, for example extensively in the Galactic centre. Tests have also been carried out looking at globular clusters (e.g. Massari et al. 2016 *A&A*, 595, L2). Specific simulations have been carried out for the MICADO SCAO case and are presented here, this has also included a list of southern targets with stars sufficiently bright to provide the required SCAO natural guide star.

Contributions:

- Report on SCAO astrometric performance, by D. Massari & S. Dreizler

Report on SCAO astrometric performance

Davide Massari, Stefan Dreizler

Aims

- To test MICADO astrometric precision in SCAO mode;
- To assess how far away from the natural guide star (NGS) the astrometric performance is still good enough to investigate the astrometric primary science cases.

Setup of the simulations

I simulated in the zoomed mode (1.5 mas/pixel) and K-band filter the central region of a Galactic globular cluster.

The globular cluster has the same luminosity function as that of Omega-Centauri (Bellini et al. 2017), and a cored density profile, such that the distribution of stars in the central chip of MICADO detector is uniform.

To simulate the effect of PSF variation induced by SCAO, I simulated fields at different distances from the nominal guide star, and assumed the PSF to be constant within those fields.

Each field has the size of the central chip of MICADO detector in the zoomed mode.

The adopted PSF is the one created by AnisoCADO, at distances (x,y) from the NGS of:

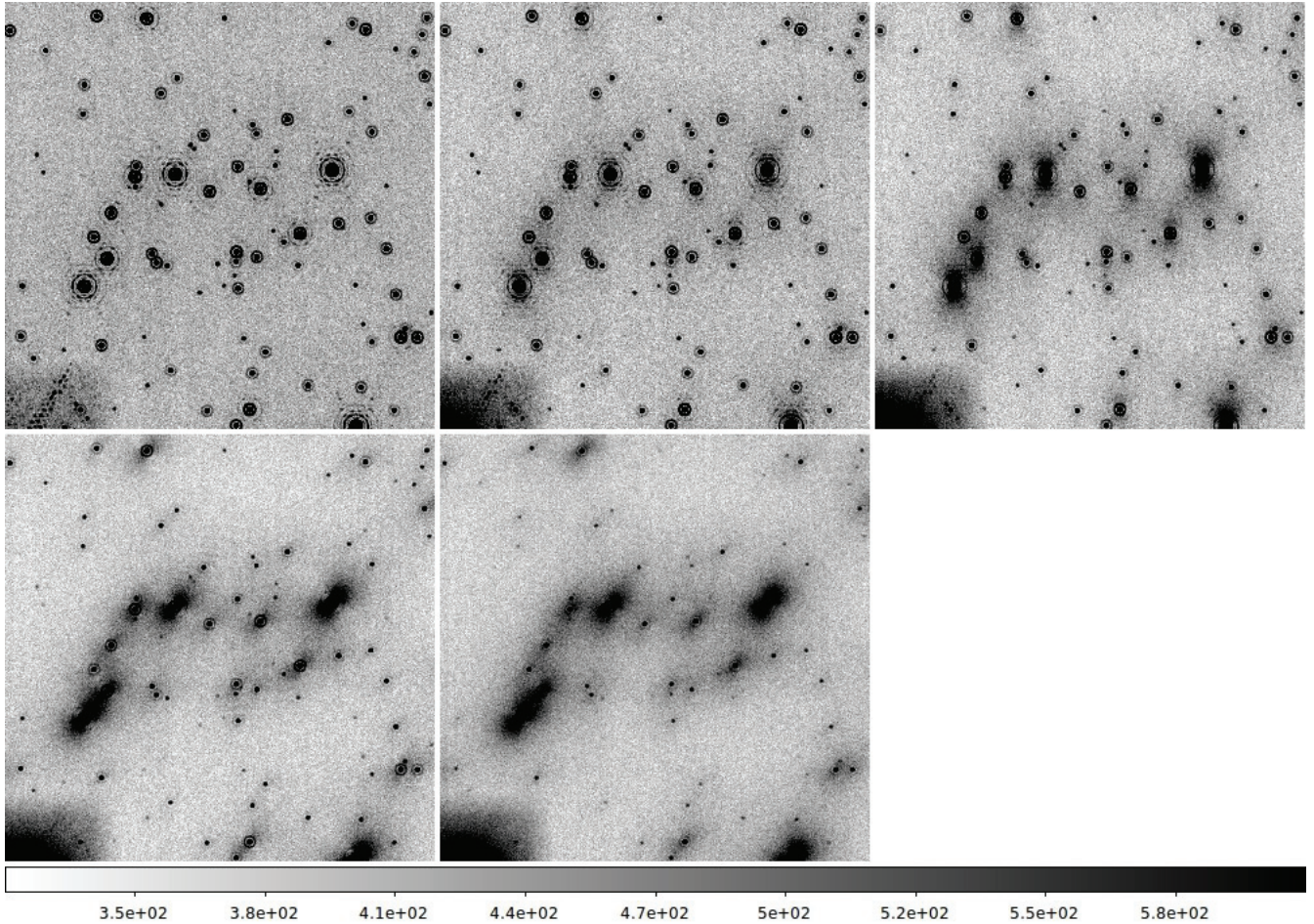
- (0,0) arcsec
- (0,7) arcsec
- (0,14) arcsec
- (15,15) arcsec
- (25,25) arcsec,

corresponding to total distances of (0,7,14,21,35) arcsec.

No geometric distortions are included, as the aim is to determine the intrinsic astrometric precision of the SCAO mode. The only contribution to the astrometric error comes from the intrinsic limit given by $\sigma \sim \text{FWHM}/\pi\text{SNR}$ (Lindegren et al. 1978), plus the PSF modelling.

PSF modelling is performed using classical astrometric techniques applied to crowded fields (e.g. Massari et al. 2016) and using DAOPHOT (Stetson et al. 1987) as software.

Simulations

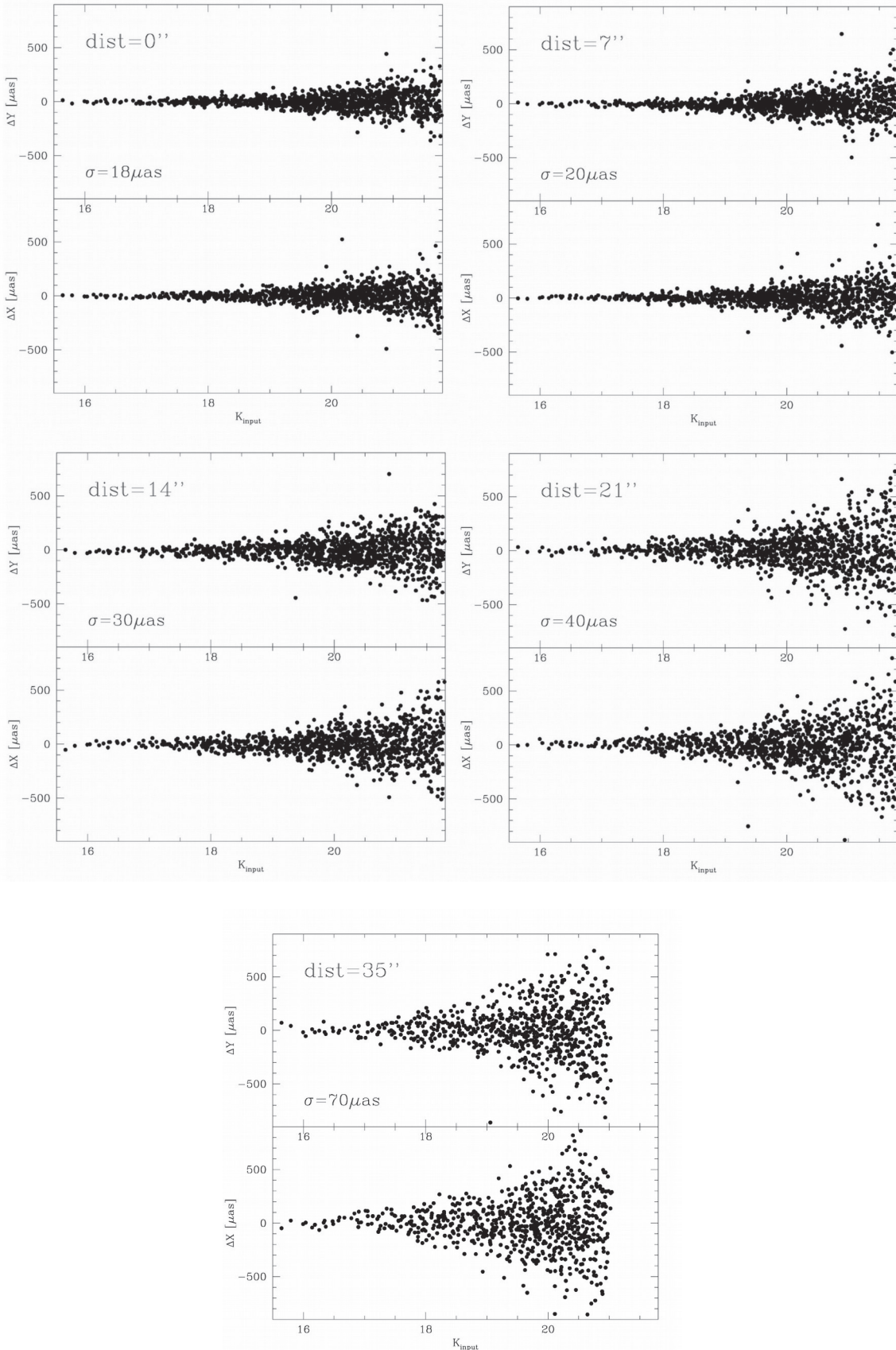


Each panel corresponds to a zoomed-in region of the five simulated fields. The NGS is located at the previously quoted distances from the centre of each field.

The results of the test are summarized in two tables.

Fig.1 provides the measured astrometric precision at K=18 for varying distances from the guide star.
Fig.2 provides the magnitude at which the requirement of 50 uas precision is achieved, as function of the distance from the guide star.

Results: individual simulations



The SCAO PSF always maintains a diffraction limited core that keeps the precision high even at large distances from the NGS. Because of this, it is possible to achieve good astrometric precision even with non optimal NGS configurations (i.e. GS located few tens of arcsec away from the ideal scientific target).

Results: summary of astrometric performance

At the typical magnitude of the Main Sequence Turn-Off of a Galactic globular cluster at 10 kpc distance ($K=18$), the astrometric performance degrades as a function of the distance from the NGS as shown in Figure 1.

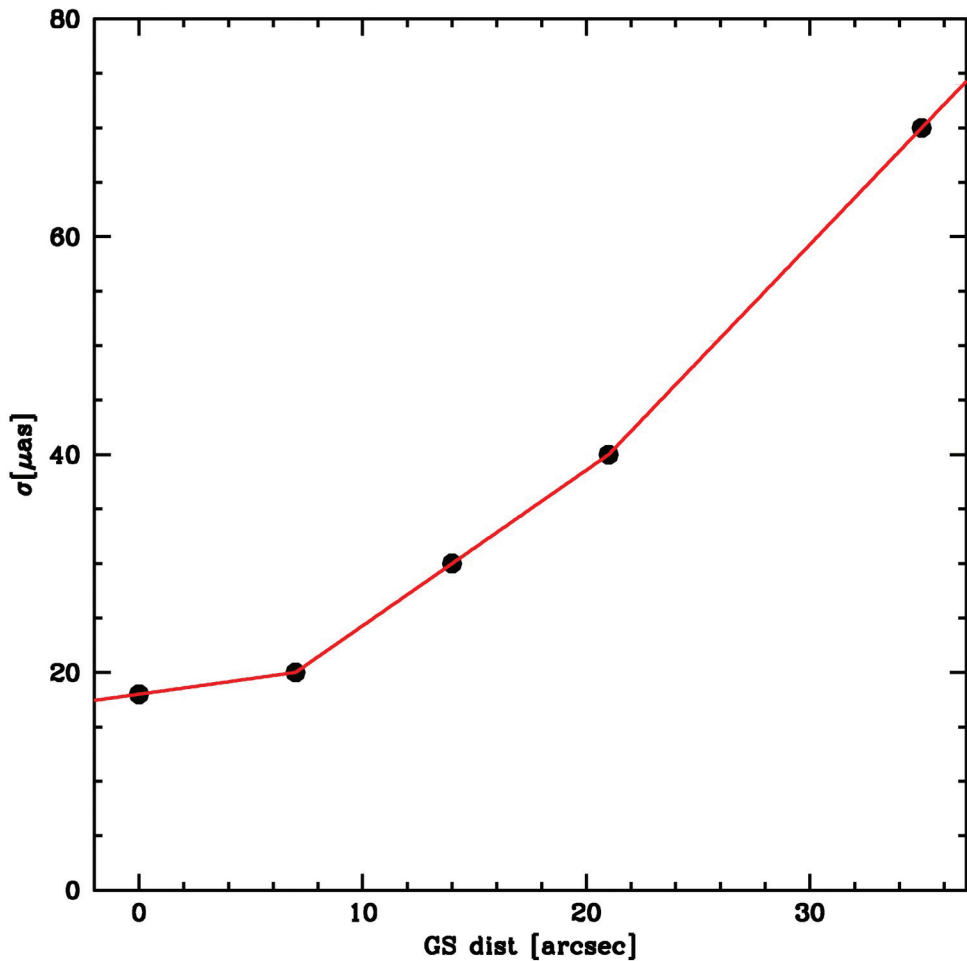


Fig.1: Astrometric precision at $K=18$ as function of NGS distance

In general, the worse performance affects the depth at which the astrometric precision requirement of 50 μ as is achieved. This is shown in the next Figure 2.

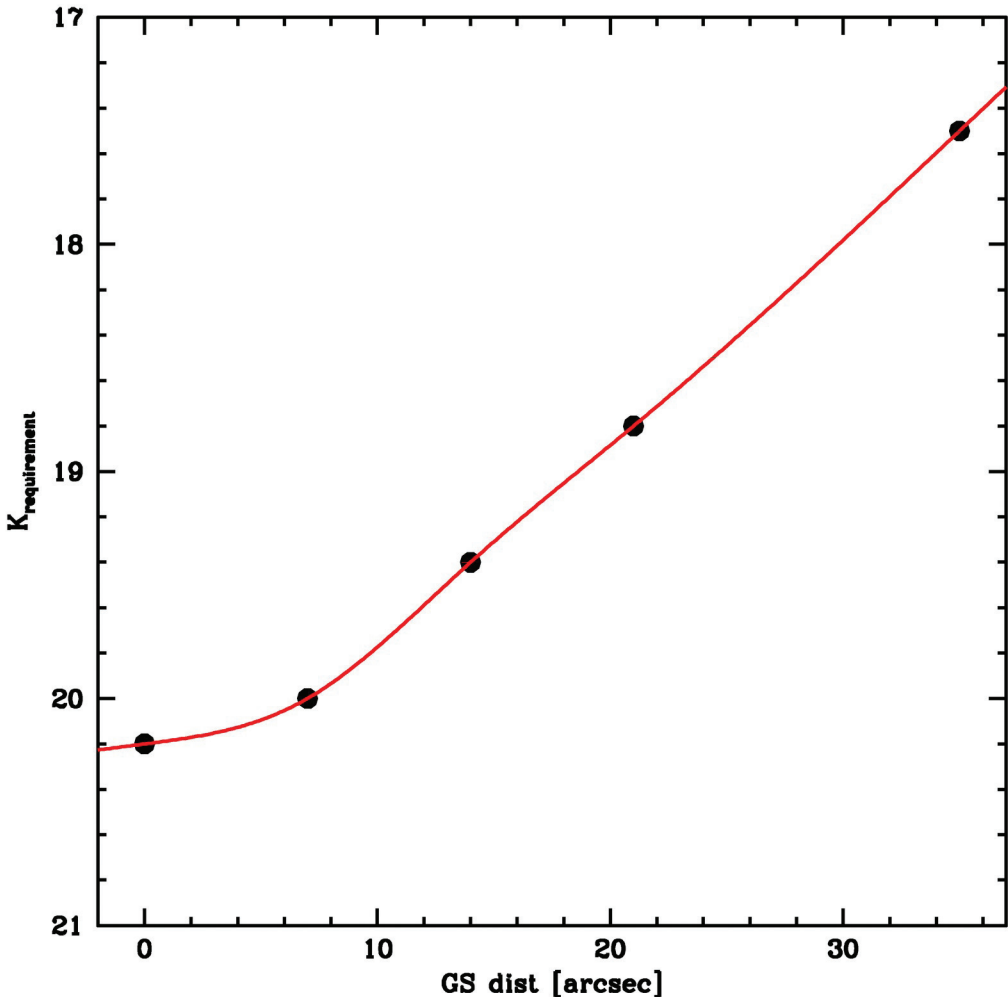


Fig.2: K-band magnitude at which 50 μ as precision is achieved as function of NGS distance

Technical issues / further remarks

Gabriele mentioned the issue of losing the stability of the plate scale during a SCAO exposure (Rodeghiero et al. 2018).

Because of how different exposures are combined together via linear transformations, this is not going to be an issue. Every exposure will be brought to the plate scale of the one used as reference (this is the plate scale that is important to know precisely).

The problem arises for longer (> 1 min) exposure, because this plate scale instability might cause the PSF to stretch along some direction, this translating to loss of astrometric precision.

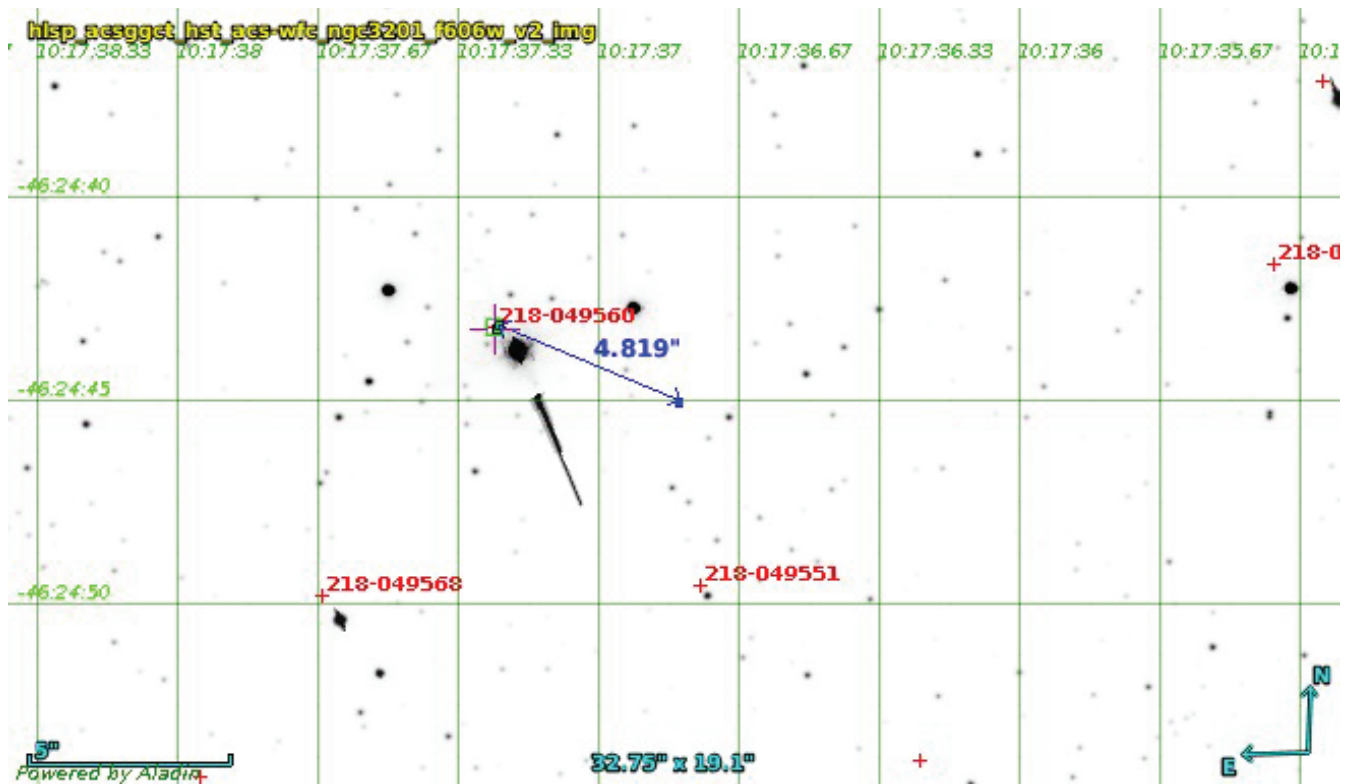
Feasibility of the Galactic globular clusters science cases

The tests performed demonstrate that SCAO will be a powerful tool to investigate astrometric science cases, and that the loss in PSF quality experienced when moving away from the NGS does not compromise the precision of astrometric measurements.

It is then possible to check the sky coverage when Galactic globular clusters (GCs) are the target of the investigation.

Given the constraints of the SCAO performance in terms of reference star brightness and distance we checked a selection of GCs based on the sample observed in the MUSE guaranteed observing time, which contains southern GCs within 10kpc.

Using the ESO GuideCam tool, HST images of the GCs were overlayed with the UCAC4 catalogue and the most suitable reference star was identified. The distance and K magnitude of those are listed in Table 1. An example (NGC3201) is shown in the next Figure.



NGC name	K mag	distance [arcsec]
104	7.4	8.5
362	8.5	1.7
419	12.2	4.0
1851	8.8	3.1
1856	10.9	3
1904	10.4	8.5
2808	9.4	2.0
3201	8.4	4.8
5139	10.8	7.1
5904	10.9	2.6
6093	9.1	1.4
6121	9.5	6.4
6254	11.6	7.3
6266	7.8	2.4
6293	9.7	3.6
6388	8.2	7.9
6441	7.9	7.1
6522	9.9	4.4
6541	9.1	2.2
6624	8.8	1.0
6656	11.1	2.7
6681	9.4	0.5
6752	9.4	4.5
7078	9.2	1.5
7089	11.0	2.0
7099	10.4	2.4

Table 1: reference star list of galactic globular clusters

This check demonstrates that sky coverage should be 100% or close to. It can be expected that the IR bright giants in the GCs are sufficiently dense in a large fraction of the galactic GCs in order to fulfill the reference star criterion.

3.2 Resolved Stellar Populations

Coordinator: Eline Tolstoy (NOVA/Groningen)

Contributors: A. Savino, D. Massari, A. Marasco, S. Larsen

This science area can benefit a lot from the increased strehl of the SCAO mode, and the resulting increase in flux sensitivity. In most of the simulations that have ever been done for this kind of observations not much more than a square arcsec has ever been simulated as this already involves extremely large numbers of individual stars. Thus even tiny SCAO fields of view will be of great scientific interest, especially in the central, most crowded regions of resolved galaxies and also in the study of individual extra-galactic globular clusters. The main limitation of SCAO is that it is not always possible to find a suitable guide star in representative places in and around individual galaxies. Thus MCAO will be a more comprehensive way to study a range of different galaxy types and usefully cover the range of the physical conditions found in individual galaxies. However, SCAO will be an excellent path finder, and it will also provide images with the highest flux sensitivity and spatial resolution in the cores of galaxies that will be excellent synergy with later wide field MCAO imaging, as well as JWST imaging. These type of simulations have already been published (Deep et al. 2011 A&A, 531, A151; Greggio et al. 2012 PASP, 124, 653) and in the attached report we show updated simulations using Simcado and up to date SCAO PSFs. Tests have also been carried out with existing AO instrumentation (e.g., Fiorentino et al. 2011 A&A, 535, A63; Massari et al. 2016 A&A, 586, A51).

To carry out accurate photometry in crowded stellar fields with a varying PSF will require new and more sophisticated tools. Also attached to this section is a preliminary report of investigations and tests made of a new software, SuperStar, that will make use of additional information (such as PSF-R estimates of PSF shape and variation over the field) in crowded fields that will enable accurate PSF-fitting photometry, even when the PSF is varying quite strongly. This will be critical to obtain accurate deep photometry for faint resolved stellar populations with SCAO images, and it will also be useful for MCAO imaging, where the variations in strehl over the field of view are likely to be difficult to disentangle from intrinsic flux variations in the stars themselves.

In addition, a science case is given for the SCAO spectroscopy of individual extragalactic globular clusters in relatively nearby galaxies. The main issue is the requirement to find a guide star, and several galaxies are shown to have sufficiently bright guide stars in their fields.

Contributions:

- Simulated MICADO/SCAO photometry of resolved stellar populations in the Virgo Cluster by A. Savino
- SuperStar: a new software for astrometry and photometry in the AO era, by A. Marasco & D. Massari
- Spectroscopy of Extragalactic Massive Star Clusters, by S. Larsen

Simulated MICADO/SCAO photometry of resolved stellar populations in the Virgo Cluster

Alessandro Savino

To characterize the expected photometric performance of MICADO/SCAO on crowded, resolved stellar populations, we rely on a suit of simulated observations of a giant elliptical galaxy in the Virgo Cluster. This analysis relies on the following steps: generation of an input stellar catalogue, representative of the astrophysical object of interest, with apparent magnitudes and positions on the sky; simulation of MICADO/SCAO observations for different lines of sight, photometric bands and exposure times; reduction of the synthetic frames and creation of an output stellar catalogue; cross-match between the input and output catalogue to calculate single-band photometric performance; creation of a multi-band output catalogue to build an observed colour-magnitude diagram. In this report we describe the details of our procedure and the conclusions that can be drawn from the reduction and analysis of this dataset.

1 Generation of input stellar catalogue

The input catalogue we use in this work is meant to be representative of a giant elliptical galaxy. We use a star formation history of an old stellar population that very rapidly self-enriched itself to solar metallicity. We assumed the stellar population was formed in three events of star formation, separated by different metallicity intervals. One of our final goals will be to asses how well we can identify the different stellar subpopulations. The synthetic stellar population was generated using alpha-enhanced BaSTI isochrones, with mass-loss coefficient $\eta = 0.4$ (Pietrinferni et al. 2006). We simulated all the stellar evolutionary phases up to the first thermal pulse on the AGB. We applied a distance modulus of 31.15, corresponding to 17.6 Mpc, the approximate distance of M87 in the Virgo Cluster. We generated a master catalogue with a large number of stars, provided they satisfied one of the following criteria:

- $J < 32.3$ (VEGA)
- $H < 32.5$ (VEGA)
- $K_s < 31$ (VEGA)

This ensures that we have stars down to at least ~ 2 magnitude below the expected SCAO detection limit (for 100h exposure). Having a deep catalogue en-

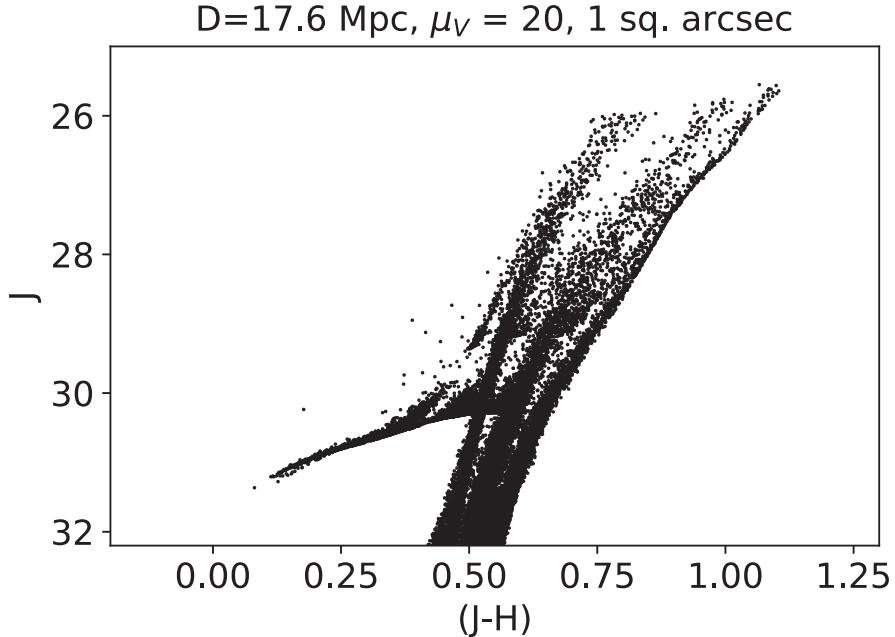


Figure 1: J vs (J-H) color magnitude diagram of the input stellar catalogue used to create the synthetic MICADO/SCAO frames, for the $\mu_V = 20$ case.

sures that unresolved stars make a realistic contribution to the sky background. The contribution to the unresolved background of even lower mass stars, not included in this catalogue, is found to be negligible (at the distance of Virgo) compared to the sky brightness in J, H and K_s , expected at the observing site.

From the master catalogue, we can extract a subset of stars to serve as input catalogue, whose size will depend on the observed line of sight in the galaxy. The number of stars N is chosen depending on the observed surface brightness and field of view, to satisfy the following criterion:

$$\sum_{i=0}^N L_{K_s}^i = f \cdot L_{K_s} = f \cdot \text{FoV} \cdot 10^{-0.4 \cdot (\mu_{K_s} - M_{K_s}^\odot - DM)} \quad (1)$$

Where $L_{K_s}^i$ is the K_s luminosity of a randomly selected star in our master catalogue (expressed in solar luminosities), L_{K_s} is the total K_s luminosity of the observed stellar population, integrated down to $0.1M_\odot$, FoV is the field of view in arcsec², μ_{K_s} is the observed K_s surface brightness, $M_{K_s}^\odot$ is the Sun's absolute magnitude in K_s band (3.27, from Willmer 2018), DM is the distance modulus (31.15 for M87) and f is the fraction of the total K_s luminosity coming from stars brighter than our magnitude threshold (estimated from the Kroupa initial mass function, the BaSTI stellar models and the adopted star formation history).

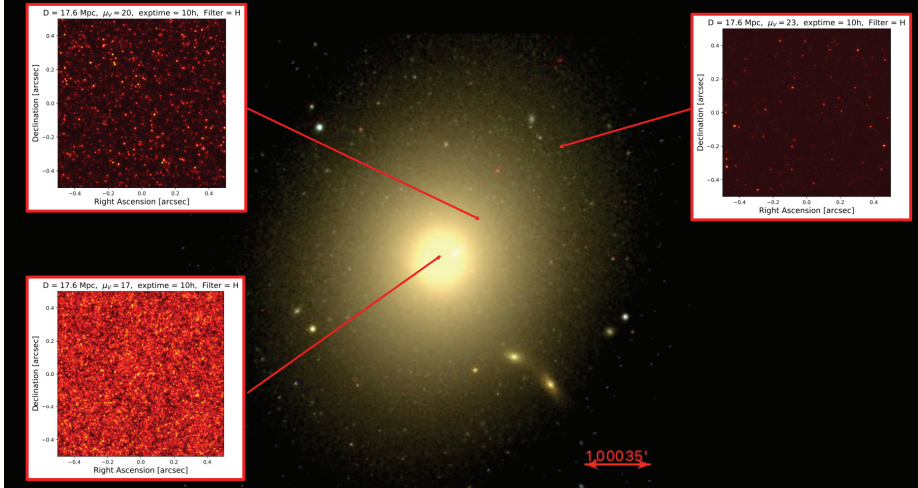


Figure 2: Color-composite image of M87, from the Sloan Digital Sky Survey. The insets show the expected (1 arcsec^2) frames that could be observed with MICADO/SCAO, at different positions in the galaxy, with a total exposure time of 10h in H band.

We generate 3 input catalogues, sampling 4 arcsec^2 at V surface brightness of $\mu_V = 17$, $\mu_V = 20$ and $\mu_V = 23$. Combining the M87 V surface brightness profile (Kormendy et al. 1990) with the 2MASS K_s profile, these values correspond to $\mu_{K_s} = 13.5$, $\mu_{K_s} = 17.4$ and $\mu_{K_s} = 20.4$, and a distance from the galaxy photometric centre of roughly 0, 50 and 150 arcsec, respectively. The chosen field of view is small enough that the surface brightness can be assumed constant. For this reason the sky positions of our stars are generated following a uniform distribution in both RA and Dec. Figure 1 shows an example CMD for one of these catalogues.

2 Creation of simulated frames

The input catalogues are converted into simulated MICADO frames using the SimCADO package (Leschinski et al. 2016). The frames are observed in ZOOM mode ($0.0015 \text{ arcsec}/\text{px}$), using the on-axis SCAO PSF, generated for the ESO median atmospheric conditions of the AnisoCADO package (seeing 0.67 arcsec , zenith angle 30 degrees, wind speed 10 km/h). We simulate observations of 1, 10 and 100 hours (summing the appropriate number of 20 min exposures) in the

J , H and K_s photometric bands. The assumed sky surface brightness is 16.5, 14.4 and 13.6 in J , H and K_s respectively (from SimCADO). We simulate a 2x2 arcsec field of view and then extract the central 1x1 arcsec region as our final simulated frame. In this way we include light from bright stars outside our field of view and avoid edge effects. Figure 2 shows an overview of the (1 arcsec²) images that could be expected at different distances from the center of a Virgo elliptical galaxy and thus at different surface brightness, which corresponds to different densities.

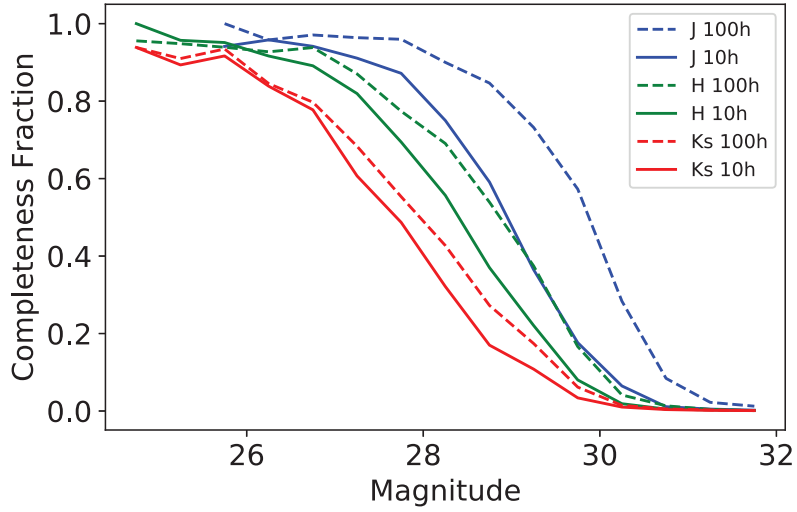
3 Reduction of the synthetic frames

We reduce the synthetic frames using DAOPHOT and ALLSTAR (Stetson 1987). We use between 25 and 100 bright isolated stars to generate a model PSF for each frame. We use this model PSF to recover position and magnitude of the detected stellar sources, which are subtracted from the original frame to generate a new frame with the residuals. We use the residual frame to identify additional faint stars and run ALLSTAR again, with a larger star list. We iterate this procedure to greatly increase our detection efficiency, while consistently getting rid of eventual duplicate sources. The output of this procedure is a separate stellar catalogue with position and magnitude for each filter, exposure time and surface brightness combination.

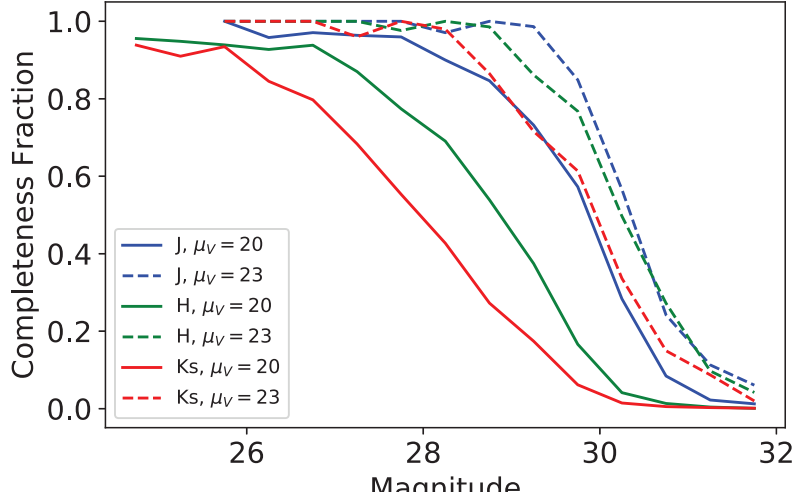
4 Cross match with the input catalogue and performance calculation

In order to estimate our photometric performance we need to cross-match the sources in our output catalogue with those in the input one. We run this cross-match on the individual passbands rather than on the multi-band catalogue (which by construction is less complete). For each star in the input catalogue (in order of increasing magnitude), we search for all the sources in the output within a given tolerance radius (0.006 arcsec). One of the following cases can happen:

- **No corresponding source is found in the output:** In this case the input star is undetected and it is flagged as such.
- **One corresponding source is found in the output:** In this case the matching is straightforward. The output star is flagged as already detected and it is never used again in the cross-match.
- **More than one corresponding source is found in the output:** In this case the brightest output star is assigned as the matching one. The output star is flagged as already detected and it is never used again in the cross-match.



(a)



(b)

Figure 3: Completeness fraction of our simulated observations as function of input (VEGA) magnitude, for different photometric bands. a) Performance on the $\mu_V = 20$ field, with exposure times of 10h and 100h. b) Comparison between the performances on the $\mu_V = 20$ and $\mu_V = 23$ fields.

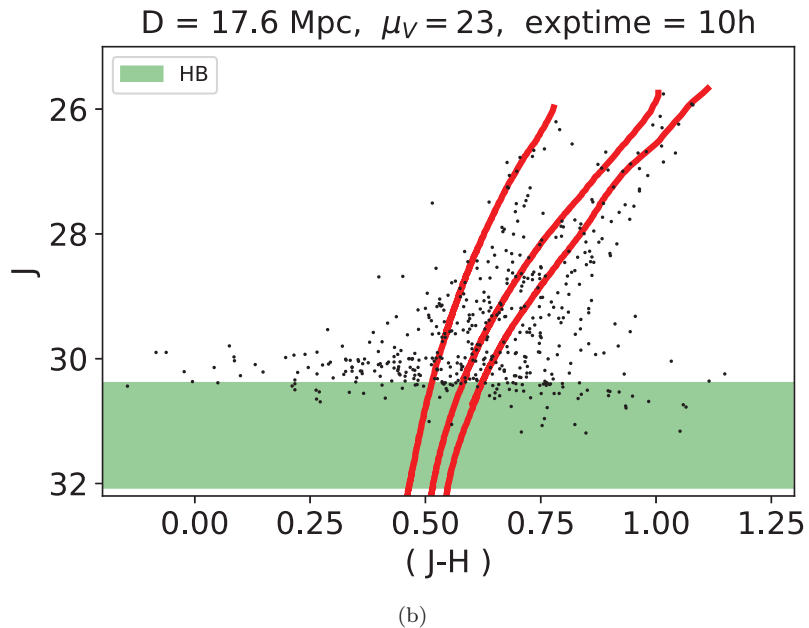
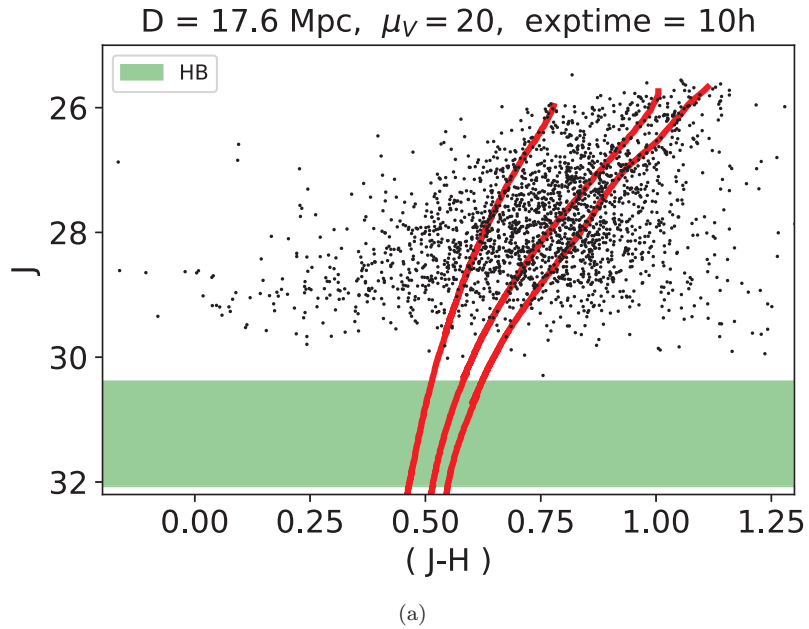


Figure 4: Recovered J vs $(J-H)$ color-magnitude diagram for the $\mu_V = 20$ (a) and $\mu_V = 23$ (b) fields. The red lines are representative isochrones for the three stellar subpopulations of this simulation. The green band marks the magnitude range of horizontal branch stars.

The outputs of this procedure are: a list of undetected input stars; a list of detected input stars, with the corresponding output magnitude; a list of output stars with no input counterpart, which are flagged as false detections. The difference between the input and output magnitude (after a calibration zero-point is applied), is assumed to be the photometric error. These three catalogues are used to estimate several performance parameters, such as completeness fraction (shown in Fig. 3, for different photometric bands, exposure times and surface brightness values), false detection fraction, photometric uncretaintiy distribution and signal to noise, as function of input magnitude.

5 Creation of a multi-band photometric catalogue

For each surface brightness and exposure time, we can generate a multi-band catalogue using DAOMATCH/DAOMASTER, using the J catalogue as reference catalogue for the stellar positions. In order to be included in the multi-band catalogue we require that each star is detected in at least two filters. The output catalogue permits us to generate an observed colour-magnitude diagram for our synthetic frames (examples shown in Fig. 4).

6 Conclusions

From the analysis of the recovered output catalogues, several conclusions can be drawn about the photometric performance of MICADO/SCAO on crowded stellar populations in the local Universe:

- The sensitivity and resolution of the instrument will allow to detect stars in the Virgo/Fornax Cluster of galaxies down to several magnitudes from the tip of the red giant branch (RGB, Fig. 4).
- We find J to be the deepest band in terms of limiting magnitude (Fig. 3). However due to the increasing luminosity of RGB stars in redder bands, H is the deepest catalogue in terms of number of detected RGB stars.
- In the high surface-brightness regime, crowding is a critical factor for the detection of faint stars. An increase in exposure time has the most benefit in J, due to the sharper PSF and the least benefit in Ks, where crowding is dominant (Fig. 3a).
- In terms of photometric depth, a decrease in the observed surface brightness is more beneficial than an increase in the the exposure time (Fig. 3).
- J vs (J-H) is the most promising CMD to reach lower luminosity features, such as the horizontal branch and the RGB bump. Even at the distance of the Virgo Cluster, these stars can be marginally detected (in the low surface-brightness regions). We can therefore expect horizontal branch

stars to be well within reach for galaxies in the Local Volume ($d \lesssim 10$ Mpc).

- Photometric uncertainties make it difficult to see the multiple star formation events at $\mu_V = 20$ (Fig 4a). At $\mu_V = 23$ (Fig 4b) the smaller photometric uncertainties allow to detect the split RGB. Since these simulations refer to a field of view of 1 arcsec² (compared to the 20x20 arcsec of the full chip mosaic), the expected number of stars over the entire field of view is expected to be two orders of magnitude larger. Such populated CMD will therefore facilitate the detection of multimodality on the RGB, even when it cannot be discerned by eye.

SuperStar
a new software for astrometry and photometry in the AO era
by Antonino Marasco, Davide Massari

Introduction

The implementation of single and multi-conjugate adaptive optics (AO) on major ground-based telescopes has the potential of boosting virtually all astronomical research fields. In particular, it is of great interest the possibility of studying in detail the dynamical and chemical properties of nearby stellar systems, ranging from globular clusters and dwarf spheroidals to massive ellipticals. However, this kind of studies rely on one key assumption, i.e., that one can measure with sufficient accuracy and precision fluxes and positions of most stars in the image.

To the first order, the point spread function (PSF) in AO-assisted imaging is built by a combination of a diffraction-limited core component and a seeing-limited halo component.

The 2D morphology and flux-ratios of these components can vary across the field of view, depending on the position and brightness of the guide-stars, and in time, depending on the atmosphere variations. These variations are difficult to predict a priori.

Most image analysis software are not designed to deal with morphologically complex, spatially varying PSFs. This often results in an inadequate image modelling, as testified by poor residuals, symptomatic of a bias in the astro/photo-metric measurements.

To tackle this problem, we are developing *SuperStar*, a new software for the analysis of stellar images. SuperStar is a stand-alone software written in C++ language and is specifically designed to model stellar images with a spatially varying, complex PSF. It uses a simple yet powerful iterative approach based on two steps: a) *PSF modelling* via the stacking of isolated stars in different regions of the images, b) *source modelling* via PSF fitting. Iterating the operations above improves on both the PSF modelling and on the astro-photometric measurements.

Below we give a brief description of the software and present two applications, one on an artificial image and the other on real data.

How does a SuperStar work?

SuperStar stands on the shoulders of giants. Most of the methods employed by SuperStars are based on those previously developed in other software for image analysis. In particular, the techniques adopted for the PSF modelling are analogous to those developed for HST imaging by [1,2], while DAOPHOT [4] and StarFinder [3] have inspired many of the algorithms associated to the source modelling.

SuperStar takes as input single images in fits format. Based on some user-defined parameters, it processes the image following the flow chart that is sketched in Figure 1. The software operates on three “image spaces”: the original image, the model image and the difference between these two (residual image). We now briefly describe the various steps of the flow chart.

1 - *Sky*. Estimating the sky background and noise is a fundamental step in any image analysis software. In contrast to other software, Superstar does it a-priori, once and for all, for the entire image. [I have attempted to write the details but they were long and tedious]. A sky background map is generated and injected into the ‘model’, leading to a residual image which at this stage is simply a sky-subtracted version of the original.

2 – *Source Finder*. Sources in the image are detected based on a simple S/N threshold criterion, and a first estimate for their position and flux is derived via aperture measurements. An algorithm flags “isolated” sources, eligible for the PSF modelling.

3 – *PSF modelling*. The image is partitioned into $m \times n$ regions, and a separate numerical (i.e., non-parametric) PSF is built in each region via the normalization and stacking of the brightest, isolated stars. The user can set a minimum number of stars to be used and/or impose a S/N threshold. The PSF construction algorithm consists of many steps which are finely detailed in [1,2].

At the end of this procedure, a PSF at any (x,y) position of the image is derived by interpolating the PSFs in the various regions.

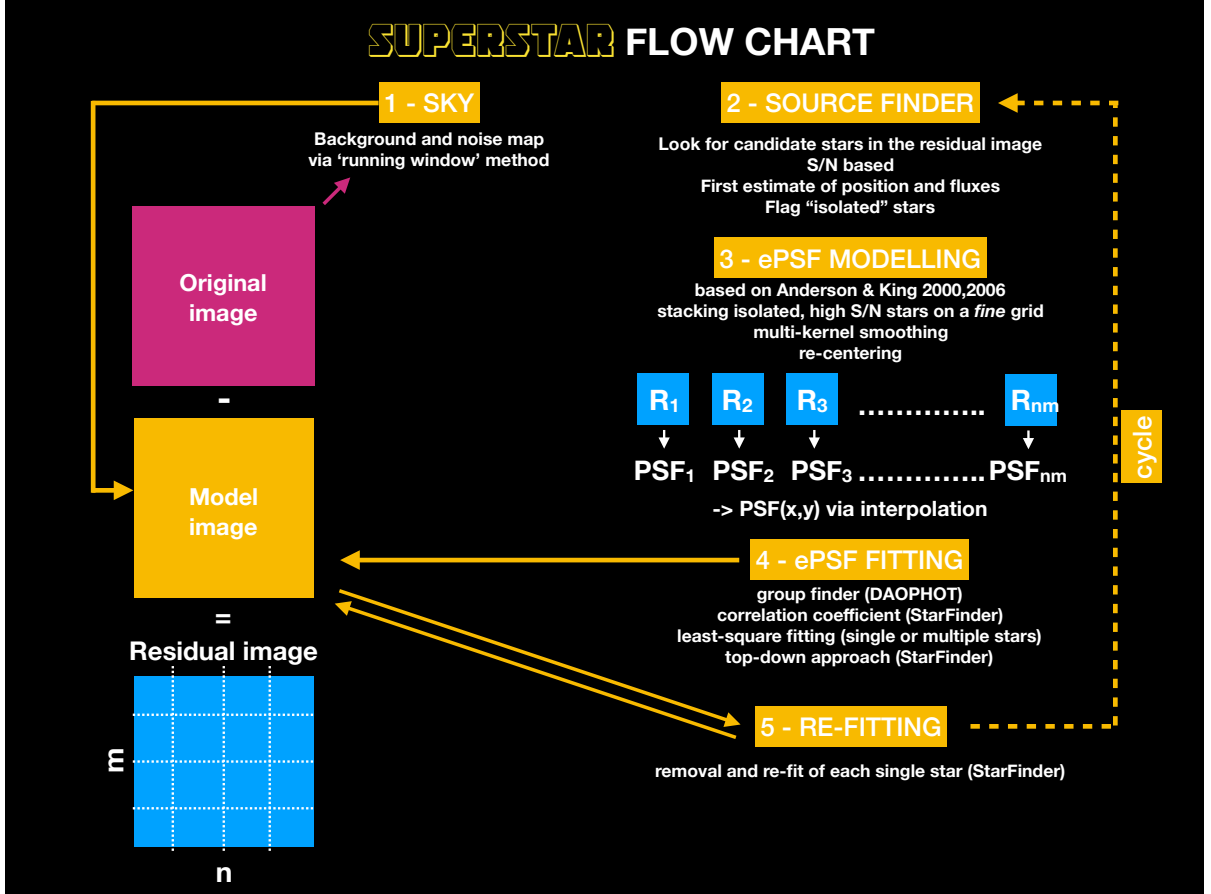


Figure 1: SuperStar flow-chart.

4 – source modelling. The PSF is fit to the sources identified in step 2, starting from the brightest down to the faintest. The sources are fit in the *residual* image. Their best-fit model gets immediately injected into the model image and the residual image is immediately updated: in this way, the star that is fit at any particular moment is not contaminated by brighter sources, as these have been effectively “removed” from the image. This process is very useful in crowded fields. Additionally, this step makes use of a group finder (stars that are “close” are fit together) similar to that of DAOPHOT, and of a PSF-source correlation coefficient test as in StarFinder.

5 – source re-fitting. As a refinement of the previous step, stars get re-fitted one by one, but this time *all* the other stars are “removed” from the image before the fit, and not only those that are brighter than the star in exam. The final position and fluxes of all stars is recorded.

Steps 2 – 5 are iterated in a loop. This is key to the success of the software, as at each iteration: 1) the PSF modelling improves, thanks to a more refined estimate for the position and fluxes of the isolated stars used in the stacking; 2) the source finder can dig into the residual image to find sources that were previously missing.

As outputs, SuperStar returns the residual image, the sky background and noise images, a datacube containing all the $m \times n$ final PSFs, and the final source catalogue.

Applications

We have tested SuperStar on both artificial and real images, and compared its astro and photometric precision to that achieved by DAOPHOT.

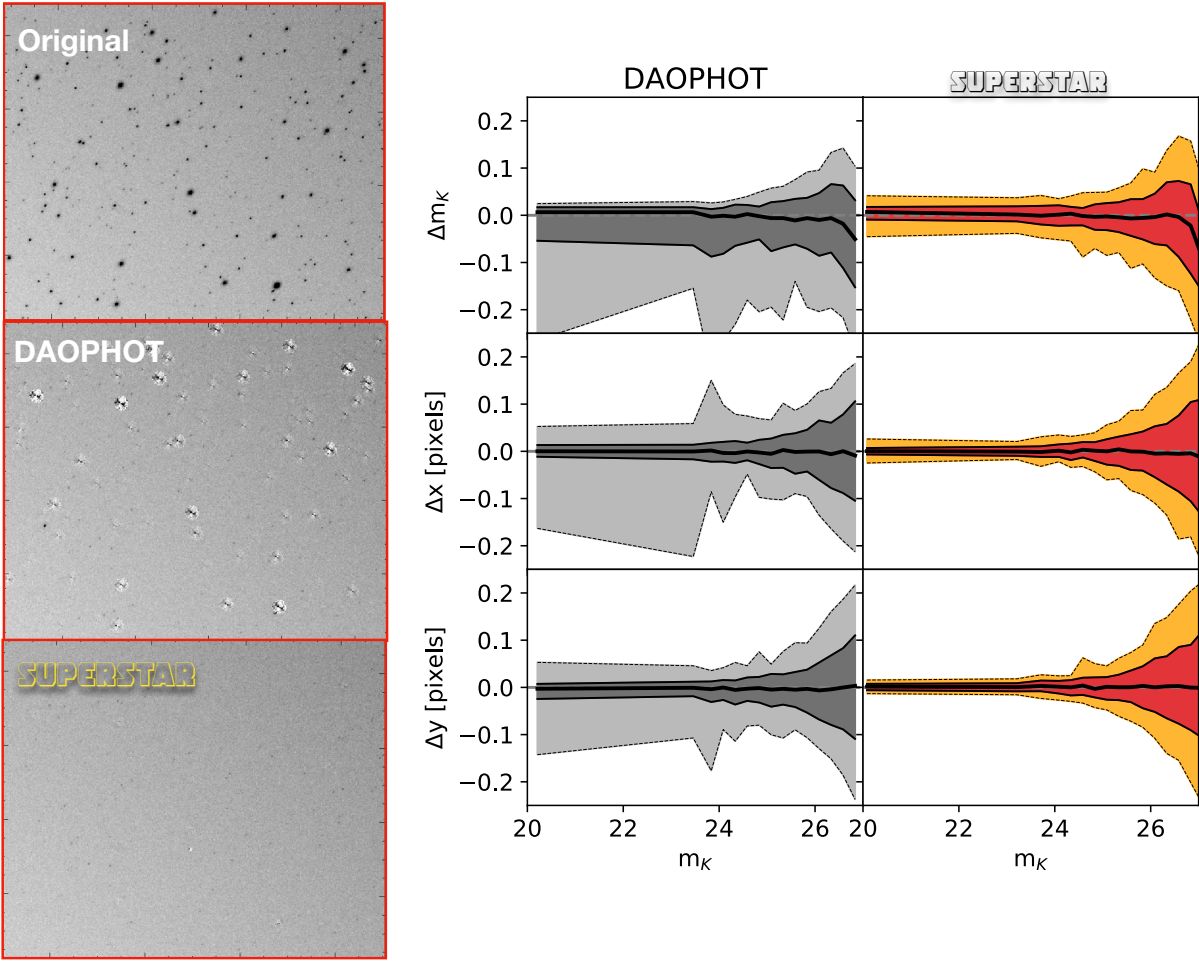


Figure 2: Comparing the performance of SuperStar and DAOPHOT on an artificial image (see text). Left panels: zoomed view on a corner of the synthetic image (on top), DAOPHOT residuals (middle) and SuperStar residuals (bottom). Right panels: photo and astro-metric precision as a function of the input stellar magnitude for the entire image.

Testing both software on artificial images is important for a robust assessment of their performance. We have created an artificial stellar field made by 10^4 sources, uniformly spaced, using a distribution in K-band magnitude analogous to that of a typical globular clusters. To mimic the response of an AO telescope, we have modelled the PSF with two Gaussian components: a core with a FWHM of 1.5 pixel, and a halo with a FWHM of 6 pixel. Both Gaussian components have the same, variable axis-ratio which is 1 at the field centre and ~ 0.5 at the corner, elongated in the radial direction. This implies that shape of point-like sources is rounder close to the centre and gets progressively stretched in the radial direction towards the field edges.

We have processed this image with DAOPHOT and SuperStar, the results are presented in Figure 2. The residual maps (left panels) show the striking superiority of SuperStar over DAOPHOT at modelling the sources in the corner of the field, where the imposed PSF distortions are maximized. This is reflected in a much higher precision on both photometry and astrometry over the entire image (left-hand panel).

We have also tested both software on real images using the GeMS data of the globular cluster NGC 6681 in K and J-band filters (Figure 3). Also in this case SuperStar gives better residual in specific regions of the field (top panels), leading to a (marginally) more detailed color-magnitude diagram (bottom panels).

Future developments

SuperStar is still under development. It is our intention to release the software to the public soon. The software will be properly documented and regularly updated.

We are now working on implementing a “fit-only” mode where the software, rather than building internally the PSF models as described above, takes as an additional input one or more PSFs

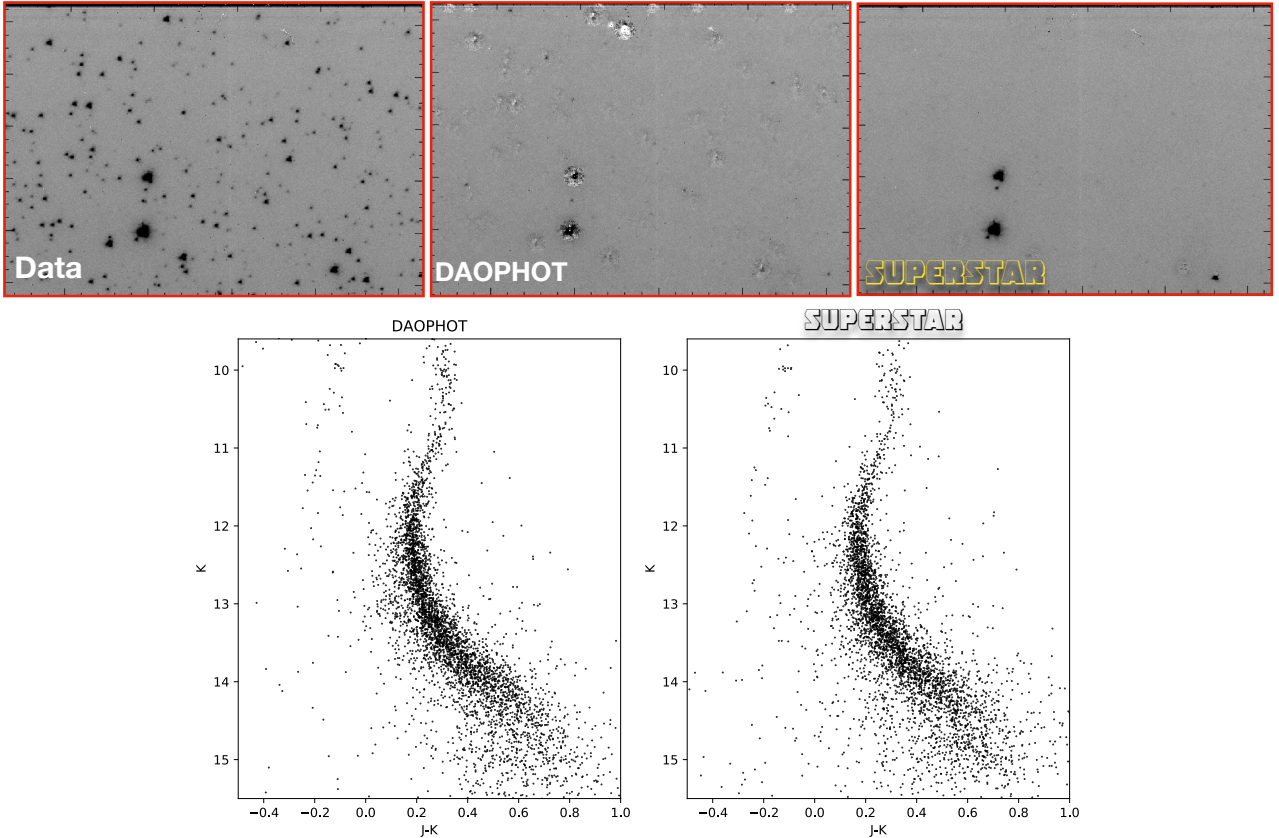


Figure 3: Comparing the performance of SuperStar and DAOPHOT on GeMS observations for the globular cluster NGC 6681. The top panels show the K-band image in a sub-region of the field, along with the DAOPHOT and SuperStar residuals. Saturated stars have been manually excluded from the SuperStar fit. The bottom panels compare the color-magnitude diagrams derived with both software.

given externally by the user in fits format. This is relevant in cases where the number of isolated stars in the field is inadequate to provide an accurate PSF model, and – most importantly – synergizes well with PSF reconstruction strategies aimed at determining a PSF model *a-priori* by exploiting the AO telemetry data and atmospheric information from weather stations. While PSF reconstruction techniques are now extremely popular, surprisingly little effort has been done to convey their application to real astronomical data. We gladly take this opportunity with SuperStar: the reconstructed PSFs can be used to model directly the sources in the image or, in a more refined approach, as a “first guess” upon which our data-driven machinery can improve.

We are currently testing the performance of this “fit-only” mode using data from SPHERE, the AO-aided high-contrast imager at the VLT. The data consist of 24 exposures (12 per CCD) of the same 3.5”x3.5” field, which is dominated the extremely bright (10.5 magnitude) guide star. The left panel of Fig 4 shows (a portion of) the mean image obtained by combining the 12 exposure from the first CCD.

We have measured the variations in flux and position of the guide-star across the 24 exposures using three different approaches: a simple aperture method, DAOPHOT, and SuperStar in fit-only mode using a reconstructed PSF. The PSF-reconstruction strategy is based on the data from AO telemetry and is further fine-tuned on the image itself for a detailed modelling of the PSF wings (Beltramo-Marten et al. in prep). This method provides an excellent model for the on-axis PSF (central panel of Fig. 4) and leads to high-quality residual (right panel).

Fig. 5 compares the astro and photo-metric precision achieved with the different methods over the 24 exposures. Clearly, the PSF-R method is ~ 10 times more precise than DAOPHOT.

Additional details will be given in Massari et al. (in prep), but this simple case highlights already the use and importance of PSF-R methods in real astronomical applications.

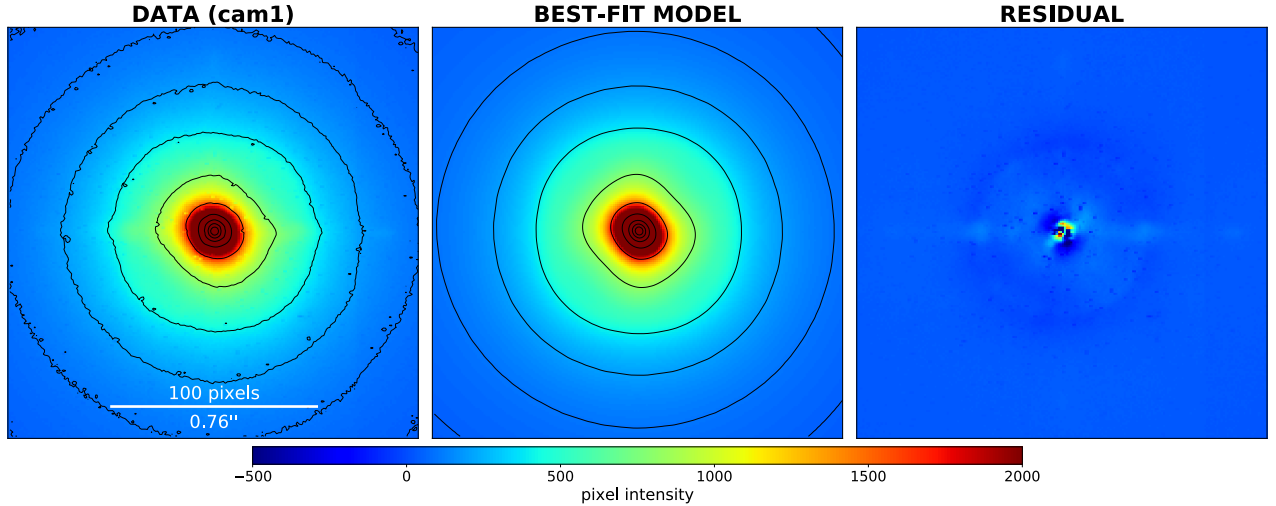


Figure 4: SPHERE data and model. Left panel: mean image derived by combining 12 exposures from the first CCD. Central panel: mean best-fit model obtained with SuperStar using the PSF-reconstruction method of Beltramo-Martin et al. (in prep). Right panel: mean residual image. All images use the same intensity scale.

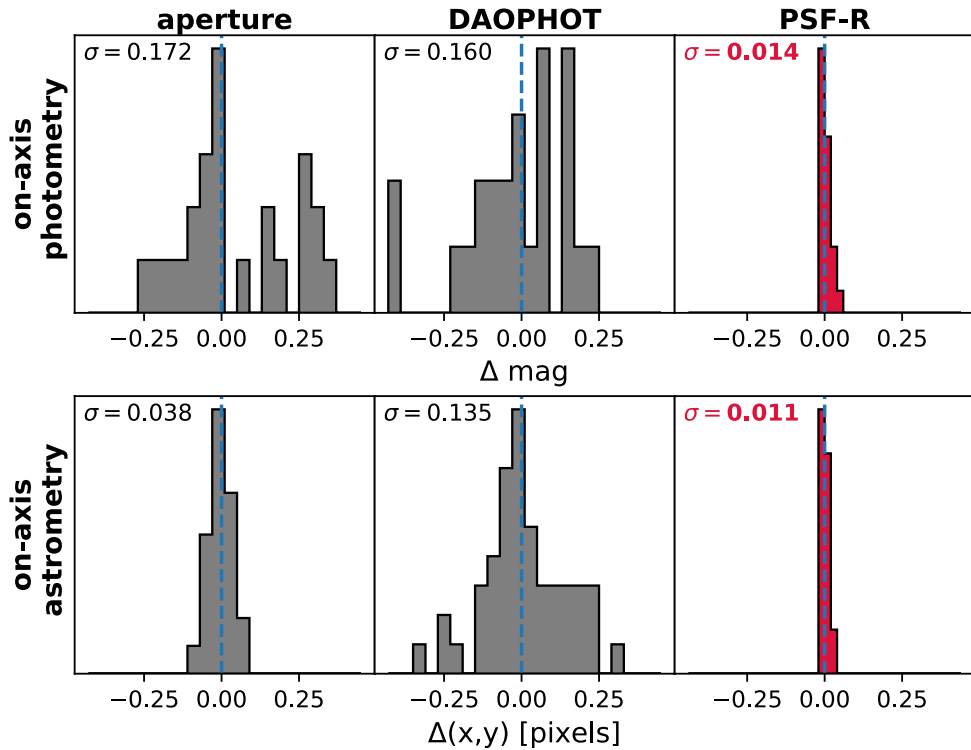


Figure 5: photo and astro-metric on-axis precision achieved by three different methods using the 24 images from SPHERE. The PSF-R method is by far the most precise.

References

- [1] Anderson J. and King I. R., Publications of the Astronomical Society of the Pacific, 112, 1360. 2000
- [2] Anderson J. and King I. R, Instrument Science Report ACS2006-01. 2006
- [3] Diolaiti E. et al., A&A Suppl. Ser., 147, 335. 2000
- [4] Stetson P.B., Publications of the Astronomical Society of the Pacific, 99, 191. 1987

Spectroscopy of Extragalactic Massive Star Clusters

Søren S. Larsen, Department of Astrophysics/IMAPP, Radboud University, Nijmegen, NL

The main impact of SCAO on this science case will be the greatly reduced sky coverage and corresponding decrease in the number of observable targets. Some of the classical Toomre-sequence mergers, such as the Antennae (NGC 4038/39) and NGC 7252, with well-studied and rich populations of young massive clusters (YMCs), are located at relatively high latitudes ($42^\circ, -56^\circ$) and lack suitable bright guide stars.

In most cases, the YMCs themselves are too faint to be used as guide stars, but one potential exception is the cluster NGC 1705-1, which has an apparent V magnitude of 14.7. At a distance of about 5 Mpc the cluster is, however, not a point source, but is resolved with a FWHM of about 40 mas. Figure 1 shows the field of view of the HST Planetary Camera (about $36'' \times 36''$) for the central regions of NGC 1705. In the vicinity of NGC 1705-1, several other fainter clusters and individual stars are visible, which are also potential spectroscopic targets for Micado.

At lower Galactic latitudes, the density of potential guide stars increases. One promising target is NGC 3256, also a recent major merger, at a latitude of 12° and located at a distance of about 36 Mpc. An HST/ACS optical image is shown in Figure 2, where circles with radii of $20''$ are drawn around three potential guide stars that have Gaia g magnitudes in the range 15.3 to 15.8. Stellar clusters (Mulia et al. 2016, ApJ 826, 32) are marked with smaller circles, labelled with their apparent V magnitudes. Two clusters fall within $20''$ of a guide star. According to Mulia et al., these clusters have ages of 50 Myr and 200 Myr and are therefore expected to be bright in the near-IR ($V - K \approx 1.8$). Several additional targets become available just outside the $20''$ circles – some of which are in fact even brighter, and may thus be better spectroscopic targets despite the expected lower Strehl.

Based on experiments with the Precado tool, a few known clusters in the nearby (4-5 Mpc) southern galaxies NGC 5236 and NGC 5253 may also have suitable guide stars.

In conclusion, we expect that it is possible to find a limited number of targets at a range of distances for this science case that will be observable with Micado in SCAO mode. This will be sufficient to demonstrate the potential of MAORY-assisted spectroscopic observations of a larger sample of YMCs in external galaxies.

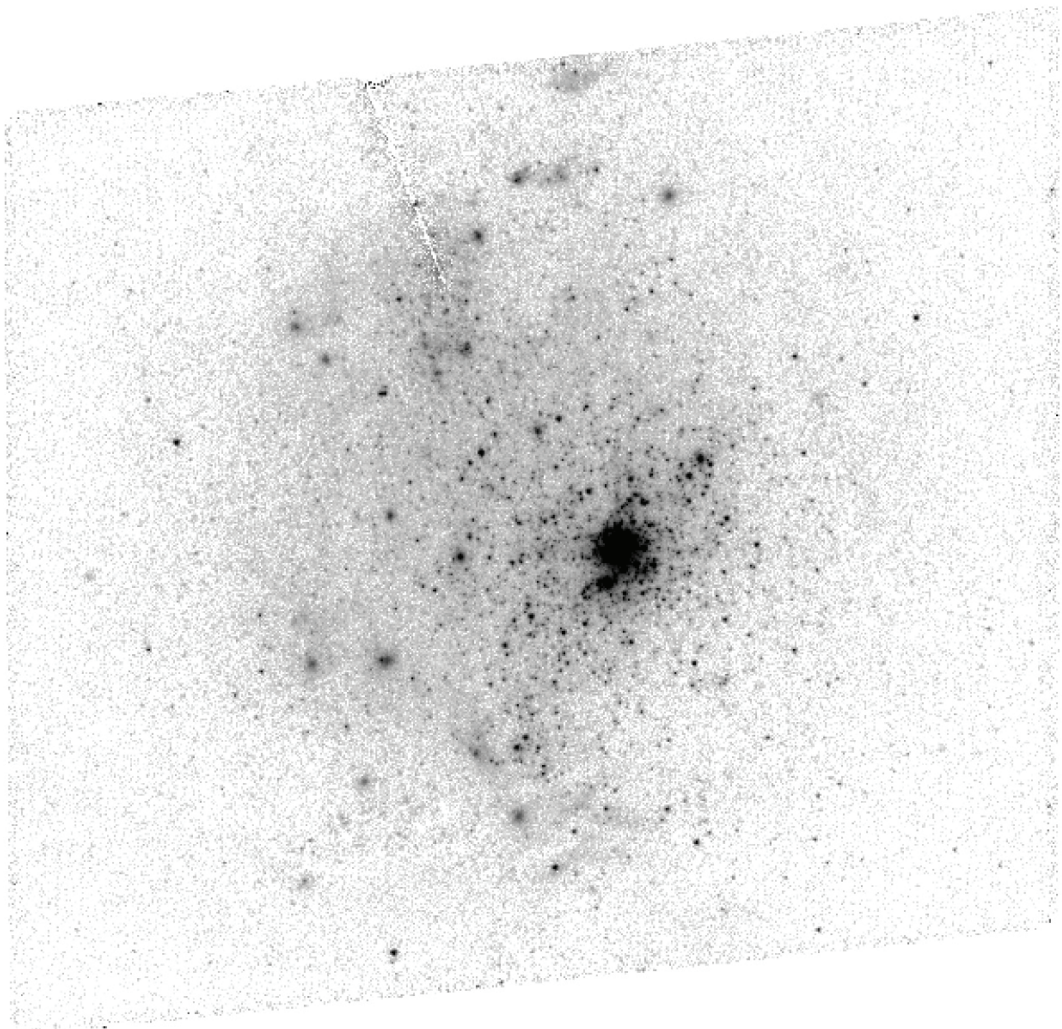


Figure 1: The blue compact galaxy NGC 1705. The image shows the field-of-view of the HST Planetary Camera, about $36'' \times 36''$. The massive cluster NGC 1705-1 is the bright object near the centre; several fainter clusters and individual stars are visible.

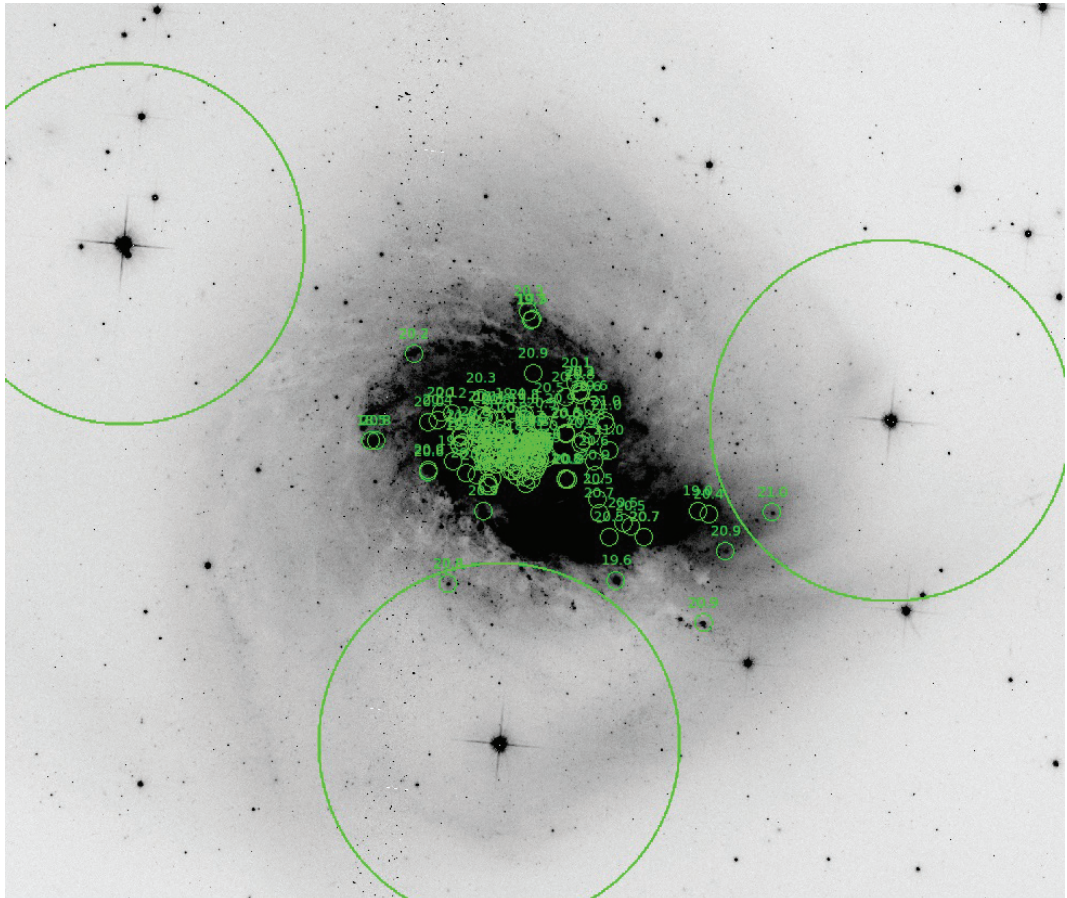


Figure 2: The interacting galaxies NGC 3256. Small circles indicate star clusters identified in HST images by Mulia et al. (2016), labelled with their apparent V magnitudes. The three large circles, each with a radius of $20''$, are centred on potential guide stars with Gaia g magnitudes in the range 15.3 to 15.8.

3.3 Galaxy Evolution: detailed properties of distant galaxies

Coordinators: Natascha M. Förster Schreiber/MPE

Contributors: Simona Mei, S. Vegetti, O. Czoske, B. Vulcani, G. B. Caminha, K. Caputi

This science area arguably suffers the most using SCAO mode alone. However, there do exist interesting and sizeable samples of galaxies (~ 150) known to have sufficiently bright guide stars nearby, for example those galaxies that have already been studied by SINFONI in AO mode (e.g. Förster Schreiber et al. 2018, ApJ, 238, 21), and more details are given in the first attachment. The simulations performed as part of the MICADO Primary Science Case remain relevant for the SCAO case as the typical angular size subtended by $z > 1$ galaxies is a few arcsec at most, and thus the effects of anisoplanatic angle are minimal for individual targets.

There are also a number of serendipitous cases which have been found in careful searches of deep images around the (few) bright stars, and the second attachment contains a very interesting example of such a case of highly lensed galaxies very close to bright foreground star.

Contributions:

- Galaxy evolution, by N. Förster Schreiber et al.
- Probing dark matter and the distant Universe with galaxy clusters, G.B. Caminha & K.I. Caputi

Galaxy Evolution

Natascha M. Förster Schreiber et al.

This science area arguably suffers the most using SCAO mode alone because of the effective loss in multiplexing from the reduced area with diffraction-limited resolution. Nonetheless, the immediate return from MICADO + SCAO observations will be tremendous even with the smaller samples. The science goals detailed in the MICADO Primary Science Case document are largely driven by fundamental questions on the structure of distant ($z > 1$) galaxies raised by studies not only with HST but, importantly, with ground-based AO-assisted near-IR integral field spectrometers (VLT/SINFONI, Keck/OSIRIS, Gemini/NIFS). Over 150 galaxies at $z > 1$ have been observed with IFU + AO to date, with typical effective PSF FWHMs $\sim 0.1'' - 0.2''$ or $\sim 1 - 2$ kpc at those redshifts, or even smaller for the subset of ~ 35 strongly-lensed sources. Many of these galaxies further benefit from exquisite multi-wavelength coverage including HST imaging at similar resolution, and an increasing number is being observed at comparable or higher resolution with ALMA. The majority of current IFU + AO samples lie at declinations accessible from the ELT (indeed, a majority were obtained with VLT/SINFONI). By the time MICADO will start observing, IFU + AO samples with suitably bright nearby stars will undoubtedly have grown substantially from new major observing campaigns with VLT/ERIS and the upgraded Keck/OSIRIS.

Consequently, *existing and future IFU+AO samples* observed with current 8-10m-class telescopes constitute an *ample and prime choice* of MICADO + SCAO targets to deepen our understanding of the physical processes driving galaxy evolution. One specific example is the SINS/zC-SINF AO sample of 35 $z \sim 1.5 - 2.5$ (Förster Schreiber et al. 2018) shown in Figure 1 below. Simulations performed as part of the MICADO Primary Science Case remain relevant for the SCAO case. We stress that the typical angular size subtended by $z > 1$ galaxies is a few arcsec at most, such that the effects of differential anisoplanatic angle are minimal for individual targets.

For these 35 galaxies, the parameters relevant to the adaptive optics performance are shown in Figure 2 (with colours denoting NGS vs LGS observations). For those observed with NGS, the typical guide star magnitude was $R \sim 15.3$ mag, at a typical off-axis distance of $\sim 20''$. They were observed at a typical zenith angle of $\sim 37\text{deg}$ due to the declination of the deep field. The resulting mean Strehl ratio was 17% in K-band. For MICADO, assuming a seeing of $0.7''$, the estimated adaptive optics performance for these same targets is shown in Figure 3. Typically one can expect K-band Strehl ratios in the range 10-30% for SCAO targets. This sample had 18 targets observable with NGS. For the larger samples that will become available in the coming 5 years, one can expect a rather larger number of potential SCAO sources suitable for studies of galaxy structure in the early universe.

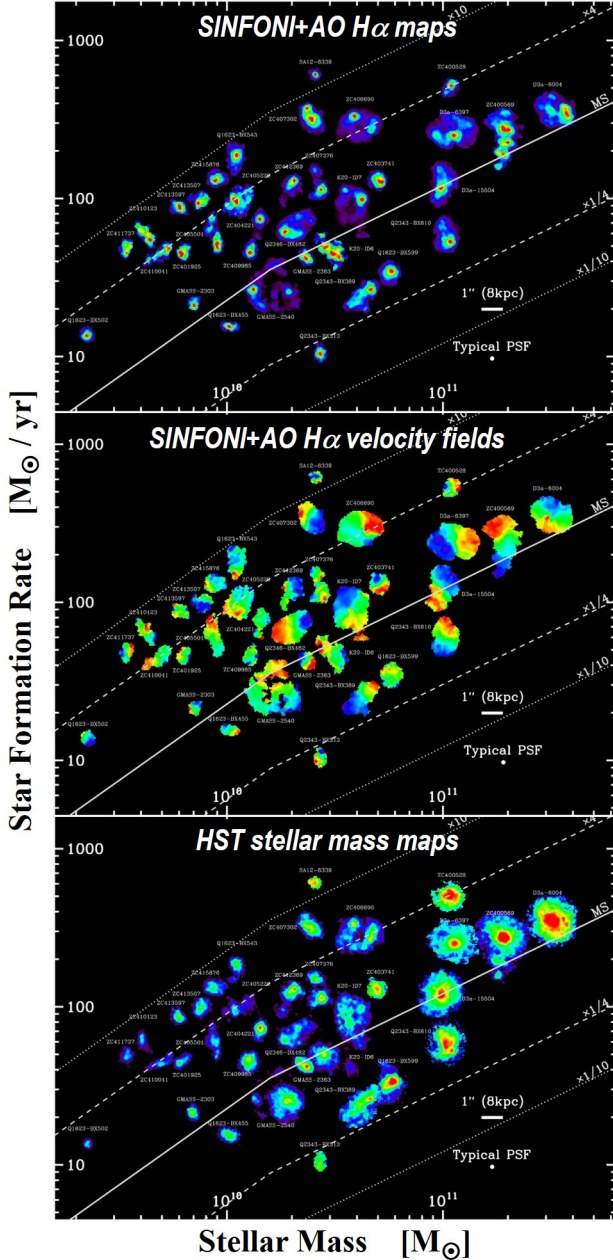


Figure 1: Example of a prime sample for MICADO + SCAO observations, from the SINS/zC-SINF AO survey of $z \sim 1.5 - 2.5$ star-forming galaxies with AO-assisted VLT/SINFONI. By necessity of the SINFONI+AO observations, all targets have a suitably bright nearby star. From top to bottom, the panels show an overview of their $H\alpha$ emission line maps and velocity fields, and of their stellar mass maps derived from HST (I)JH color maps (Förster Schreiber et al. 2018, ApJ, 238, 21). The galaxies are plotted at their position in the stellar mass vs. star formation rate. Among other goals, MICADO + SCAO observations will enable us to resolve the small-scale structure down to ~ 100 pc scales of the bright star-forming clumps and massive dense bulge-like components, whose nature cannot be elucidated at the ~ 1 kpc scale of current data but is fundamental to our understanding of the physical processes driving the growth of galactic disks and bulges at the peak epoch of galaxy formation. Collectively, IFU+AO samples amount to > 150 galaxies at $z > 1$, and many more are anticipated in the until MICADO starts observing.

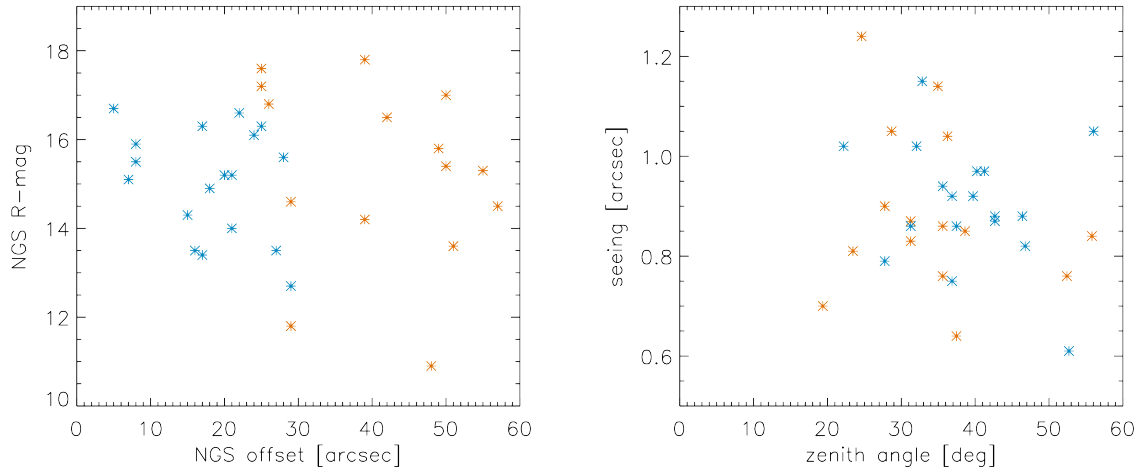


Figure 2: Parameters for the SINS/SINF-zC AO sample of 35 galaxies relevant for the adaptive optics performance. Points in blue were observed with NGS those in red were observed with LGS. All the blue points, and some of the red points would be possible with MICADO SCAO.

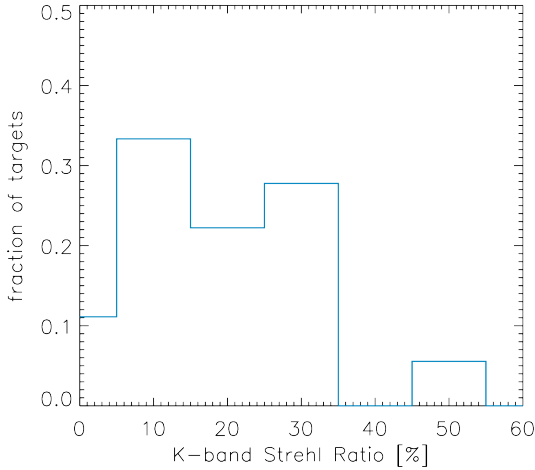


Figure 3: Predicted K-band Strehl ratios – typically in the range 10-30% – for SCAO observations with MICADO of the 18 sources in the SINS/SINFzC sample that were observed on the VLT with NGS.

Resolving the structure of star-forming galaxies at high redshifts is key to understand how star formation in galaxies proceeded at early cosmic times and test different mechanisms for galaxy growth, e.g. via galaxy mergers or cold flows. Combining high angular resolution instrumentation with the power of gravitational lensing allow us to investigate the morphology of such regions with unprecedented details, impractical in blank fields. In order to select possible targets for MICADO, we examined strongly lensed galaxies with spectroscopic confirmation in known galaxy cluster lenses that satisfies the SCAO requirements. Among the ≈ 15 cluster lenses we considered (most of them presented in Caminha et al. 2016, 2017a,b, 2019), we have identified a group of four galaxies at $z = 4.3$ that full fill the observational constraints. These four galaxies are close to a bright star with $mag_{AB}^H = 15.56$ that can be used as a natural guide star for MICADO/SCAO. We have used SimCADO (Leschinski et al. 2016) to simulate the near-infrared structure of these sources. The aim of the simulation is to verify if we can resolve clumpy star-forming regions in this system, focusing in the galaxy id ID3-b which has the highest lensing magnification (≈ 10) and observed magnitude ($mag_{AB}^H = 23.61$).

In Figure 1, we show the HST imaging of the four lensed objects indicated by green circles and the bright star in red. Even with the lensing magnification, the limited HST image resolution of 90 mas and 180 mas in the i_{814} and H_{160} filters, respectively, is not sufficient to resolve the morphology of these galaxies. Only with high-resolution Ks band observations, we will probe the optical-restframe continuum emission of this system and trace the morphology of star-forming regions in this object.

In the left panel of Figure 2, we show an idealized simulation of two sources with clumpy and smooth light distributions in the left and right panels, respectively. The original (input) images are based on the observed size and total flux of ID3-b and shown in the bottom row. In the top row, we show the two simulated images considering a two hours exposure on target. It is clear that with MICADO we can distinguish between a clumpy and smooth light distribution, which is not possible with HST, and also detect and possibly resolve some individual regions of star formation in this galaxy at $z = 4.3$.

In a second step, we performed a set of simulations in order to quantify the detection limits of size and magnitude of individual clumps. The clumps are parametrized by a steep Sersic profile with $n=10$ and the smooth light component has $n=4$. These values are chosen to be consistent with observations of high- z sources in lensing fields (see e.g. Vanzella et al. 2017), however robust measurements are (naturally) not available. In each simulation, we add to the smooth component one clumpy object with different values of size (R_{eff}) and magnitude. On the simulated images, we run the software SExtractor (Bertin & Arnouts 1996) in order to check if we can detect or not the small extra component. In the right panel of Figure 2, we show the grid of R_{eff} and magnitudes we used as input in the simulations. These values are corrected by the lensing magnification estimated by our lens model, that is ≈ 10 for ID3-b. In the right y-axis, we show the corresponding observed size in milliarcseconds (i.e. not corrected by the magnification effect), thus we can compare this quantity directly to the instrument final point-spread-function (psf) that is expected to be around 10mas in the Ks filter. In each point of the grid, we indicate if SExtractor detected or not the clumpy component. For values brighter than intrinsic $mag_{AB}^{Ks} = 29.5$ we can detect all clumps in the considered range of sizes, from 3pc to 600pc. On the other hand, fainter objects are easier to be detected

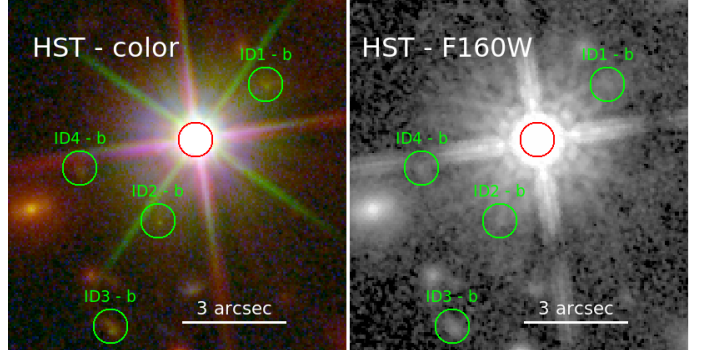


Figure 1: HST imaging of the $z \approx 4.3$ system gravitationally lensed. The blue circles indicate the position of the four background galaxies. The natural guide star is marked in red.

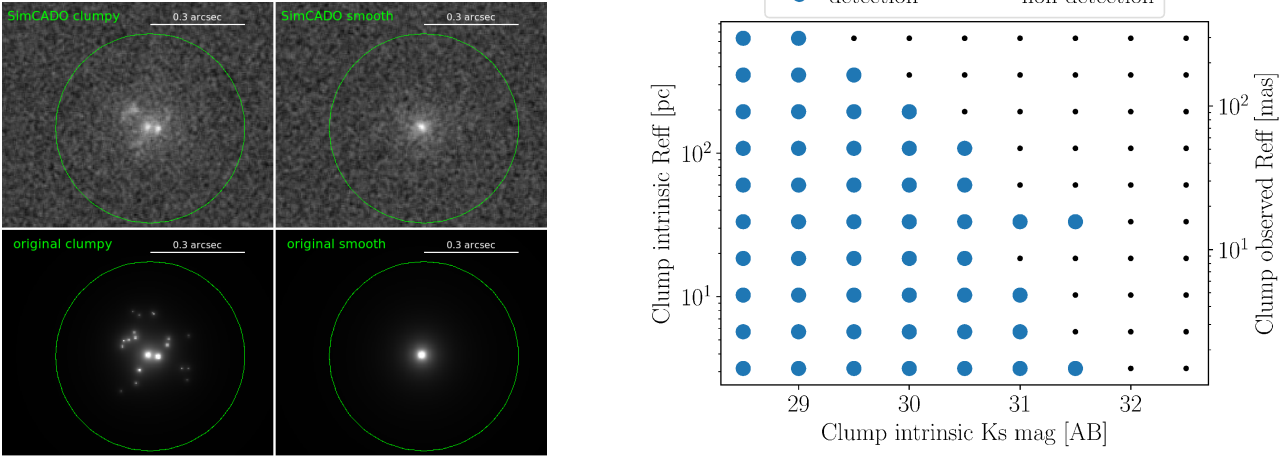


Figure 2: Left panel: simulation of two sources with clumpy and smooth light distributions performed with SimCADO. The original input images are shown in the bottom panels. Right panel: Detection limits of size and magnitude of individual clumps. Blue circles indicate a detection and small dots non-detections.

if they are more concentrated, i.e. with higher surface brightness. Moreover, detected objects with sizes of $\approx 50\text{pc}$ or larger have around 3 times the instrumental psf size, allowing unprecedented shape and light-profile measurements with MICADO. With MICADO we will be able to probe in detail the morphology of star-forming regions at cosmological distances and detect objects as tiny as star clusters.

The identification of such fortunate alignment of a spectroscopic confirmed high-redshift galaxy and a bright star is relatively challenging to find with the current cluster lensing surveys. However, thanks to the large areas covered by the EUCLID and LSST surveys, thousands of high- z massive/bright galaxies will be detected. From this total, around 1.8% will be suitable targets, i.e. located within 7 arcsec from a natural guide stars if we assume a star density of 1000 deg^{-2} . On the other hand, JWST will provide excellent complementary spectroscopic measurements of Balmer lines at redshifts higher than 3. The combination of high resolution imaging and spectroscopic in the optical rest-frame wavelength of $z = 4 - 6$ galaxies will shed light on the complex mechanism driving the star formation in the early stages of the Universe.

References

- Bertin, E. & Arnouts, S. 1996, A&AS, 117, 393
 Caminha, G. B., Grillo, C., Rosati, P., et al. 2016, A&A, 587, A80
 Caminha, G. B., Grillo, C., Rosati, P., et al. 2017a, A&A, 600, A90
 Caminha, G. B., Grillo, C., Rosati, P., et al. 2017b, A&A, 607, A93
 Caminha, G. B., Rosati, P., Grillo, C., et al. 2019, arXiv e-prints, arXiv:1903.05103
 Leschinski, K., Czoske, O., Köhler, R., et al. 2016, in Society of Photo-Optical Instrumentation Engineers (SPIE) Conference Series, Vol. 9911, Proc. SPIE, 991124
 Vanzella, E., Calura, F., Meneghetti, M., et al. 2017, MNRAS, 467, 4304

3.4 Exoplanets and planet formation

Coordinators: Pierre Baudoz/Obs. Paris

Contributors: A. Boccaletti, G. Chauvin, F. Snik, J. Birkby, J-M. Desert, E. Huby, Y. Clénet, D. Doelman

This science area always has been a pure SCAO case, and the original science case needs little clarification or addition. There are extensive targets, both exo-planets and proto-planetary disks that can be studied in exquisite detail on-axis with SCAO. Some updates and more careful simulations have been added here to the original science case presentation.

Contributions:

- Exo-planets and planet formation, by Baudoz et al.

Exoplanets and planet formation

Pierre Baudoz

The exciting science objectives presented below could easily take up to 20 nights per years during the SCAO-only mode of MICADO.

1. Direct detection/characterization of new exoplanets

a. Getting closer and fainter

Following the strategy that the chance of finding new exoplanets is actually higher within a system with already one planet detected, prime targets of interest of the high-contrast mode of MICADO will be young, nearby systems with either known exoplanets previously imaged in direct imaging (β Pic, Fomalhaut, HR8799, HD 95086, 51 Eri, GJ504, κ And b, HIP65426, PDS70, HIP107412, HR2562...) or systems suggesting the presence of planetary perturbers (disk vortex, gaps, asymmetries, exocometary activity...) but also blobs that could be linked to the presence of planets in formation (HD100546, HD169142, LkCa15...). Given the gain in angular separation and contrast achieved with MICADO, the goal will be to search for inner planets in those systems, but also separate the possible contributions between the planets and the disk. For the very close candidates with significant orbital motion, a dedicated monitoring strategy will be necessary to increase the chance of probability. The case of the young radial velocity planet Bpic c, a 10 M_{Jup} planet located at 2.7 au (Lagrange et al. 2019), has been simulated considering the MICADO detection limits and will be easily detected supporting the importance of accessing closer separation and the synergy with indirect techniques.

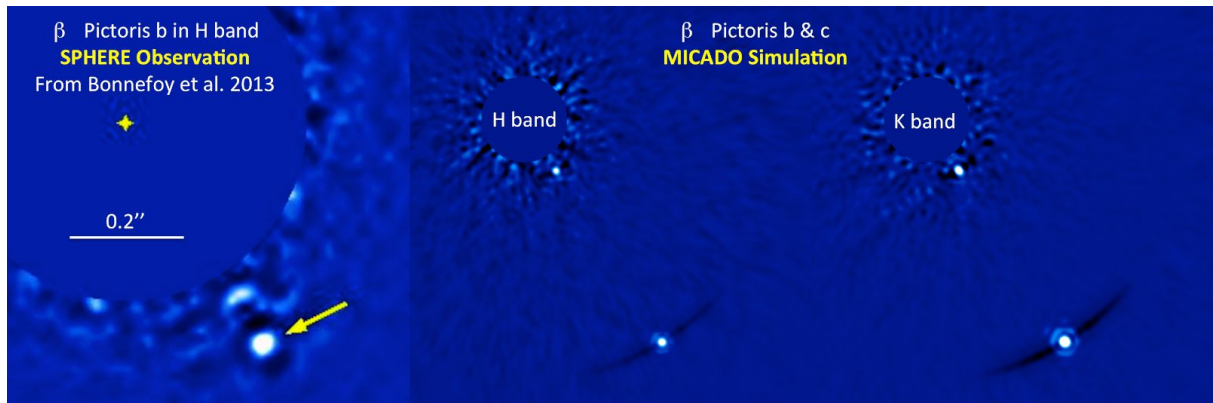


Figure 1: Comparison between SPHERE observations of Beta Pictoris b and simulated observation of Beta Pictoris b & c. Position and brightness of planet b is the same as the one given in Bonnefoy et al. 2013. Planet c is placed at a physical distance of 2 AU (0.1'') assuming a mass of 10 M_J. The 3 images show the same field of view.

b. Building the bridge with indirect methods

The overlap between radial velocity (soon astrometry with Gaia) and direct imaging is nowadays marginal (Lannier et al. 2017; Lagrange et al. 2018), and a prime scientific goal of the high contrast mode of MICADO will be to bridge that gap to exploit the synergies between these techniques in order to further explore the physical properties of young Jovian

planets, which remain highly uncertain at young ages. Direct imaging gives access to the photometry, the luminosity and the spectral energy distribution of exoplanets, but not directly the mass.

In this context, we have to rely on evolutionary model predictions that are not well calibrated at young ages. In addition to the system age uncertainty, the predictions highly depend on the formation mechanisms and the gas-accretion phase that will form the exoplanetary atmosphere. The way the accretion shock will behave (sub or super-critical) on the surface of the young accreting proto-planets during the phase of gas runaway accretion will drive the initial entropy or internal energy, hence its initial physical properties (luminosity, effective temperature, surface gravity and radius) and their evolution with time. These different physical states are described by the so-called hot-start (sub-critical shock), cold-start (super-critical shock), and warm-start (intermediate case) models. They predict luminosities that are spread over several orders of magnitudes for young, massive giant planets. Getting closer and deeper to access physical separations down to 1 au (see Figure 3) will be therefore a prime goal to explore the physics of young Jupiters by imaging and characterizing the young giant planets that will be discovered with Gaia in the context of the Data Release 4 (2022) and in the course of radial velocity campaigns targeting young, nearby stars with HARPS/3.6m, NIRPS/3.6m, CFHT/Spirou, ESPRESSO at VLT.

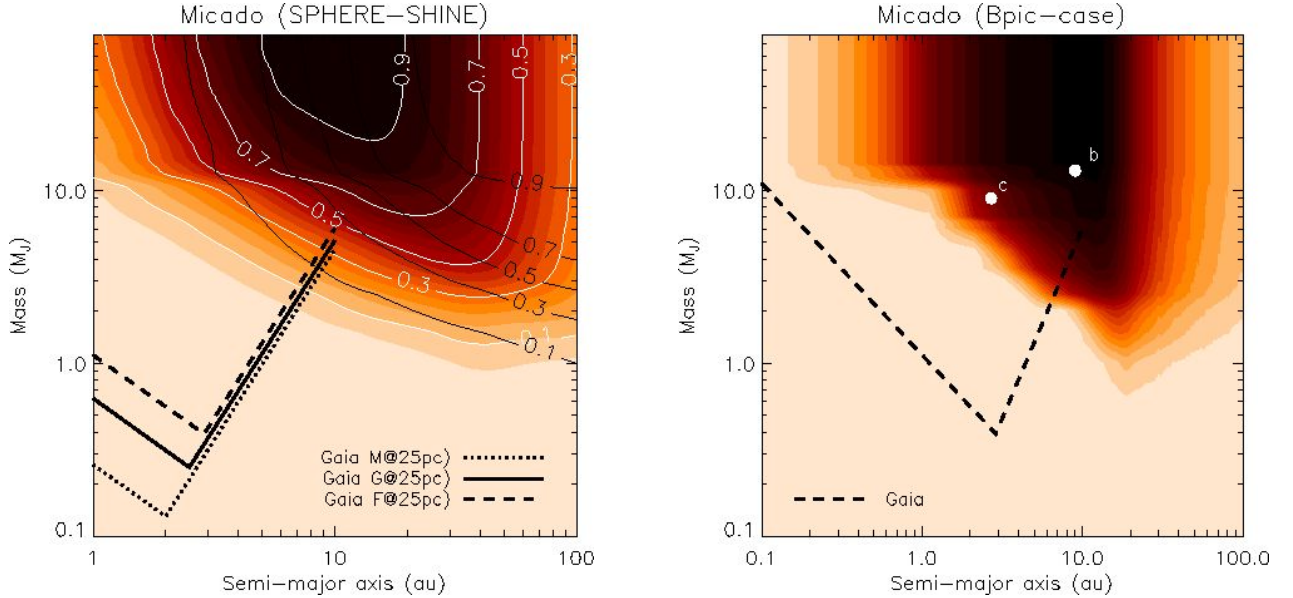


Figure 2: Left, detection probability map of MICADO for a typical mini-survey of young (< 100 Myr), nearby (< 100pc) stars to illustrate the 1- 30 au window opened by MICADO compared with SPHERE (SHINE survey in black solid line) and with GAIA detection limits. Right, simulation for the specific case of Bpic with the MICADO performances reported in terms of detection probability with the GAIA detection limits and the semi-major axis and mass position of Bpic b and potential c (Lagrange et al. 2019b).

2. Characterization of known and future systems

a. Orbital properties and system architectures

Among the known imaged planets which are mostly located at wide orbits (≥ 10 au), orbital motion has been resolved for a few cases. It actually concerns the case of β Pic b, Fomalhaut b, HR8799 bcde, HD 95086 b, 51 Eri b, GJ504 b, κ And b, HIP65426 b and more recently PDS70 b and c. Accurate astrometric monitoring allows to study, in addition to the planet's orbit, the global system architecture including the planet-planet and planet-disk interactions and the system stability. The orbital monitoring of β Pic b enabled for instance to witness the planet's revolution around its star and to confirm its role in the formation of the disk inner warp and in the exocometary activity witnesses for years. For HR8799, the long-term monitoring actually enabled to test the dynamical stability of the whole system. The derived orbital properties of each planet showed that all planets evolve on coplanar and circular orbits except HR 8799 d which seems to be misaligned by 15–20 degrees and significantly more eccentric (~0.3). This configuration likely suggests remaining imprints of dynamical interactions between the planets in this system. The system seems however stable as indicated by the existence of several mean motion resonances. Using the SCAO mode of MICADO at ELT, we will be able to characterize the orbital properties of a dozen of exoplanets discovered in direct imaging, and even more considering the upcoming detection. The coronagraphic imaging mode can obtain accurate astrometric measurements at K band. Our prime goals will be: i/ to refine the orbital properties of these known systems, ii/ study the dynamical stability of the system if additional planets or disks are present, iii/ explore the possibility to derive dynamical mass measurements of such objects in order to test their evolutionary models, which are widely used, although poorly calibrated, to infer the mass of imaged companions using luminosity measurements and age constraints.

b. Characterization of exoplanet atmosphere (species, time evolution, etc)

Nowadays, most imaged exoplanets are young, early-L to early-T type massive planets with red, dusty atmosphere. To reproduce their anomalous observables, enhanced cloudy atmospheres are invoked in which lower surface gravity alters the vertical mixing which then leads to high altitude clouds depending one physical conditions (e.g. thinner or thicker aggregation; Faherty et al. 2016, ApJS, 225, 10). Here, atmosphere models play a key role to test our understanding of the atmospheric physics of exoplanets involving at least hydrodynamics, radiative+convective energy transport and gas-phase chemistry, and sophisticated models of clouds of different compositions (silicates, fosterite, sulfites...). Additional processes such as disequilibrium chemistry induced by advection of hot CO gas from deeper and hotter layers or thermo-chemical instability might help to explain the peculiar near-infrared colors of young L dwarfs as well as the warming up of the deep atmosphere along the L/T transition (Tremblin et al. 2015, 804, L17). However, today's low-resolution spectra of imaged exoplanets covering a small portion of the planet spectral energy distribution do not allow to explore and remove the atmospheric model degeneracies. Using the SCAO Long-Slit Spectroscopic mode of MICADO at ELT, we could characterize more than 20 planetary-mass exoplanets discovered in direct imaging to further explore the physics of exoplanetary atmospheres. With high-quality medium/high-resolution ($R = 20000$) spectra over the near-infrared spectral range (0.95 – 2.4 μ m), our prime goals will be: i/ to

empirically characterize the spectral properties of these exoplanets and brown dwarf companions through their atomic and molecular lines (spectral indexes and equivalent widths) and identify any signs of accretion, ii/ to determine the effective temperatures, surface gravities, metallicities, chemical abundances and cloud properties with the latest generation of self-consistent and parametric models but test at the same time the development of new cloud models and treatment of non-equilibrium processes and thermo-chemical instability, iii/ finally, to explore the radial and rotational velocities of each companion to explore their formation and dynamical evolution, and potentially the presence of zonal winds, accretion processes, and even surface molecular mapping through time monitoring observations.

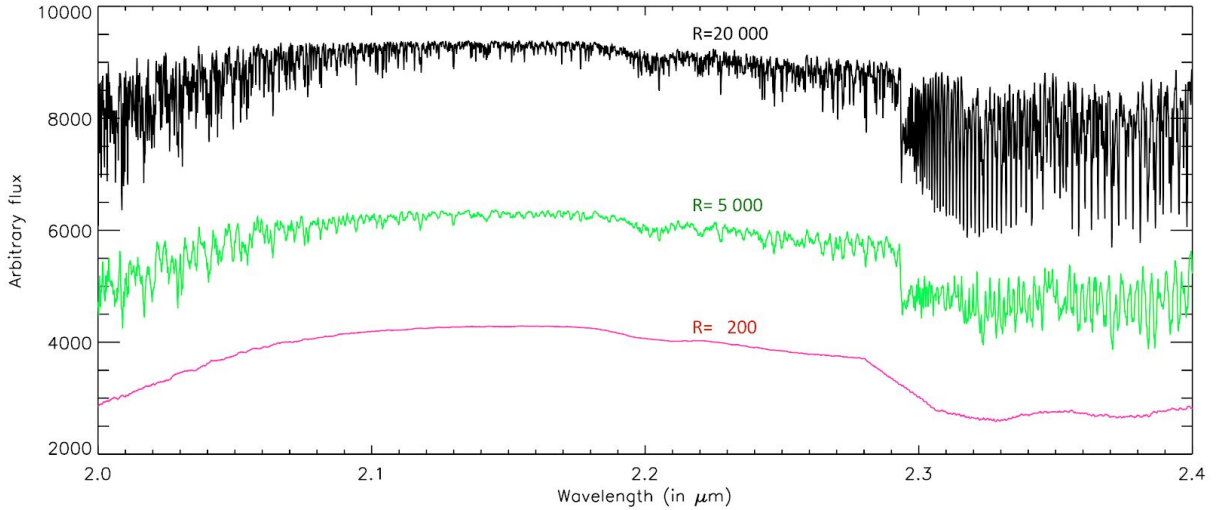


Figure 3: Theoretical spectrum for a planet with the following characteristics: $T_{eff}=1100\text{ K}$, $\log(g)=4.0$, $C/O=0.44$ (Corresponding to the best model for HR8799e using ExoREM model, Charnay et al. 2019). The spectrum shows part of the K band at MICADO resolution and for smaller spectral resolutions. The high resolution spectrum is rich enough to allow molecular mapping retrieval (Hoeijmakers et al. 2018).

3. Understanding planet formation and planet/disks interaction

Understanding planetary systems formation and evolution is one of the main quest in modern astrophysics. One way to address this paramount question requires imaging these systems directly at various stages of their evolution, from the formation of disks around embedded protostars to more tenuous environment in which planets are warm enough to be detected by their emission light. Several instruments covering a very broad spectral range from the optical to the millimeter can tackle this question. However, the spatial resolution is here of great importance to resolve the scale of planetary systems at the distances where young star associations reside. ALMA, has been extremely efficient to spatially resolve planet-forming disks (Andrews et al. 2018). Interestingly, the presence of fine structures is ubiquitous in these systems either in the form of spirals or cavity or gaps (Huang et al. 2018a,b, Dullemond et al. 2018). All these characteristics are supposedly resulting from the

interaction of massive bodies with the gas and dust present around young stars, therefore leading to the indirect identification of planetary objects (Zhang et al. 2018, Dong et al. 2015, Dipierro et al. 2015, Pinte et al. 2019) or even to direct proofs of ongoing planetary formation. However, other origins are also proposed which do not involve a massive body as a perturber, but some other type of instabilities, either gravitational instability (Boss 2000), which can lead also to planet formation eventually, or gas-dust interactions (Lyra & Kuchner 2013).

Later in the evolutionary sequence, when the first generation gas component has dissipated, planetesimals and planets are formed. The remaining dust content is constantly produced by collisions leading to the formation of debris disks (some can contain second generation gas released by collisions). In this phase, the material is arranged in planetesimals belts presumably shepherded by planets. More complex planet-disk interactions can lead to variations around this ring-like geometry (Lee and Chiang 2016). It is interesting to note that all giant planets imaged directly (Marois et al. 2008, Lagrange et al. 2009, 2018, Macintosh et al. 2015, Chauvin et al. 2017, Kepler et al. 2017) are actually found in systems where the presence of circumstellar disks is attested. With the current high contrast instruments like SPHERE and GPI many structures are reported both in protoplanetary and debris disks but because of the distance of these targets the observed patterns are located far from the snow line (except a few favorable cases), but planet formation should be more efficient at the snow line. While it is known that planets can generate patterns at much larger separations (like the warp in the beta Pic disk), we are still blind to the most important region, the snow line. Structures can be static or in rotation around the star depending on their origin. A dust clump will have different dynamic whether it is produced by massive collisions or from mean motion resonances. Spirals are density waves and rotate with the planet so can be super or sub Keplerian. Constraining planet formation form direct imaging of disks requires 1) to identify and resolve the fine structures resulting from planet/disk interactions and disentangle from those due to other processes, 2) to map the spatial distribution of the dust for various grain sizes and 3) to explore the variability in the time domain of all potential structures.

c. Exploring detailed structures and inner regions of disks

MICADO has the ability to provide access to the inner region of proto-planetary and debris disks by increasing the angular resolution compared to SPHERE (about a factor of 4). We will be able to probe the inner region (\sim 5-10 au) of many more systems located at 100-150 pc in star forming regions, to characterize the morphology of structures triggered by planet formation or planet evolution. The known structures in protoplanetary and debris disks will also be much more detailed for the same reason, leading to a more accurate characterization (Fig. 4).

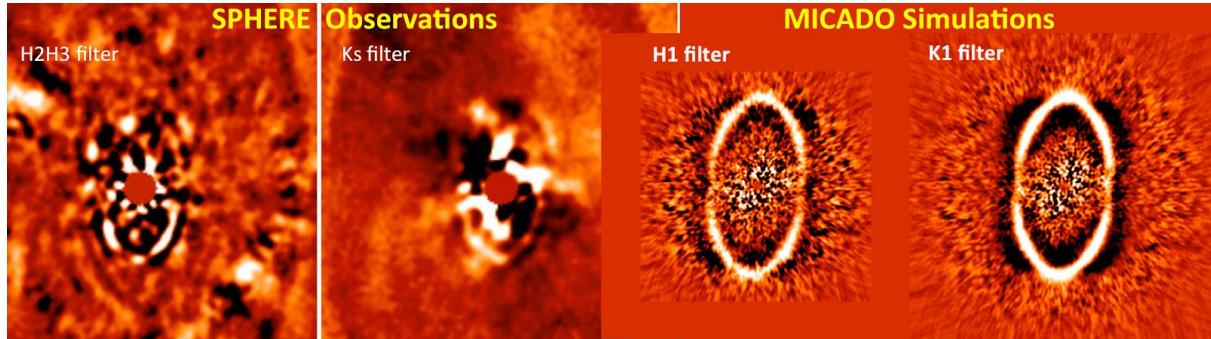


Figure 4: Example of the improvement in sensitivity and angular resolution of MICADO with respect to SPHERE. SPHERE observations are made on HD141169 (Perrot et al. 2016). MICADO simulations use the best disk model found from this observation and use it as an input to the MICADO simulation. The disk is simulated with GRaTer (Augereau et al. 1999).

d. Disk morphology in scattered light compared to sub-millimeter regime

MICADO will also provide a better sensitivity to fainter stars (gain of 3 mag) compared to SPHERE. This will open up access to a large population of systems observed with ALMA and not accessible to SPHERE. The connection between the spatial distribution of the gas, the millimeter-size grains and the micrometer-size grains is key to understand how the dust grows and evolves. Some differences are already observed in systems for which the targets are bright enough for SPHERE. Extending the comparative analysis to a larger sample of stars will allow to better constrain the planetary system evolution. Mid-IR is also necessary to complete the global picture and identify different type of grains. Such images and data will be provided by JWST (MIRI in particular) but with much lower angular resolution with respect to MICADO. It will take METIS to perform such comparison at similar spatial scales. In this respect MICADO has strong synergies with other current and future facilities.

e. The dynamics in the disks

AU Mic hosts a debris disk conveniently close (~ 10 pc), and extensively observed with SPHERE and STIS/HST. Dust structures were observed (Boccaletti et al. 2015) in the form of « arches » located between ~ 1 and $5''$, and propagating outwards, with large projected velocities (4-12 km/s). The velocity of structures is increasing with stellocentric distances but the edge-on orientation of the system complicates the interpretation. Between 2014 and 2018, a program combining SPHERE monitoring together with archival HST data has allowed to identify new structures emerging from the central part of the image (angularly close to the star) or converging towards the star (Boccaletti et al. 2018). The most likely hypothesis to explain such a behaviour of dust particles involves the stellar wind from this low mass but very active M star, and a site of dust production either located at a fixed position in the system (leftover from massive collision) or in keplerian orbit round the star (a planet).

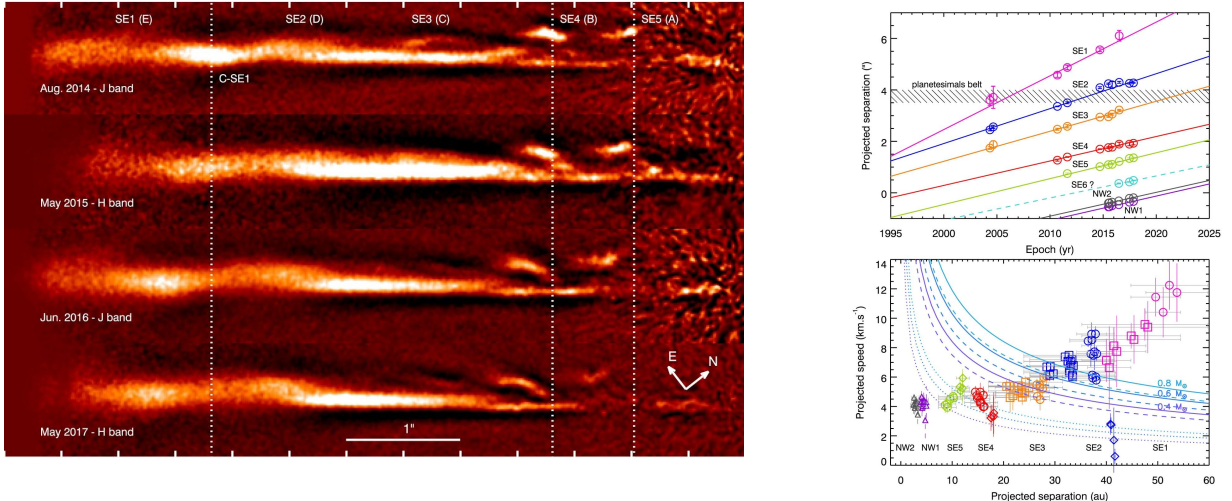


Fig. 5 : Left: southeast side of the AU Mic disk at 4 epochs as observed with SPHERE (2014 to 2017). **Right:** Projected separations of the 5 structures as a function of time (top) and corresponding projected speeds (bottom) evidencing non-keplerian velocity.

A dynamical model taking into account the trajectories of dust particles shows that the grains are necessarily very small (sub-micron) and the mass loss very large (tens to hundreds of solar mass loss). The site of dust production would be also relatively distant from the star (10-30 au). The structures themselves are a few au wide and their exact shape changes with time on a very short timescale (months), which should be related to the magnetic field topology. AU Mic might be the first and unique example of a directly observed interaction between stellar activity and another body (dust reservoir or planet) at large physical separation. The improved angular resolution of MICADO (equivalent to au at the AU Mic distance) compared to SPHERE and HST will be key to understand the on-going interaction in this system. MICADO observations in the H band (same as SPHERE filters) will provide the ability : 1/ to detect closer in ($<1''$) structures possibly emerging from the central part of the system (or disappearing), 2/ to extend the monitoring on a long timescale, and 3/ to measure the detailed shape of the structures. Items 1 and 2 will allow to put strong constraints on the dynamical behaviour, to solve the 3-D geometry of the system, and to solve the origin of these structures (dust reservoir, or planets). Item 3 will allow to derive constraints on the stellar magnetic field and how it interacts with the dust particles. Finally, MICADO will allow to extend the search of similar behaviour around other, more distant, young M stars.

3.5 The Solar System

Coordinators: Frédéric Merlin/Obs. Paris, Benoit Carry/Obs. Côte d'Azur

This scientific area was always predominantly a SCAO case, as many solar system objects are intrinsically bright enough (and small enough) and the SCAO system is flexible enough to be able to use them as a guide star. All Solar System objects move rapidly across the sky and so it is possible to wait to observe them for the moment when they pass by a bright background star that can be used as a guide star. This last mode requires careful planning and execution, but it is already in use with current telescopes.

Contributions:

- The MICADO/SCAO Solar System science case, by F. Merlin & B. Carry

Observation with ELT-MICADO using SCAO only. The Solar System Science Case – Detailed Document

I present the different science cases as well as several simulations done using SimCADO and SpecCADO allowing us to indicate the requested exposure times for each target or family of targets.

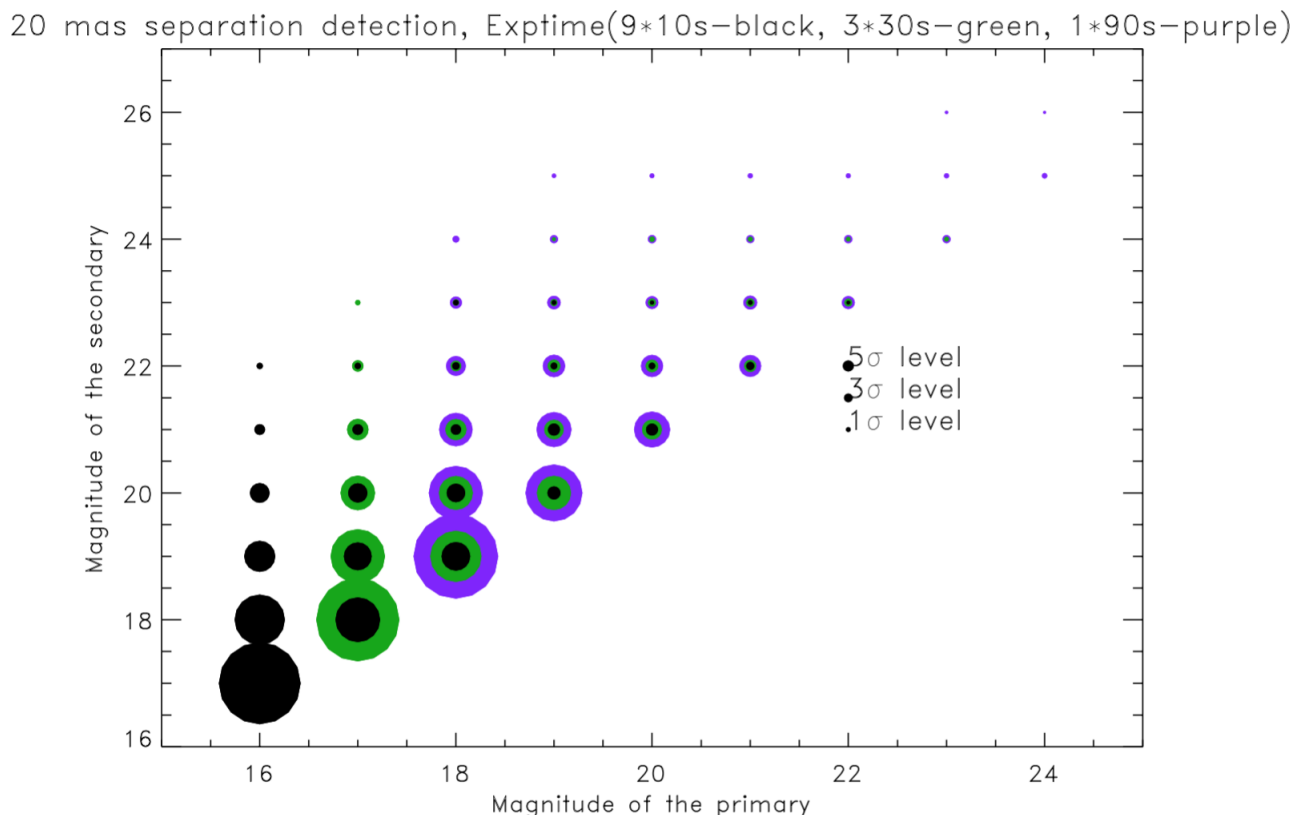
SCAO MODE 1 : NGS = MOVING TARGET

SCAO MODE 2 : NGS = NEARBY STATIC STAR (<20" FROM OUR MOVING TARGET)

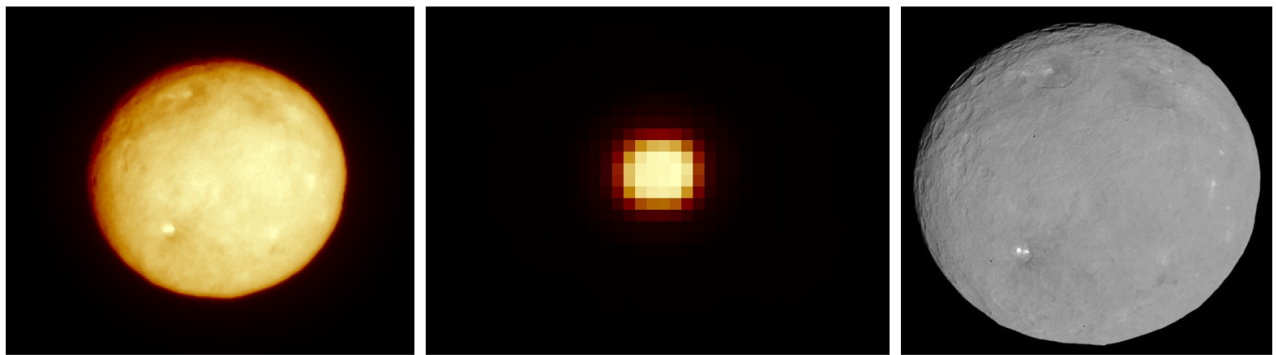
SCAO MODE 3 : NGS = NEARBY MOVING SATELLITE (FOR OTHER DIMMER MOVING SATELLITES OR SURFACE OF THE MOVING GIANT PLANETS)

A) Physical properties of the small bodies populations. Retrieve the albedo, the shape, the bulk density. USING SCAO MODE 1 & 2 – IMAGING

The advent of large telescopes equipped with adaptive-optics will enable direct imaging of the asteroids and their possible satellites. The shape and colors of the targets will give us the possibility to retrieve the shape, albedo and a first mass estimation of most of the different families existing in the asteroid main belt. From the study of the companion orbit, the mass can be obtained, and once combined with the volume estimate (see above), this yields the bulk density of the minor planet, a key parameter to infer its composition and internal structure (e.g. Merline et al. 2002) and the mass and density distribution for these different objects.



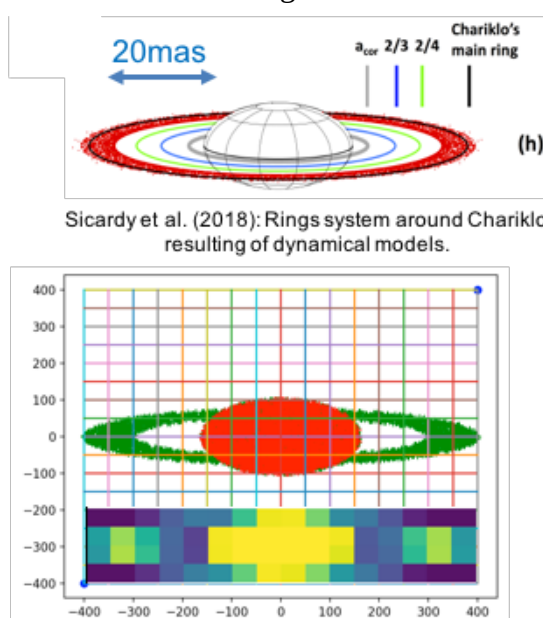
Summary of simulation done with SimCADO for multiplicity detection as a function of the primary and secondary magnitude for a 16mas separation. Depending of the target distance, individual exposure time have to be short enough to avoid smearing due to the rotation of the secondary around the primary. For a 20 mas separation, this means that secondary found is very close to its primary for asteroids and more farther for Trojans and TNOs, allowing us to increase the individual exposure time from 10 to 90s in the three different cases. Results obtained for a total exposure time of 90s, could be increased to several minutes, keeping the same individual exposure time (done considering NGS=target!).



Simulation to reproduce acquisition of Ceres (magnitude 7) and smaller asteroid (scaled to magnitude 9-10) obtained in the H band from image obtained with the DAWN spacecraft.

B) Rings, formation and stability. The case of the Centaurs Chariklo and Chiron, and the TNO Haumea. USING SCAO MODE 2 – IMAGING

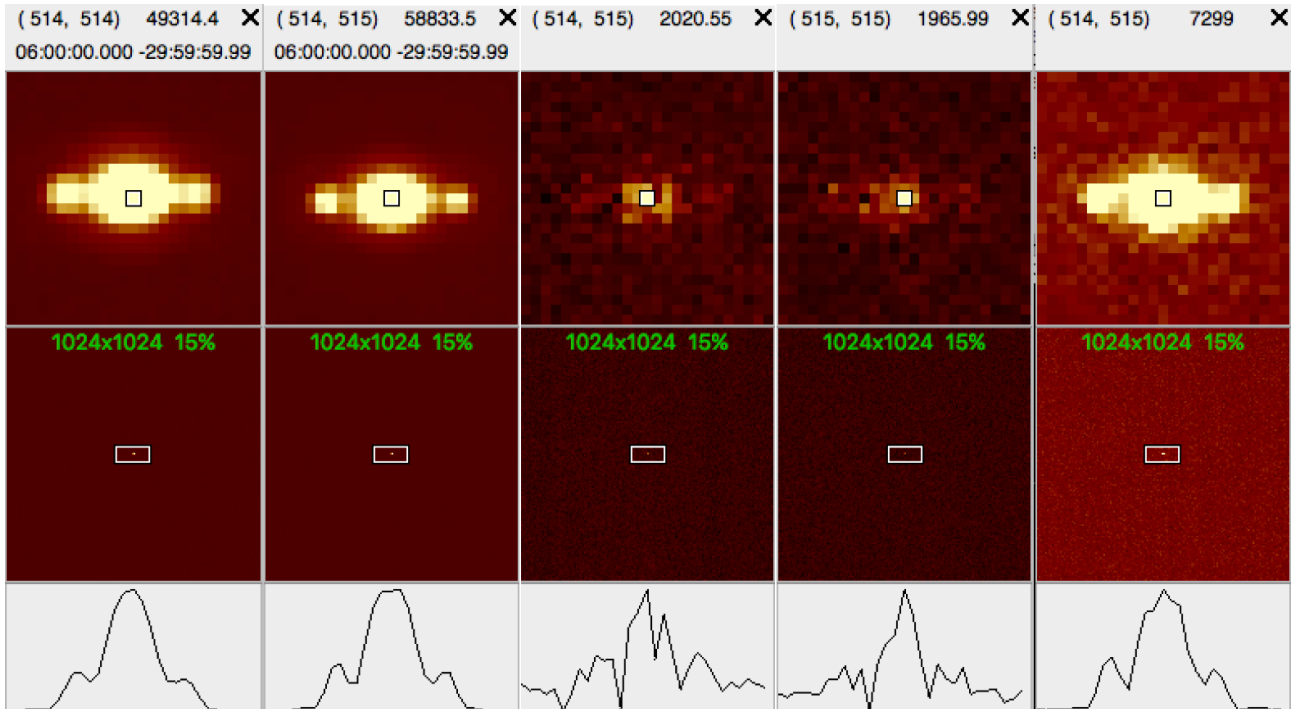
Dense and narrow rings have been discovered recently around the small Centaur Chariklo and the dwarf planet Haumea, while being suspected around the Centaur Chiron (see Sicardy et al. 2018). They are the first rings observed in the Solar System elsewhere than around giant planets. Contrarily to the latters, gravitational fields of small bodies may exhibit large non-axisymmetric terms that create strong resonances between the spin of the object and the mean motion of rings particles. Since a part of the rings only have been detected from stellar occultations, direct imaging of the rings is highly requested to have a complete view of them. For this purpose, high spatial resolution imaging provided by MICADO will be crucial. In addition to the determination and distribution of the matter in the rings, different models suggest that the inner part of the disk may be deposited on the equator of the body forming a ridge akin to that of the Saturnian satellite Iapetus, requesting multi-color analyses of both surface and rings. On the left: Simulation of the flux distribution of the light incoming in MICADO for a plate scale of 0,004" assuming similar orientation of the object and its main ring at the date of the first lights compared to that defined during the previous stellar occultation. It is highly probable than the ring aperture will be greater, allowing a better view of the whole main ring.



Simulation (this work). Monte Carlo simulation to generate the profile of Chariklo (in km) and flux (converted in magnitude) received by each pixel as seen by ELT/MICADO ignoring the real PSF at this step.

For these reasons, observations should be done using both broad and narrow band filters. The best broad band filter will be the J one, allowing us to maximize the number of photons, the magnitude of the objects are usually maximum in J band, in a spectral range where almost no absorption feature is expected. It is well suited to investigate the global shape of both 1) the object and 2) its main ring without suffering of possible chemical heterogeneity. It will also allows us to observe the system with the best spatial resolution provided by the instrument in the near infrared. Beyond the shape analysis, a first chemical composition analysis will be possible using narrow band filters. We mainly expect presence of H₂O and possibly CH₃OH ices on the surface of the objects and possible H₂O in the particles of the main rings. Good candidates to investigate this chemical components will be the H2O_204 and CH4_227 filters, probing the deepest H₂O and CH₃OH bands in the near infrared, respectively.

For simulation of the Chariklo system (almost comparable with what we can do with Haumea and Chiron, which are both brighter by 0.5 to 1.5 magnitudes), we have to take into account the need of close NGS during *appulse* events (i.e: when the object, along its path on the sky, passes nearby a bright enough star to be used as NGS). The occurrence of such phenomenon is quite rare (1 or 2 times a year usually, for a given object) but we provide the observational requirements for different cases (assuming different angular separations between the NGS and the target). At the time of first lights of MICADO, we can expect more detections of rings around Centaurs and TNOs, increasing the number of potential observable events. Such *appulse* occurs on a 3-5h temporal window per event for the Centaurs and at least the double for TNOs, which move slower on the sky.



*Simulation of the Chariklo system using AnisoCADO and SimCADO with EsoMedian atmospheric conditions. From left to right (for a total exposure time of 12*5 minutes) : image obtained in H₂O_204 filter, CH4_227 filter, difference of both images themselves compared between images obtained without and with 10% of H₂O ice with target-NGS distance set at 5'', the same with target-NGS distance set at 15'', and the same with 50% H₂O ice with target-NGS distance set at 5''. The last three composite-images inform us on the H₂O content level and its possible spatial distribution on the surface and in the ring. Need additional PSF images for reconstruction and photometrical calibrations.*

Distance to NGS\Filter	J (Co/Cn/Ha)	H ₂ O_204 (Co/Cn/Ha)	CH4_227 (Co/Cn/Ha)
5''	10 / 7 / 2	60 / 40 / 5	60 / 40 / 5
15''	15 / 10 / 3	75 / 50 / 6	75 / 50 / 6

Indicative requested exposure times (in minutes) depending on the filter for detection of the rings (J band) or chemical composition analysis of Chariklo (Co), and extrapolated for Chiron (Cn) and Haumea (Ha) systems. We assume 10% H₂O content for Centaurs and 50% content for Haumea. Clear detection of ices is achieved comparing images obtained in both H₂O_204 and CH4_227 filters, in addition to the context image obtained in the J band.

Magnitude of the target	J = 16	J = 17.5	J = 19
5"	15 min. / seq	80 min. / seq	300 min. / seq
15"	20 min. / seq	110 min. / seq.	400 min. / seq

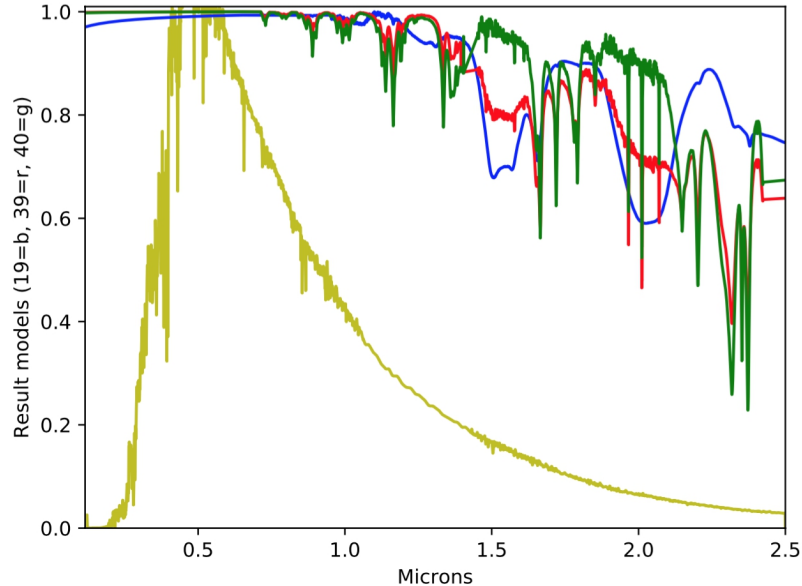
Total requested time on target for a complete sequence (i.e: complete acquisition of several colors following J, H₂O_204, J, CH₄_227, and J acquisitions) for a morphological and chemical investigation of the ring systems as a function of the magnitude, following the previous simulations using three different filters. Need additional observations to retrieve the PSF and common photometrical calibrations. The total requested times are usually compatible with the whole duration of the required appulse events.

C) Temporal evolution induced by seasonal sublimation/condensation processes. The cases of Titan, Triton and Pluto. USING SCAO MODE 1, IMAGING + SPECTROSCOPY

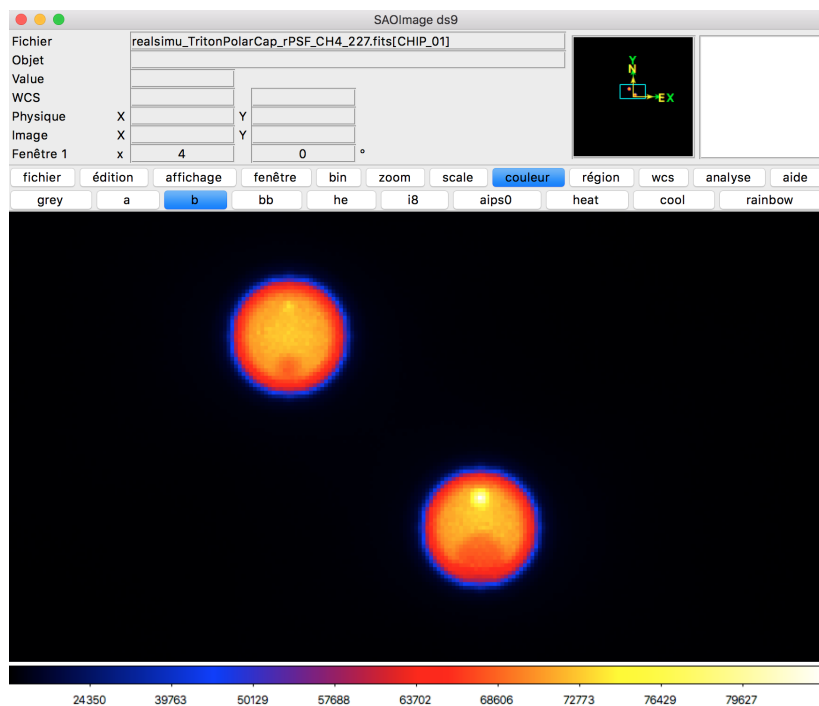
Titan, Triton and Pluto are mid-class diameter distant bodies, all three covered by large amounts of ices and surrounded by an atmosphere in interaction with the surface. Titan has a dense (almost 1-bar) atmosphere, mainly composed of methane, while Triton and Pluto have a thin atmosphere (of the order of a few micro-bars) mainly composed of Nitrogen. For Titan, imaging observation from ground-base could provide continuous monitoring of the different atmospheric structures and evolution mainly driven by the seasonal variation reaching the methane windows occurring in the near infrared range. Lellouch et al. 2014 showed from Cassini/CIRS observations that the methane abundance was not homogeneously distributed horizontally in the deep stratosphere with local abundance maxima observed near 30° latitude and at both poles. As the chemical lifetime of methane is about 10 million years, it was supposed to be well mixed in the entire atmosphere. The spatial resolution of MICADO will allow us to investigate these spatial variations as well as their potential seasonal variations in order to understand origin of this local enrichments. For Pluto and Triton, the thin atmosphere does not hamper the direct observation of the surface and imaging could provide evidence of the expected spatial and temporal surface variations also driven by the sublimation-condensation processes (Grundy et al. 2010). If these objects have been observed during close up events, thanks to the Voyager, Cassini-Huygens and New-Horizon NASA missions, the capabilities of the onboard instruments were time-constrained (due to the very short duration of their surveys), and their high spatial resolution abilities only linked to low spectral resolution analyses, with the extreme case of the lack of direct chemical identification for Triton. For these reasons, additional observations of these objects are mandatory to explore the surface variation (state on the latitudinal structures of Triton and extension of its south polar cap for instance, see Bertrand et al. 2017) as well as the chemical composition of their surface and atmosphere (constrain the location and nature of the expected irradiation-produced materials, see Merlin et al. 2018, for instance). In this topic, we identified different cases for imaging and spectroscopic investigations. We concentrate our simulation efforts on Triton but we notify that most of the technical parameters (target=NGS, requested filters, frequency of the survey, requested spectral resolution and requested amount of nights devoted for each object) and science outcomes (chemical nature and distribution, temporal evolution and dynamical atmospheric structures) are quite equivalent.

Imaging will be done, first, using typical narrow band filters, well designed to identify icy structures on the surface of these objects. The best filters for this topic are the CH₄_227 and H₂O_204 which will allow us to disentangle the chemical-components areas from the known bulk composition (see the following figure showing the mean spectrum of Triton with the expected chemical end members composed of pure H₂O or only of the N₂-CH₄ matrix). From our simulations, we assume to be able to spot, at 3 sigma levels, the smallest detectable H₂O patches in approximately 10 minutes (if pure, see the results of the simulations). If patches are even smaller than the spatial resolution of a pixel or if H₂O is not completely pure, we have to increase the exposure time by (1/f)², where f is the fraction of pure H₂O into the pixel element or the concentration variation of H₂O compared to the bulk composition. From a conservative point of view (assuming f=0.25), we need 2h30 on target for

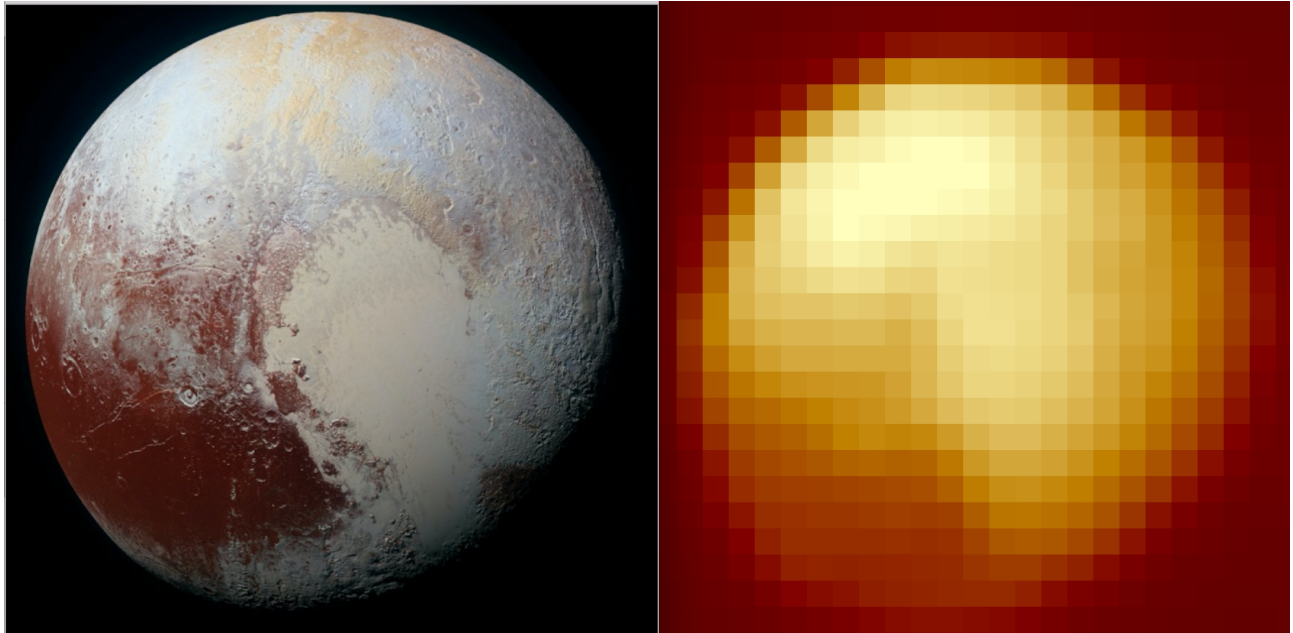
each side of the object. 5 different acquisitions obtained during 5 consecutive (or any different nights, if well sampled in agreement with the rotation period of each target) could allow a nearly global mapping of the surface of Triton with a good sampling. We could guess that a total of 12h30 on the target (well distributed over 5 nights) should guaranty to map the extension of the polar cap and point any large areas enriched in CH₄ or H₂O.



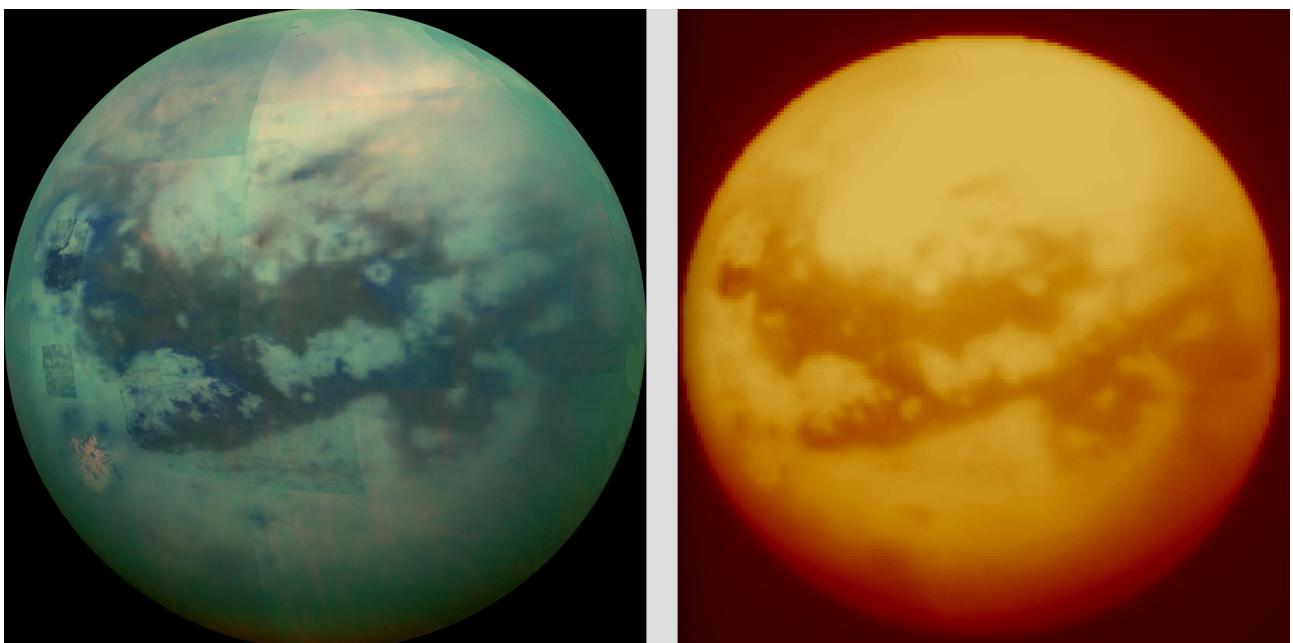
Normalized Spectra of the sun (in yellow), to be convoluted with the normalized reflectance spectrum of Triton (in red, obtained using SINFONI in the H and K spectral ranges and extrapolated in the visible and J spectral ranges using spectral-modeling), with that of pure H₂O ice (in blue) and that of N₂-CH₄ ice (in green) as derived from laboratory measurements and spectral-modeling.



Simulations using SIMCADO with different extensions of a possible H₂O-area (simulated bright spot located in the northern hemisphere) and of the expected CH₄-N₂ enriched south polar cap (slightly dark) assuming the smallest and largest expected extension (on the upper left and lower right, respectively). Filter: CH4_227 with plate scale of 0.004''. NGS=Target. Need additional PSF images for reconstruction and photometrical calibrations.

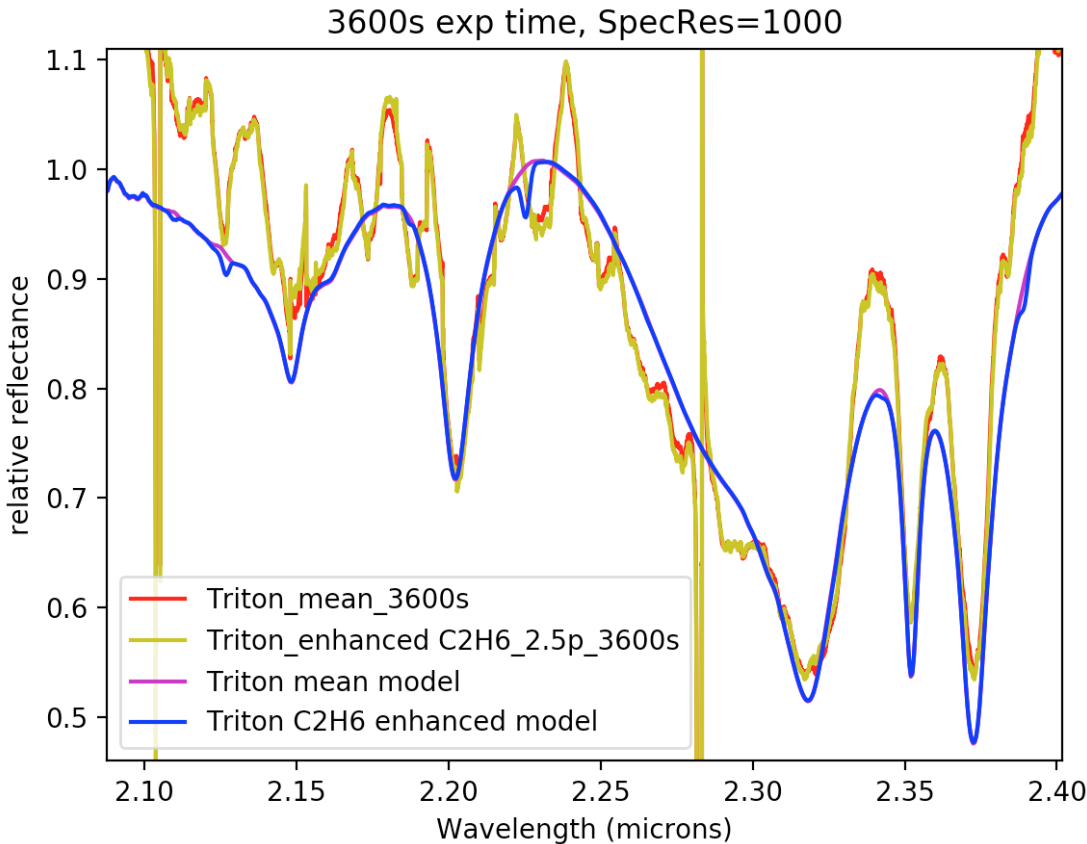


Simulation of the surface of Pluto as seen by ELT/MICADO performed with SimCADO in the H band, using the composite image of Pluto obtained by the MVIC instrument onboard the New-Horizon spacecraft.



Simulation of the surface of Titan as seen by ELT/MICADO performed with SimCADO in the K band, using the composite image of Titan obtained by the VIMS instrument onboard the Cassini spacecraft.

Based on these maps, spectral investigation will be held on the surface of Triton, as well as for Titan and Pluto for which spectral data at high spectral and spatial resolutions are more required than direct imaging due to data retrieved by the Cassini-Huygens and New-Horizon space missions. The strongest constraints on the chemical and physical properties of these objects will be obtained using the H+K grism using the longest slit in order to properly eliminate the sky contribution and observation of a nearby solar analog right after the acquisition of the target is also mandatory to remove the specular light and retrieve the reflectance spectra of the objects. This will allow us to answer the still open questions on the presence and properties of the hydrocarbons species present on the sub-surface of these objects, and constrain the temperature of several ices (see Merlin et al. 2018 for Triton, for instance).



Simulation of Triton like spectrum to search for local enhancement of hydrocarbons using SpecCADO. Firsts simulations seem indicate exposure time of several hours to fulfill our goals. Need improvement of SpecCADO to take into account extended sources.

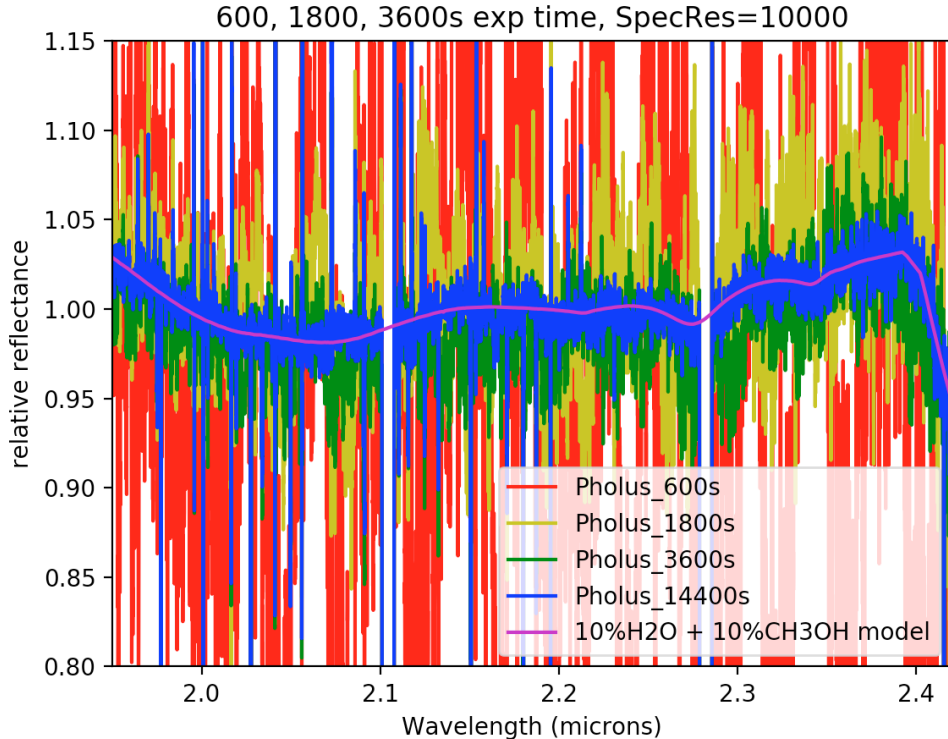
Strong limitation to properly simulate resolved disk object of this dimension due to the fact I generate multi-sources to simulate the whole disk, it is very time-machine consuming. For this purpose, I generate a “small” Triton ($\frac{1}{4}$ of the real apparent dimension) with similar brightness surface.

D) Spectroscopy of the small body populations.

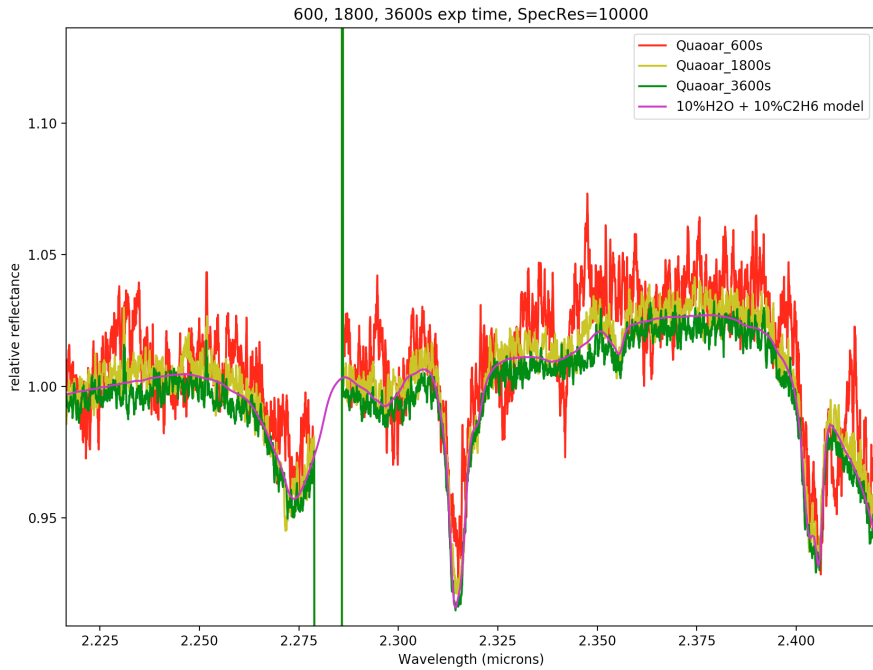
USING SCAO MODE 2, SPECTROSCOPY

The spectroscopic analyses of the Centaurs and TNOs have mainly been done on the biggest members, allowing us to dress a first portrait of these remnant and cold bodies and retrieve accurate information on the physical and chemical properties of the primitive solar nebula and processes which have been at work since the formation of these remnant bodies. However, the current sensitivity of the instrument only reveal the characteristics of the main ices (methane ice for the biggest, water ice for almost 70% of the population). With the spectral capabilities of the spectroscopic mode of MICADO, we will attempt to push back current detection barriers, especially for mid-class diameter objects that are still unresolved and for which slit spectroscopy is the best suited technique. In this topic, we will extend our investigation to constrain the chemical composition of the ultra-red objects which are suspected to host organic matter that could be primordial or formed by consecutive alteration from the space weathering (Dalle-Ore, 2015, Brunetto et al. 2011). Around 10% of the Centaurs and TNOs are known to be ultra-red members and the mean spectral spectrum obtained from this population agree for absorption features compatible with hydrocarbons and/or methanol (Merlin et al. 2017). The large number of ultra-red objects allows us to find a good number of possible *appulse* events every year. Investigation of the H and K spectral ranges of several objects will enable the detection of the expected absorption

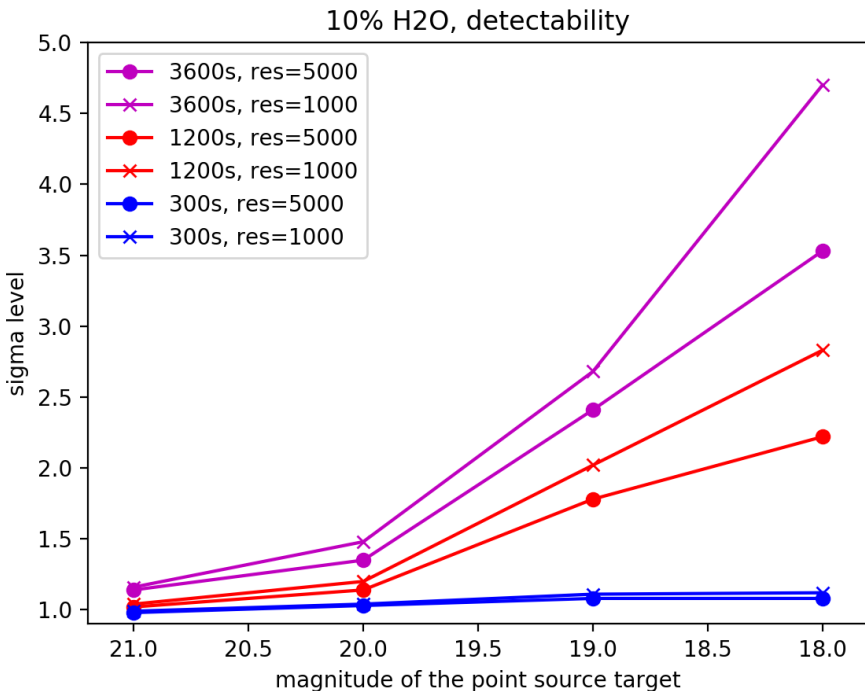
features, such as those already detected (mainly H₂O, CH₃OH, C₂H₆) that need firm confirmation and constraints (e.g: for the objects Quaoar and Pholus), and those exhibited by simple organics, composed by aliphatics or alcoholics radicals. In addition to direct detection of these ices, we expect to be able to identify the physical state of these chemical compounds, thanks to the high spectral resolution offered by MICADO. For the smallest tale of TNOs and Centaurs, the main goal will be to extend our ability to detect water ice and see if small objects share similar trends with those reported for the larger objects. In all cases, this kind of observation lets us assume that the spectroscopic mode will be fully compatible with this kind of investigation (i.e: slit could be set at any place and any orientation on the frame compared to the position of the used moving NGS).



Simulated spectra of Pholus like composition ($J_{\text{mag}}=20.6$) using SpecCADO for different exposure times in order to retrieve methanol and water ice content of the object (both set at 10 % content in this simulation). Detection of 10% methanol is barely done with exposure time of the order of 1 hour at high spectral resolution. Need additional spectra of at least one solar analog nearby our target right after the target acquisition to retrieve the required reflectance spectrum.



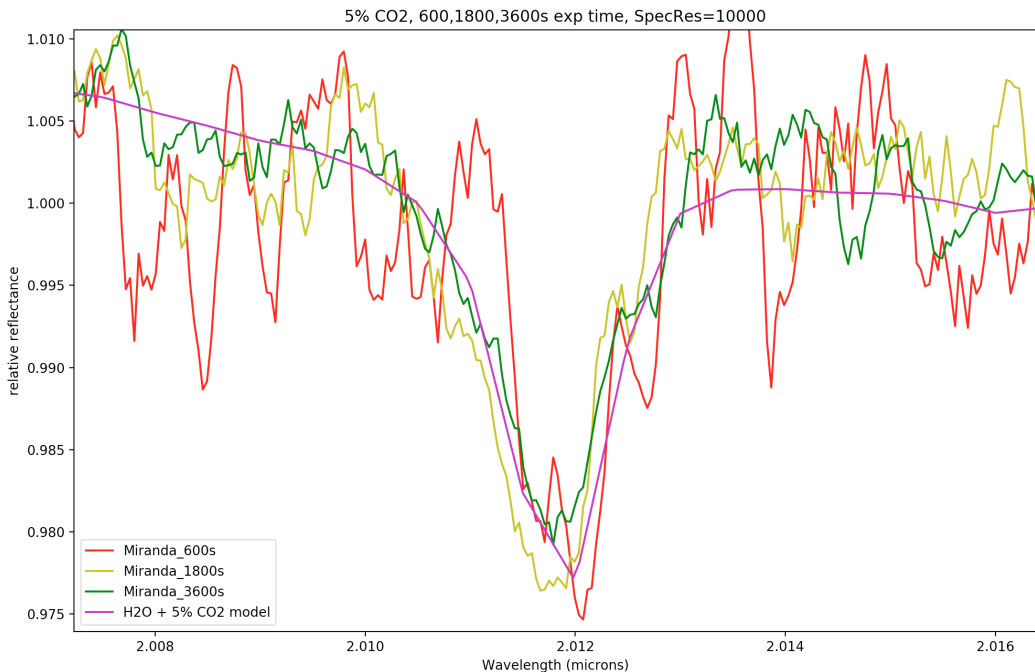
Simulated spectra of Quaoar like composition ($J_{mag}=17.4$) using SpecCADO for different exposure times in order to retrieve ethane and water ice content of the object (both set at 10 % content in this simulation). Integration time of 30 minutes on target should allows firm detection of C_2H_6 for icy content of the order of 5-10%. Need additional spectra of at least one solar analog nearby our target right after the target acquisition to retrieve the required reflectance spectrum.



Simulations using SpecCADO with NGS=Target for detection and characterization of the water ice (assuming 10% content) for different exposure times and different magnitudes (set in J band). Even for bright sources, exposure time has to be large enough to minimize noise and start to extract any information on absorption bands. Results are more compatible comparing results using exposure times at 1200s and 3600s. Note: Real exposure times have to be increased since our targets will not be NGS (need tracking mode 2).

E) Constraint the chemical properties of the satellites of the giant planets and consider possible interactions with their host planet. USING SCAO MODE 1 & 3, SPECTROSCOPY

The case of the Uranian satellites with the possible exogenic nature of CO₂ ice. SCAO tracking mode 1 (target = NGS) & C (using other satellites of Uranus), spectroscopy of unresolved and slightly resolved targets. Among the various populations of small outer solar system bodies, planetary satellites play an important role in our understanding of planet formation. Water, which is the primary “volatile” present in its solid state beyond the Jupiter’s snow line, is also the main compound found on the Uranian satellites. The largest of them, Ariel, Umbriel, Titania, and Oberon, show possible signs of resurfacing processes, whose Voyager 2 returned images of a highly perturbed geology with many surface cracks and faults possibly caused by the large-scale motion of some distinct regions on its surface. Such activity is believed to be the result of tidal forces with Uranus and Umbriel, which heated the interior ice and generated upwelling of material (Tittemore & Wisdom 1990). Previous results (Grundy et al. 2006, Gourgeot et al. 2014) indicated presence of CO₂ on the surface of the biggest satellites while the smallest seem to be depleted. This result is quite interesting since CO₂ ice is increasingly present on the spectra of the trailing hemispheres of Titania, Umbriel, and Ariel, suggesting an external source of contamination linked to the decreasing planeto-centric distance of the satellites. New investigation are needed to search for such material on the smallest Miranda to constrain the effect of both size and planeto-centric distance parameters on the distribution of CO₂ ice.



*Detection of the CO₂ main signature using a mean 5% level content in H₂O ice, for simulated Miranda spectrum (V magnitude: 16.5, from spectral modeling) with different exposure times using SpecCADO. The detection is close to 2, 3 and 5 sigma level for exposure times of 600, 1800 and 3600s. For lower mean CO₂ content, as low as 1% in H₂O, detection level at 3 sigma is granted in 5 hours on target. We could sample two opposite sides of Miranda, at least, to investigate physical mechanisms which lead to the possible presence of such exogenous material (leading and trailing sides) for a total of 10 hours on target made on 2 different nights. Similar investigation could be led on the brightest satellites (with mV=14, in such case, NGS=Target) in order to investigate more deeply the distribution of CO₂ on the whole disk of each satellite (in this case, the satellites are resolved). Extrapolation from these simulations let us assume that 5*2 h for each larger satellite (4 different) seems to be sufficient to obtain CO₂ content variation at the 1% accuracy level. Need additional spectra of at least one solar analog nearby our targets right after the target acquisition to retrieve the required reflectance spectrum.*

F) Atmospheres of the Giant planets.

USING SCAO MODE 3, IMAGING + SPECTROSCOPY

Dynamic, exchange and structure. No simulation yet done, science is that described in the scientific document.

Need better inputs in the near infrared range and better radiative models usually.

SUMMARY

A: Shape and multiplicity among small body populations.

Technique – Photometry, imaging with 0.004" plate scale. Focusing on asteroids with SCAO mode 1 (target=NGS), and on TNOs with SCAO mode 2, using nearby NGS on moving targets. Number of targets: Possibly several dozens (up to 100), required time on target between a few minutes (for most asteroids with $8 < mV < 14$, shape characterization only performed for main belt asteroids in the $8 < mV < 12$ range) and a few hours (medium size class TNOs with $19 < mV < 22$, only for multiplicity). Need observation with broad band filters (J if only focusing on shape and astrometry for binary objects) with addition to H and Ks filters to identify possible heterogeneous spatial composition. Calibration requirements: PSF images for imaging reconstruction, photometrical standards to retrieve JH and JKs colors and absolute flux between companions, if any. Astrometry calibration to retrieve accurate positions and shape.

B: Observation of rings around small bodies.

Technique – Photometry, imaging with 0.004" plate scale. SCAO mode 2, using nearby NGS on moving target. Number of targets: at least 3 (should be limited to 10 objects), required time on target between 30 minutes (best case) up to 3 hours (if not fainter than Chariklo). Need observation with different filters, such as J, H₂O_204 and CH₄_227. Calibration requirements: PSF images for imaging reconstruction, photometrical standards to retrieve JH₂O and JCH₄ colors and absolute flux of both disk and ring.

C: Temporal evolution induced by seasonal sublimation/condensation processes.

Technique – Photometry and spectroscopy, with 0.004" plate scale. SCAO mode 1 only (NGS=target). Need several filters, mostly narrow to moderately narrow band filters such as H₂O_204, CH₄_227, CO ones. H+K band coverage for spectroscopy. Number of targets: at least 3 (Titan, Triton, Pluto). Required time on target of the order of 2 hours by night per object for imaging with necessity to monitor the whole longitudes for Triton (4-5 different observations should allow us a complete monitoring of the surface). For Titan it is more relative to temporal variations rather than spatial variation. For Pluto, 2 different images is enough, since we have already context images from the New-Horizon flyby. For spectroscopy, the required time is only approximative but we need at least 1-3 hours for a complete H+K spectroscopic coverage. Calibration requirements: PSF images for imaging reconstruction, photometrical standards to retrieve absolute flux and spectroscopic solar analogues to retrieve the reflectance. Strong limitation yet to simulate large extended spectroscopic sources, SpecCADO is very long for this purpose replacing extended sources by a large number of point sources.

D: Spectroscopy of the small body populations.

Technique – Spectroscopy, mainly done in H+K band. Number of targets: a few (<10, with $19 < mV < 21$). Need SCAO mode 2 (NGS=nearby star). Required time on target of the order of 1-4 hours (compatible with the time of appulse events). Calibration requirements: Spectroscopic solar analogues to retrieve the reflectance.

E: Constraint the chemical properties of the satellites of the giant planets.

Technique - Spectroscopy, mainly done in H+K band. Number of targets: 10-20 ($6 < mV < 19$). Need SCAO mode 1 (NGS=target, most of the time) or 3 (NGS=nearby another satellite, for a very few object). Required time on target of the order of 1-2 hours per side (need at least 3 different sides, the best is 5 for a complete coverage of the surface). For spectroscopy, several hours are needed to extract a complete spectrum in H+K range. Need new simulations and perhaps improved SpecCADO procedures. Calibration requirements: Spectroscopic solar analogues to retrieve the reflectance. Note: For the larger satellites, possibility to have better results using Harmony. Strong limitation yet to simulate large extended spectroscopic sources, SpecCADO is very long for this purpose replacing extended sources by a large number of point sources.

F: Atmospheres of the Giant planets.

Technique – Photometry and spectroscopy, with 0.004" plate scale. SCAO mode 3 only (NGS=nearby satellite). Required time on target : still not simulated, but probably $< 1/2\text{h}$ for imaging and 2hours for spectroscopy (using a “scanning mode”) per each observation. Calibration requirements: PSF images for imaging reconstruction, photometrical standards to retrieve absolute flux and spectroscopic solar analogues to retrieve the reflectance. Strong limitation yet to simulate large extended spectroscopic sources, SpecCADO is very long for this purpose replacing extended sources by a large number of point sources.

3.6 Black-holes in Galaxies

Coordinators: Nadine Neumayer/MPIA, Maximilian Fabricius/MPE, Jens Thomas/MPE

Some aspects of this scientific area suffer quite a bit using SCAO-mode alone, as the most distant black holes are not necessarily bright enough to be suitable guide stars by themselves, and in these cases it is extremely unlikely to find a chance overlap with a bright foreground star. However relatively nearby systems, within $\sim 100\text{Mpc}$ (and there are many of these) are bright enough in their centres that the targets can themselves be used as on axis guide stars and this is the perfect situation for SCAO observations. This will allow detailed studies of black hole properties and their surroundings for a large range of nearby galaxies, as is laid out in the accompanying document.

Contributions:

- Black holes in galaxies: from the lowest to the highest masses, by N. Neumayer, M. Fabricius & J. Thomas

Black holes in Galaxies: from the lowest to the highest masses

Nadine Neumayer (MPIA Heidelberg), Maximilian Fabricius & Jens Thomas (MPE, Garching)

1) Low mass galaxies in the local universe: While the bulge mass to black hole mass relation is well established at $10^6 - 10^{10} M_{\text{sun}}$, little is known yet about the existence of any possible scaling below $10^6 M_{\text{sun}}$. This is the realm of intermediate mass black holes that potentially exist in the centers of globular clusters, nuclear star clusters, and dwarf galaxies. With masses below $10^6 M_{\text{sun}}$ these putative black holes will gravitationally influence only a small region of less than 1pc at the center of these galaxies. With the unprecedented spatial resolution of MICADO, this spatial scale can be resolved in galaxies out to a distance of about 50Mpc. The most promising galaxies to be targeted in the search for low mass black holes are low mass galaxies that host a nuclear star cluster. Their high central stellar densities are a prerequisite to enable the detection and mass measurement via stellar kinematics, one of the most accurate ways to measure black hole masses. Moreover, many of the nuclear star clusters will be bright enough to serve as the guide star for SCAO observations.

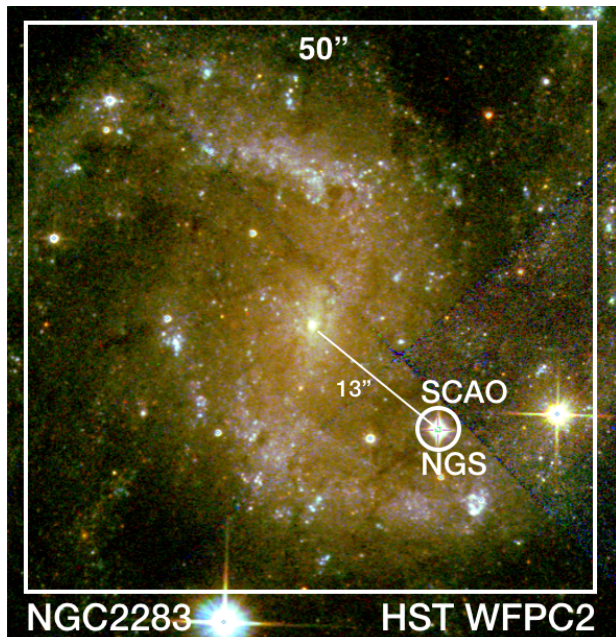


Figure 1: This shows the nearby spiral galaxy NGC2283 that hosts a nuclear star cluster at its center, and has a nearby natural guide star suitable for MICADO SCAO. Given the mass of this galaxy, the mass of the putative central black hole is expected to be below a few times $10^5 M_{\text{sun}}$ – a mass regime unaccessible to current observing facilities outside of 5Mpc.

We know from our own Milky Way that nuclear star clusters in galaxies do contain massive black holes. Stellar dynamical detections are exceedingly challenging with current observing facilities and only a handful of cases exist today with solid detections (e.g. Seth et al. 2010, den Brok et al. 2015, Nguyen et al. 2018, 2019). These are limited to the nearest galaxies (<5 Mpc) due to the limits in currently available spatial and spectral resolution.

MICADO will be a game changer for this field: with a spectral resolution of $R \sim 5000 - 10\,000$ MICADO is able to measure velocity dispersions (σ) as low as 10 - 20 km/s. While at the moment direct measurements are lacking at the low σ end, and are essentially limited to the nearest galaxies, MICADO will be able to spatially resolve the dynamical influence of “seed black holes” in local inactive bulgeless or dwarf galaxies out to ~ 50 Mpc.

How many targets can we expect to observe with SCAO?

There are more than 110 galaxies known to host a nuclear star cluster within a distance of \sim 40Mpc. Restricting ourselves to targets observable from the ELT and with a suitable natural guide star (<15Gmag) within a distance of 15" from the galaxy nucleus leave us with a **sample of seven galaxies**, currently known.

If we can use the nucleus itself to guide on, the sample size will be increased by a factor of \sim 10.

How long do we need to integrate?

These galaxies have central surface brightness of \sim 14-18 mag/sqarcsec in Iband and we expect to get very accurate and deep photometry for the mass profile modeling within a few minutes. For spectroscopy we estimate a required exposure time of 2h per target on source, providing a signal-to-noise of about 30 per resolution element.

With a total time investment of about 20h (including overheads), we would get a sample of 7 galaxies, to address the science questions of how supermassive black holes form and how they relate to galaxy evolution.

By the time of the first light of MICADO current and future gravitational wave observatories will have measured several hundreds of stellar mass black hole mergers. MICADO will be the first instrument to close the evolutionary gap between these and the IMBH intermediate mass black hole population and to follow the black hole mass function throughout all ranges up to most massive object in the universe.

2) The highest mass black holes out to $z \sim 0.3$ – galaxy cores in the making

Most high mass elliptical galaxies exhibit flattened central light profiles as compared to the power law profiles of lower mass elliptical galaxies (e.g. Lauer et al. 1995; Dullo et al. 2014). For these core galaxies, black hole masses correlate strongly with the size of the core region (Thomas et al. 2016) while the amount of missing light — or better mass — is related to the total number of merger events (Merritt 2006). In the current understanding, cores are formed in the late stages of major dry galaxy mergers. As the central black holes of the two progenitor galaxies spiral into the center of the new system, stars are ejected from the central region. This process is referred to as core scouring (Faber et al. 1997, Rantala et al. 2018). The core sizes are found to be identical to the black hole sphere of influence (Thomas et al. 2016).

In the local universe, essentially all galaxies at $M_V < -21$ exhibit these flattened central stellar light profiles and core sizes scale linearly with the mass of the central black hole. Core scouring is an essential process in the evolution of the largest galaxies. However, are there other processes that can result in low-density cores but do not require gasless mergers without star-formation, like strong AGN feedback? This would fundamentally change our understanding of galaxy evolution. It is crucial to determine exactly at which mass and when in the evolutionary histories of massive galaxies cores are formed. Our current ignorance comes largely from the lack of instrumental capabilities to study core properties and black hole masses in statistically meaningful numbers and in representative cosmological volumes.

At $M_V > -21$ galaxies exhibit centrally peaked surface brightness profiles. The corresponding SMBH masses result in projected sphere of influence sizes that currently cannot be observed stellar dynamically further out than 20 Mpc. This hinders a systematic sampling of the SMBH scaling relations in the mid-mass range, introduces potential biases (Shankar et al. 2016) and avoids any studies of the development of scaling relations with redshift or environment.

Census of the supermassive black hole mass function out to $z = 0.3$ and beyond: With its exquisite spatial resolution MICADO will be able to resolve the black hole sphere of influence to about 5 times larger distances than current ground based instruments and 2 times larger distances than the future JWST will be able to do. Following the $z = 0$ scaling relations MICADO will be able to detect and measure black holes in galaxies with velocity dispersions above 270 km/s out to a redshift of $z = 0.3$ or a comoving distance of as large as 1.2 Gpc. The corresponding 300-fold increase of available volume will result in tens of thousands of observable targets. This is a comfortable number of objects to test for time evolution of the mass function and to probe correlations with the environment.

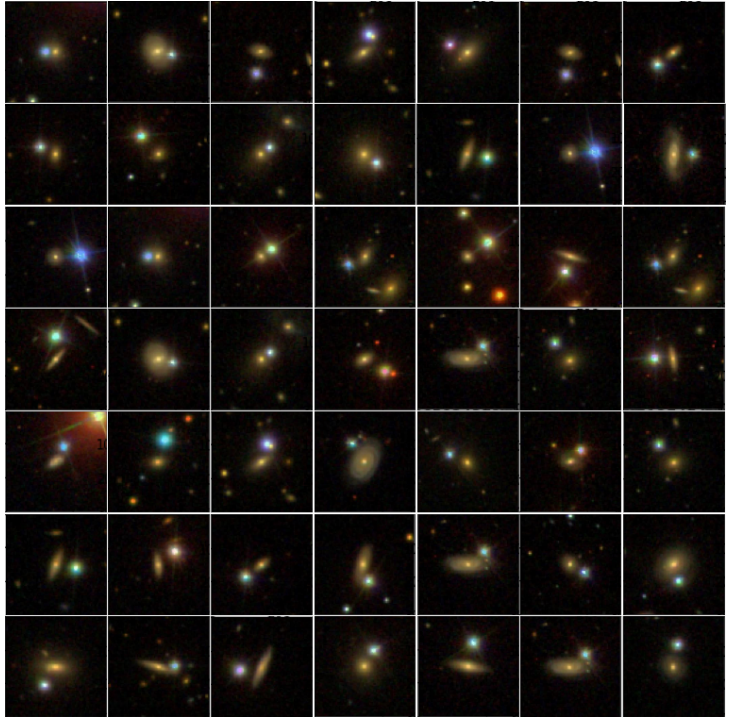
How many targets can we observe with MICADO in SCAO mode?

Local power law galaxies reach central surface brightnesses of 10 mag/sq.arcsec or 15 mag/sq.arcsec at $z= 0.2$. The central surface brightness for local core galaxies is about 15-17 mag/sq.arcsec in K-band. A five minute exposure will reach a SN ~ 200 in spectroscopy at 10 mag/sq.arcsec. At 15 mag/sq.arcsec, exposure times of a few minutes for imaging and an integration time of about 3h in spectroscopy, reach a SN ~ 35 per resolution element – sufficient for stellar kinematic measurements. The limiting factor for a systematic survey will thus be the availability of targets that do have a suitable AO target in their close vicinity ($m_V < 15$ and within 15").

For the target selection it is not possible to rely on current imaging and spectroscopic galaxy surveys (like SDSS or BOSS), since those have avoided the Galactic plane, and hence do not have bright stars close to the targets that could be used as SCAO guide stars. Using statistical arguments, we expect (extrapolated from SDSS) a density of 4.8 ± 0.9 galaxies per square degree within $z < 0.3$ and a central velocity dispersion of more than 150 km/s placing them in the desired mass range. The nuclei of power law galaxies are – even to a redshift of 0.2 – bright enough to serve as AO target themselves, resulting in the best possible Strehl ratio around the region of interest. Thus for power law galaxies, observing time will be the only limiting factor enabling a survey of a few hundred galaxies in imaging and a few dozen spectroscopic mass measurements over the course of a few nights

As their centers are much fainter, core galaxies on the other hand will require an actual AO star at distance of about 15". We estimate the available AO guide stars using the Besançon model for the Milky Way, and arrive at a parent sample of 12000 galaxies observable from the ELT. Limiting our selection to the ones where we expect to resolve the sphere of influence of the black hole, leaves us with a sample of ~ 700 suitable targets for a survey. In order to preselect suitable objects for observation additional spectroscopic information will be needed: On the one hand one needs to be reasonably sure that the projected sphere of influence is large enough such that MICADO is able to resolve it and therefore have prior information on the target's central velocity dispersion, on the other hand we must avoid an overlap of kinematically important features with strong atmospheric emission or absorption lines. While existing spectroscopic extragalactic surveys typically avoid the Galactic plane, for SCAO mode, observations in the proximity of the plane is desirable as it holds a higher probability of the existence a suitable guide star. A systematic spectroscopic survey of candidate galaxies can however easily be executed at future facilities like 4MOST and potentially even be added to their survey programs.

Figure 2: Example of target galaxies selected from SDSS. The selection criteria were a redshift of < 0.3 and $\sigma > 150$ km/s and the availability of a suitable AO star within $15''$. For many of the objects shown here, actually their nucleus would already be sufficiently bright to serve as AO target. A spectroscopic campaign – specifically targeting galaxies with close by stars – would easily deliver hundreds of candidate targets for a spectroscopic mass measurement with MICADO.



3.7 The Centre of the Milky Way

Coordinator: Stefan Gillessen/MPE

Contributor: R. Genzel

The centre of the Milky Way is a renown SCAO target, and it can continue to be studied in SCAO-mode with MICADO. All the studies relating to the properties of the black hole itself and the motions of objects in the vicinity of the black hole will be suitable for observations with SCAO, as these require high spatial resolution and flux sensitivity over a small field of view. The study of the central regions of the Milky Way will also benefit from MCAO observations to study the wider area around the Black hole in more detail, and to relax the requirement on using the single known SCAO guide star in the central field.

Contributions:

- The Galactic Centre, by S. Gillessen & R. Genzel

The Galactic Centre

Coordinator: Stefan Gillessen

Contributors: Reinhard Genzel, Stefan Gillessen

Outstanding Questions

The centre of the Milky Way is a unique laboratory for exploring strong gravity around the closest massive black hole, and for studying fundamental and broadly relevant processes happening in the very dense star cluster surrounding this massive black hole, at a level of detail and quality that will never be possible in external galaxies. The Galactic Centre also serves as a crucial guide for theoretical studies of accretion onto massive black holes and the important issue of co-evolution of massive black hole activity and nuclear star formation.

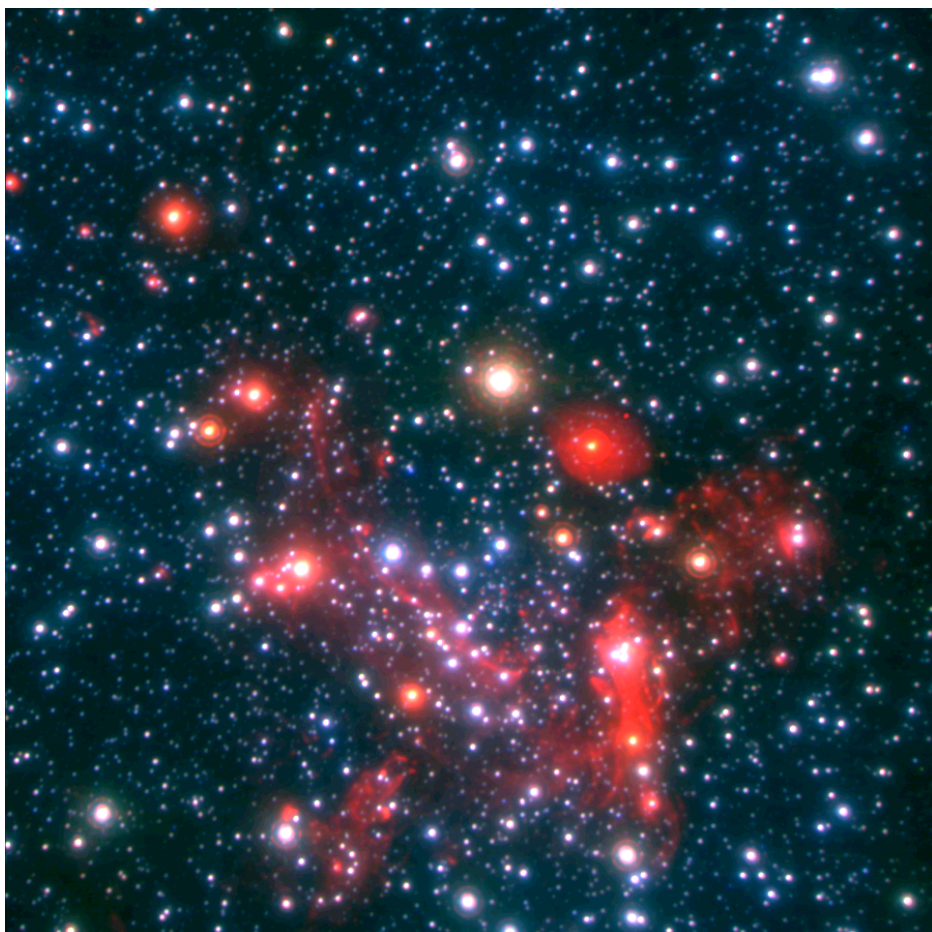


Fig. 1: Three-color composite of the Galactic Center region obtain in H-, K- and L-band with the adaptive optics imager NACO at the VLT. The field of view is roughly 20'', corresponding to around 1pc.

A prime target for MICADO / ELT

Located at a distance of 8kpc only, the Galactic Centre harbors the closest massive black hole, nicknamed SgrA*. The proximity allows for very detailed observations, unparalleled by any other astrophysical system (Genzel et al. 2010). The extinction along the line of sight through the Galactic Disc imposes the use of infrared wavelengths for Galactic Center observations. Since the beginning of the observations in the early 1990's it has been a quest for high resolution and sharpness. With the advent of adaptive optics at the very large telescopes (mainly VLT and Keck), the stellar system could be fully resolved for stars brighter than

around $m_K = 17$. Surprisingly, a rather large sample of 40 so-called S-stars resides in the immediate vicinity of SgrA*, whose gravity forces the stars into orbits with periods short enough to be followed individually by the observations. The shortest period star known so far revolves in 12 years (Meyer et al. 2012), and the brightest star in the system, called S2, is on a 16-year orbit (Schödel et al. 2002, Ghez et al. 2005, 2008, Gillessen et al. 2009a,b, 2017).

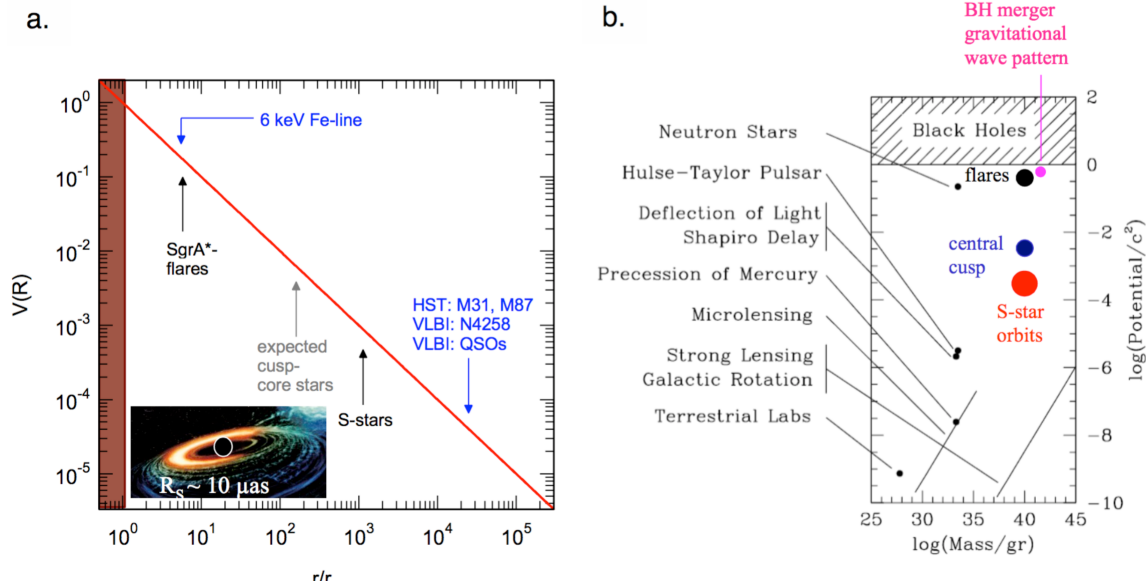


Figure 2, left: Gravitational potential around a (massive) black hole, as a function of radius in units of the radius of the event horizon. Current dynamical measurements in the Galactic Centre ('S-stars') probe to $\sim 1000 R_s$, while external galaxies (blue) probe to $\sim 3 \times 10^4 R_s$. Measurements with MICADO will probe faint cusp stars ten times closer to the event horizon, where β^2 -effects of Special and General Relativity, as well as the Schwarzschild precession term can be observed. The recent GRAVITY-VLTI observations of infrared flares and potentially also spectrally resolved X-ray reverberation mapping of the 6.4keV Fe-line push dynamical measurements into the very strong curvature regime at a few times R_s . Right: comparison of different probes of gravity, as a function of mass scale (horizontal) and field curvature (vertical). The Galactic Centre stellar orbits and flares probe a hitherto totally untested regime of mass and field curvature.

Arguably the most fundamental goal of Galactic Centre research in the next decades will be dynamical measurements of the gravitational potential ever closer to the event horizon, with the ultimate goal of testing General Relativity in the strong field limit. Until very recently the adaptive optics observations have been the cleanest dynamical measurements of the gravitational potential to a scale of $\geq 10^3$ times the radius of the event horizon, R_s (Figure 2). Since 2017, the VLTI instrument GRAVITY delivers a full order of magnitude improved resolution and astrometry (GRAVITY collaboration 2017), pushing the scales probed to $\geq 10^2 R_s$ for stellar orbits, and potentially to very few R_s for the astrometry of flares. For comparison, the best observations in external galaxies can sample $> 3 \times 10^4 R_s$. GRAVITY has already detected the gravitational redshift and relativistic Doppler effect for S2 during its pericenter passage in May 2018 (GRAVITY collaboration 2018a), and the Schwarzschild precession of the S2 orbit is on top of the goals for GRAVITY in 2019 / 2020.

The single-telescope VLT/Keck observations are strongly limited by confusion, while the VLTI can only cover a limited field of view and has a smaller throughput. Fainter stars further in than presently observable are very likely present, as the observed K-band luminosity function (KLF) is very steep (see Figure 3). The volume density of the S-stars increases inward with $R^{-1.3 \pm 0.1}$, such that it is likely that higher resolution and sufficiently sensitive measurements will find a sample of faint stars at $10^2 - 10^3 R_s$. At that radius, orbital velocities approach $0.1c$ and orbital periods may be as short as a few years, allowing the routine detection of the effects of

Special and General Relativity (SR and GR) on these orbits. Such measurements will test SR and GR in an otherwise unexplored regime of field curvature and mass scale (Figure 2).

Still further in, at a radius of a few R_S , variable infrared emission from transiently accelerated electrons ('flares') probe the innermost accretion zone around the massive black hole. Occasionally, SgrA* flares up in the infrared by a factor 100 to 1000 (Genzel et al. 2003). During such an event probably a magnetic reconnection locally heats some of the electrons to relativistic energies ($\gamma \approx 1000$) such that a hot spot occurs, emitting synchrotron light in the infrared, sometimes even up to the X-ray regime (Baganoff et al. 2001, Dodds-Eden et al. 2009, Ponti et al 2017). The detection of orbital motions of this hot gas with GRAVITY (GRAVITY collaboration 2018b) has shown that IR observations can access dynamics at the event horizon scale, a fully relativistic regime. Technically, this required an astrometric precision and stability of about $10\mu\text{as}$ for a time scale comparable to the orbital time scale, i.e. an hour.

Because of the effects of confusion, the current precision of astrometric measurements is significantly worse than the fundamental measurement limit. Higher resolution observations (with higher precision and lower confusion) are required to detect the Newtonian precession of these orbits due to any extended mass outside of the central massive black hole. Such a mass distribution consists of the observed stars themselves ($< 10^2 M_\odot$ in the central $0.1''$) and in addition, stellar remnants (stellar black holes and neutron stars: estimated to be $\leq 10^4 M_\odot$) and perhaps dark matter. Detection of these components is obviously of great interest, also for determining the expected rates of extreme mass ratio in-spiral events leading to gravitational waves.

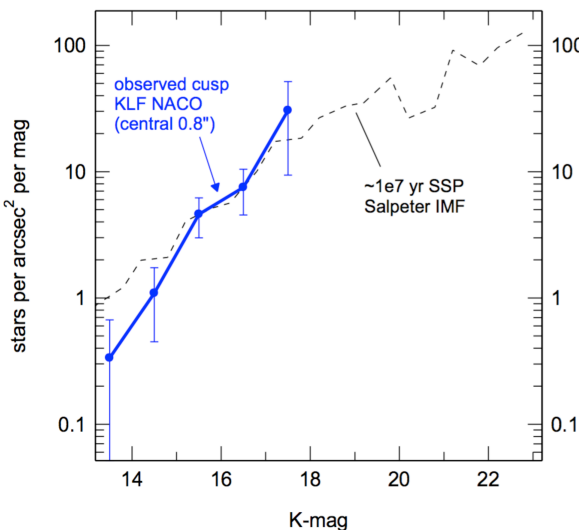


Figure 3: Observed K-band luminosity function (KLF) of the central $0.8''$ as observed with NACO on the VLT (solid blue line), compared to a $t = 10^7$ yr age population with a Salpeter IMF (dashed black line). Combined with the observed $R^{-1.3 \pm 0.1}$ power law stellar density distribution, there are likely to be ~ 5 - 10 $K < 20$ stars in the central 0.1 - $0.2''$.

Another important issue is whether the gas that falls into the nuclear region forms stars near the massive black hole, or whether it is accreted directly into the massive black hole, and whether nuclear star formation and massive black hole activity are related. Observations of population of young stars in the Galactic Centre have yielded the remarkable result that episodic star formation deep in the sphere of influence of the massive black hole appears to be efficient, and has a top-heavy mass function. A better quantitative determination of the processes involved in stellar formation in this extreme environment, a precise determination of the resulting stellar mass function and density profile, and the exploration of the connection between the rates of star formation and black hole accretion are critical for understanding the cosmological co-evolution of galaxies and massive black holes.

Finally, SgrA* is the prototype of the very common class of radiatively inefficient accretion sources ($L/L_{\text{edd}} \sim 10^{-8} - 10^{-6}$). Detailed multi-wavelength observations of SgrA* have shed light on the complex physics underlying this inefficient accretion process that appears to dominate at relatively low accretion rates and is guiding current theoretical work. The fact that the IR emission from SgrA* is sporadic and faint and at a very confused location makes further substantial observational progress difficult without instrumental advances. Future work could emphasize high time resolution, spectrally resolved observations, polarization studies and eventually astrometry. Routine astrometry of the ‘infrared’ flares would be extremely exciting, but requires unconfused astrometry at the $\sim 10\mu\text{as}$ level.

Importance of MICADO

MICADO is uniquely suited for the exploration of the Galactic Centre. The central stellar cusp around SgrA* is strongly confusion limited for current AO observations on 8m class telescopes, limiting the reliable detection and measurement of positions of stars to $m_K \sim 16 - 17.5$, which corresponds to main sequence B-stars. The combination of MICADO and the ELT will push the effective stellar detection sensitivity by $\geq 5\text{mag}$ in modest integration times, making studies of even sub-solar mass stars possible and allowing mass function studies across the entire range of stellar masses. It should be possible to carry out astrometry with a long term precision of $50 - 100\mu\text{as}$ with MICADO, this is 3–6 times better than currently with NACO at the VLT. At this level of precision a number of key issues of the physics of massive black holes and their surroundings can be tackled.

Synergy with GRAVITY

Compared to VLTI/GRAVITY, MICADO will excel with its much higher sensitivity and the larger field of view: Imaging with GRAVITY is limited by principle to a 50 milli-arssec field of view (the single-telescope beam size); and astrometry is limited by the need to find a suitable fringe-tracking star nearby. GRAVITY offers the higher resolution (by roughly a factor 3), though.

In 2018, GRAVITY at the VLTI has delivered two important results in the Galactic Centre:

- S2's motion has been followed in great detail, as the star passed the pericenter of its orbit on May 19, 2018 reaching a speed of around 8000 km/s or more than 2.5% the speed of light. Since S2 is bright enough for measuring its radial velocity spectroscopically with $< 10\text{ km/s}$ error the orbital data allow for a 0.3% accurate measurement of the distance to the Galactic Center (GRAVITY collaboration 2019). Further, relativistic effects in its motion (the β^2 -effects in the radial velocity, namely gravitational redshift & transverse Doppler effect) have been detected at more than 20σ significance (GRAVITY collaboration 2018a, 2019).
- Occasionally, GRAVITY has observed that these flare move clockwise with an orbital radius of few gravitational radii ($\approx 9 R_g$). While the hot spots constitute the probe closest to the event horizon so far, their motion also constrains the system's inclination to be moderate (GRAVITY collaboration 2018b). It is worth noting that for a weakly accreting system, the gas dynamics is governed by the accretion flow angular momentum, and not by the black hole spin.

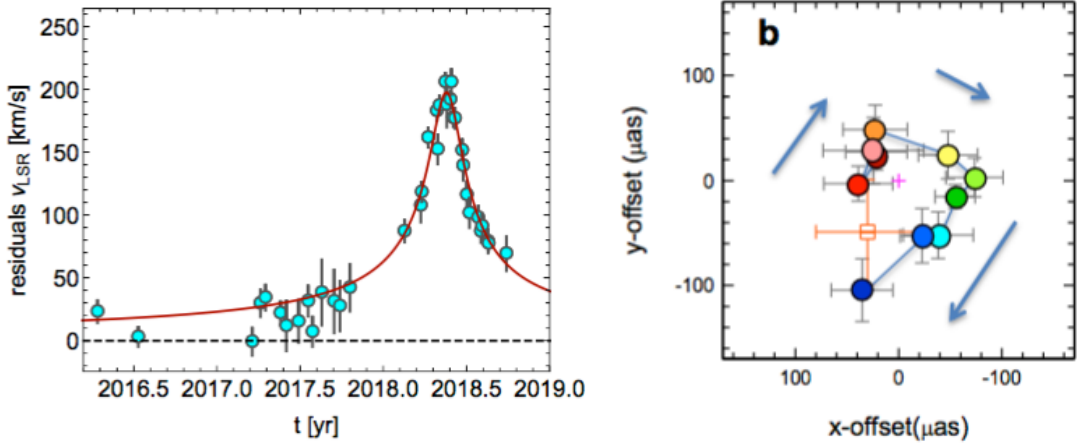


Fig. 4: Left: The gravitational redshift due to SgrA* as measured from the spectra of the star S2 as it passed the pericenter of its orbit during 2018. Right: clockwise, orbital motion of the flaring emission from SgrA* has been observed in 2018 in three flares.

Those two results constitute the first big success of GRAVITY, capitalizing on the 3 mas resolution and the position precision down to 20 μas .

While unrivaled in precision and resolution, by principle the interferometer has an extremely small field of view. Given the number of telescopes it also has only limited imaging capabilities, and it is obviously much less sensitive than a filled aperture. It will be impossible to track more than a few, selected stars with VLTI. This is where MICADO will open a up a new era: Over a field of view 10s of arcseconds across, it will deliver high-quality images with 12mas resolution with a superb sensitivity. The comparison with 8m telescope data is stunning (Figure 5). In the following, we present a few science cases for MICADO, exploiting the resolution and sensitivity of the ELT.

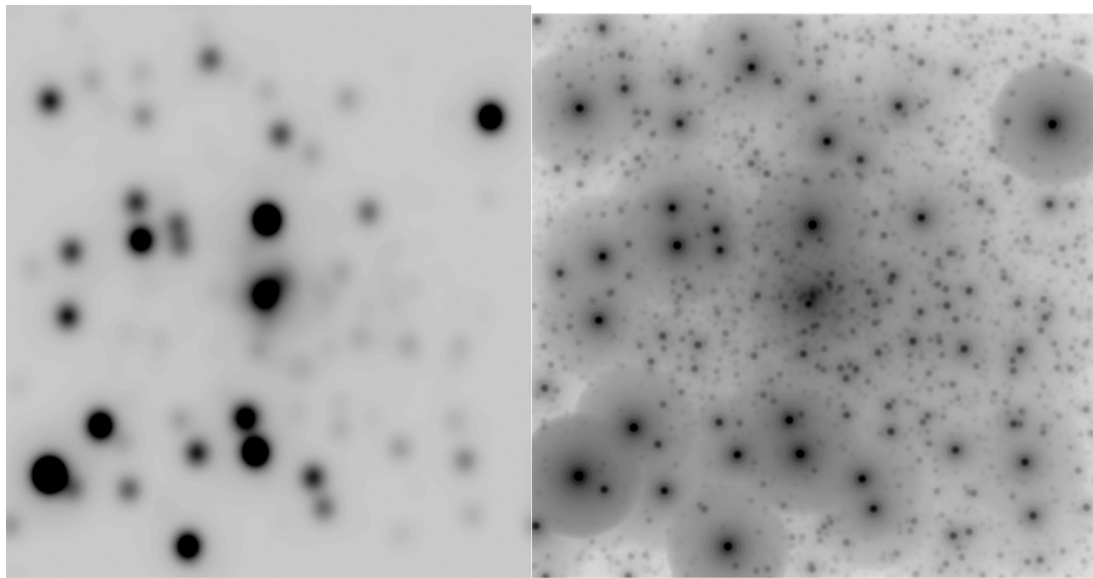


Fig. 5: The impact of the very high resolution achievable with the ELT illustrated in the Galactic Center field. Left: a current high-quality VLT/NACO K-image of the central arcsecond around SgrA* at 60mas, adaptive optics resolution. Right: The KLF- and surface density information and extrapolating NCAO results to fainter magnitudes with a Salpeter IMF yields the simulated MICADO image in the central panel (on the same scale as the NACO image). The field shown roughly matches the area over which the gravity of SgrA* is strong enough to impose detectable accelerations with current AO instruments at the 8m class telescopes. With MICADO, not only the number of stars detectable will be larger, but also the area over which accelerations can be measured.

Case 1: Statistics of stellar orbits

Currently, ~ 40 stellar orbits around SgrA* are known. This relatively small number only allows for very limited statistical statements. The current limitation comes from stellar crowding: While the brighter stars can be seen, stars fainter than $m_K = 18$ are hidden in the stray light of the surrounding brighter ones. The only way to overcome crowding is resolution and high Strehl ratios - hence MICADO will lift the current limitation. Reaching fainter magnitudes and higher precision positions than with 8m telescopes, the number of stellar orbits will increase into the hundreds, and the radial distance out to which one can detect orbits via accelerations will be increased. As a result, one will be able to analyze the orbital properties statistically.

The central arcsecond

Surprisingly, a large fraction of the orbiting stars in the central arcsecond is of stellar type B - massive main sequence stars, with young ages such that their motions still contain information on how these stars came to reside so close to the a massive black hole. Formation on the current orbits is excluded due to the tidal forces, and a slow migratory process would take more time than the lifetime for these stars. Some more violent mechanism must have placed these stars deep in the potential well of SgrA* - like the so-called Hills mechanism, in which the stars are leftovers from field binaries broken up during a close fly-by at SgrA*.

- One statistical quantity to measure with MICADO is the eccentricity distribution. For a relaxed stellar system $n(e) \sim e$. Current data show that indeed high eccentricities are favored, but the sample size is too small to make a detailed comparison with the various proposed formation scenarios.

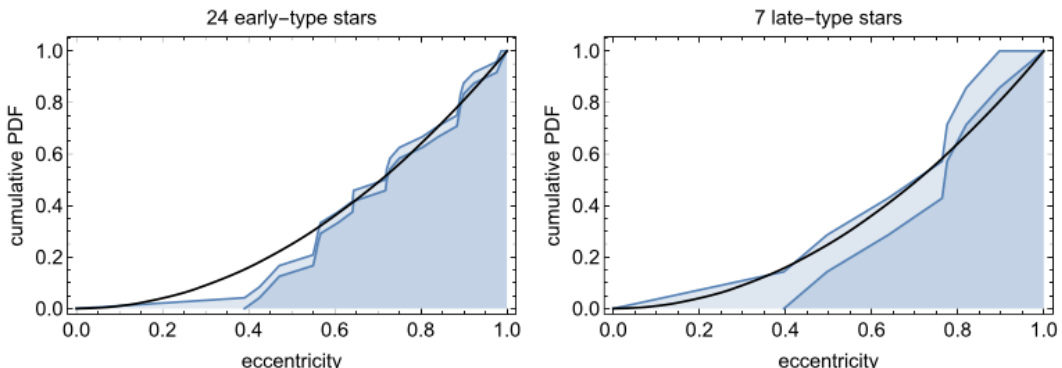


Fig. 6: The measured cumulative eccentricity distributions for main-sequence stars (left) and red giant stars (right) from the sample of stellar orbits. The solid line shows a thermal, relaxed distribution $n(e) \sim e$.

- A second statistical quantity to determine with MICADO is the distribution of specific angular momentum vectors. For stars at radii $> 1''$ and revolution times of a few 1000 years, coherent motion in two stellar disks has been found, but it is not clear, how these disks - if at all - relate to the stars further in. Again, a larger sample size would allow determining dynamical structures in the stellar system, which would give us the clues, how the stars can reside where we find them today.

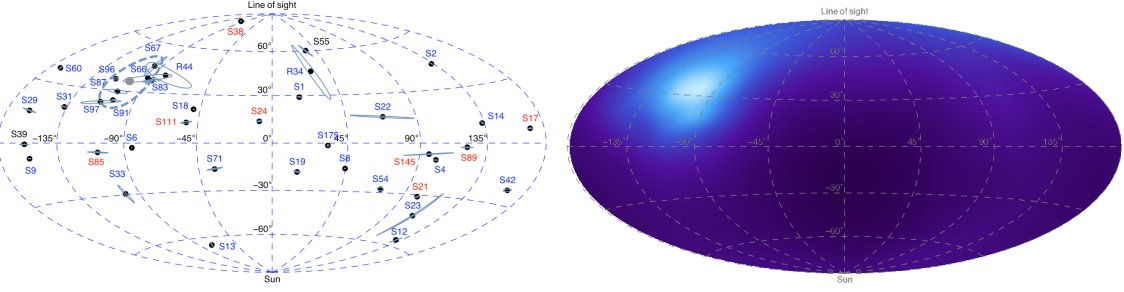


Fig. 7: Left: The orientations of the ~40 stellar orbits determined so far. The figure shows the directions of the angular momentum vectors, where along the line of sight is at the top, and towards the observer at the bottom. Edge on orbits lie on the 'equator'. One can see that the orbits are oriented mostly randomly, with the exception of one overdensity at ($l=104^\circ$, $b=106^\circ$). **Right:** For stars further out one cannot determine a full orbit, but from measuring the five quantities x , y , v_x , v_y , v_z one gets per star a linear features on the angular momentum sphere, in which direction the vector points. Using the sample of young massive O/WR stars, one finds that a large fraction of these linear features intersect in one point. These stars move on a clockwise rotating disk, located at the same position as the overdensity in the left figure.

The regime of the stellar disks

Beyond one arcsecond, the dynamical state of the stars is not random. Many of the O-stars belong to one of two disks. Here the increased statistics with MICADO will better characterize the disk properties: What is their mass function? - How strongly are they warped? - How eccentric are the disk orbits? - Are there cut-offs in radius or mass of the disks? - How do the disks relate to the S-stars?

Case 2: Detection and characterization of relativistic post-Newtonian effects

For stars currently tracked, the β^2 -effects in the radial velocity as well as the Schwarzschild prograde precession term will almost certainly not be measurable using only spectra and proper motion data from current 8m-class telescopes, because of confusion with fainter stars.

- Here, GRAVITY has excelled already, and the combination of MICADO and GRAVITY will be most fruitful: GRAVITY is suited best to follow close peri-centre passages; while MICADO can track the orbits more easily out to the apocenter. Given the degeneracies between Keplerian and relativistic orbits, both a good determination of the orbital elements as well as following in detail the moment of closest approach is needed.
- Exploiting the sensitivity and resolution of MICADO, we might detect stars on even shorter period orbits. Those stars would be suspect to stronger relativistic effects, and they would orbit with few years - ideal probes for the effects we wish to measure. Again, the combination with GRAVITY data might be very powerful here.

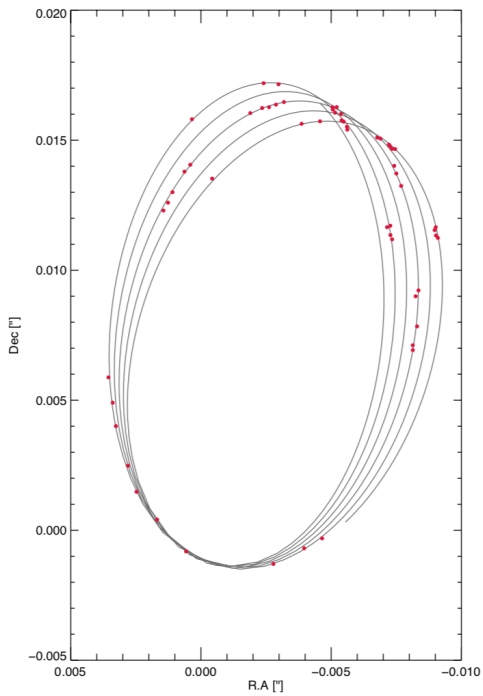


Fig. 8: Illustration of the relativistic motion of a hypothetical star in the Galactic Centre. The star has the same orbital elements as S2, but a semi-major axis $10 \times$ smaller.

Case 3: Towards measuring the spin of SgrA*

Measuring the spin of SgrA* from stellar orbits via astrometry is a very tough problem - even at the accuracy of GRAVITY. It is not clear, whether a suitable star (with short enough an orbital period and high enough an eccentricity) exists (Waisberg et al. 2018). However, stars on very close orbits experience extreme radial velocities, overcoming the confusion in the spectral domain.

If a star on the same type of orbit like S2, but with 10x smaller semi-major axis can be followed ("S2/10"), at a radial velocity accuracy of < 10 km/s the data start getting sensitive to the spin. In the 1 km/s regime, the spin might be measured at the 1% level, and going down to the sub-km/s level opens up the sensitivity to the quadrupole moment. Measuring the latter would constitute a very fundamental test: If general relativity is the correct theory to describe SgrA*, the quadrupole moment is fully determined by the spin already. Measuring it thus constitutes a test of this statement, which is often called the "no-hair-theorem" test.

Rad err [km/s]	Schwarzschild precession	Lense-Thirring precession	γ (light delay & lensing)	Quadrupole Moment
10	0.6%	3%	-	-
1	0.4%	0.7%	35%	-
0.1	0.02%	0.04%	4%	11%

Table 1: Precision by which the given relativistic effects can be measured as a function of assumed error in the radial velocity data (left column) for the hypothetical star "S2/10".

Case 4: The mass distribution in the Galactic Center

With many more stellar orbits, there will also be a much larger number of orbits for which the coverage is good enough to measure the enclosed mass. Gillessen et al. (2017) showed that currently at most 17 stars fulfill this criterion, but none is as constraining as is S2.

- MICADO will yield for a few more stars mass (and distance) measurements that can compete with the S2 based estimates, that have errors $< 1\%$ by now due to the recent GRAVITY observations of the 2018 pericenter passage.

- With MICADO, we expect to get more mass measurements referring to a range of radii, mapping out the radial mass distribution. While it is clear that the gravitational potential is dominated by SgrA*, theory predicts that there should be a population of stellar remnants who have sunk down in the nuclear cluster due to dynamical friction (Morris 1993). Detecting this population would test our fundamental understanding of the evolution of dense stellar systems.
- Another route to detecting such an extended mass component is via detecting the effect in the shape of the orbits. An extended mass component will show up as a retrograde precession of the stellar orbits. The effect competes with the relativistic prograde pericenter precession imposed by the Schwarzschild nature of the metric around SgrA*.
- Further, with a much larger number of stars being monitored, we increase the chances of detecting an actual flyby. We might witness how one or more of the stars experience a "kick" along its path, from which one can estimate the mass of the perturber (Gualandris et al. 2010).
- In a variant of this, one can systematically look for and eventually detect or exclude the presence of an intermediate mass black hole in the Galactic Center. One suspected such host might be the dense cluster of stars called IRS13, roughly 3.5" southeast of SgrA* (Maillard et al. 2004, Fritz et al. 2010).

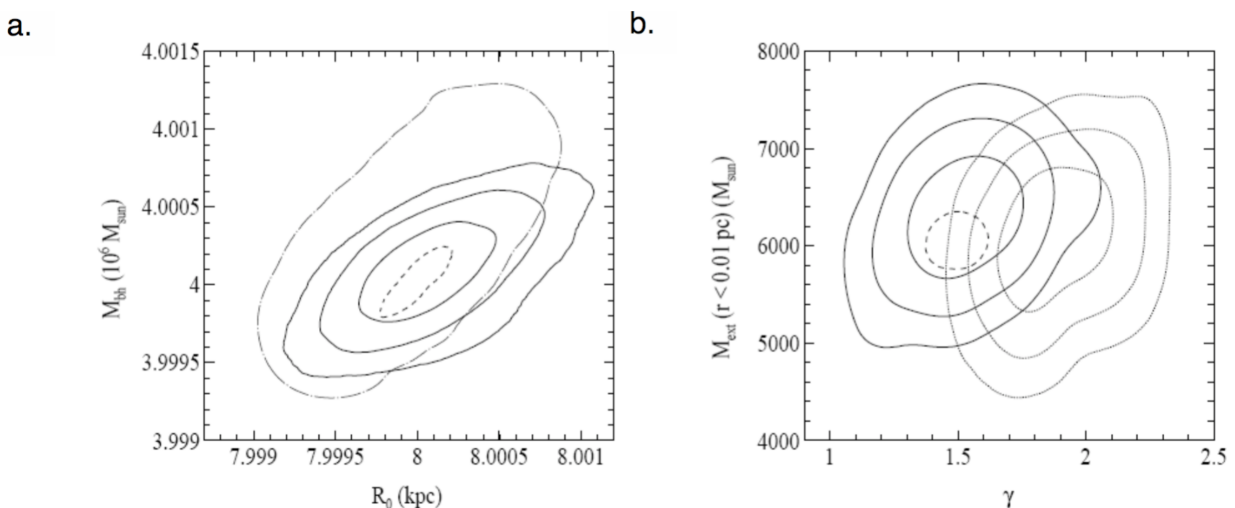


Fig. 9: Examples of the precision of parameter estimations in the Galactic Centre, obtained from simulations of stellar orbital astrometric and radial velocity data with an ELT (from the TMT study by Weinberg, Milosavljevic & Ghez 2005): a. 1, 2 and 3σ uncertainty contours (solid) of mass and distance to the Galactic Centre massive black hole obtained from an astrometric study of 20 stars with a modest precision of $500\mu\text{as}$ and 10 km/s . The dotted contour gives the 3σ contour for a 5 times higher precision, which will be achievable with MICADO; b. Same for the estimate of the extended mass around the massive black hole for two different choices of the power law slope γ of the cusp's density distribution.

Case 5: The mass function in the Galactic Center

The sensitivity & resolution of MICADO will be good enough to see and count stars to $< 1 M_{\odot}$. This will allow for a robust determination of the initial mass function (IMF) in the Galactic Centre and test the emerging evidence that the IMF in the Galactic Center region is much flatter than that in the Galactic disc, indicative of a different mode of star formation close to the massive black hole.

Case 6: Lensing in the flares of SgrA*

The astrometric effects of gravitational lensing are rather small, and it might be impossible to actually see a displacement of the flaring emission, which one can ascribe to lensing. However, lensing can lead to very sharp features in the light curve due to the caustic nature of the lensing geometry. These variations might be much shorter than current integration times. One can thus use the superb sensitivity of the ELT, to obtain a sufficient signal-to-noise ratio of the flaring emission with integration times short enough to resolve such lensing features. Instead of going faint, one would here try to go "short".

Case 7: Dynamics of the prominent young star clusters in the central 50pc

Outside of the central parsec MICADO astrometry will allow dynamical measurements of the other prominent young star clusters in the central 50pc (Arches, Quintuplet etc.). Perhaps the most intriguing issue is the search for possible intermediate mass black holes there (as in globular clusters). The unambiguous detection of an intermediate mass black hole in such a cluster has far-reaching consequences for seed black hole formation during the epoch of reionisation.

Case 8: Gaseous objects in the central arcsecond

Most of the objects seen in the Galactic Centre are stars. Yet, a few gaseous objects have been discovered, and their nature is subject of current research. Most prominent is probably the gas cloud G2 (Gillessen et al. 2012) who passed the pericentre of its orbit in 2014, and for which the tidal evolution has been followed in great detail with SINFONI at the VLT (Figure 10). Recently, G2 has been observed to deviate from a Keplerian motion. Including a drag force acting on the gas can describe the observed radial velocities much better. The measured strength of the drag force can be used to estimate the density of the ambient medium through which G2 rushes, the accretion flow of SgrA* (Gillessen et al. 2019).

But also other gaseous objects have been studied (Clenet et al. 2005, Pfuhl et al. 2015). All these objects are rather faint in line emission, and require in the order of 10 hours of integration with the VLT for getting a high SNR position-velocity diagram. With MICADO, accordingly shorter integrations will suffice, and deeper, more detailed spectra will become accessible. Here, the light-gathering power of the ELT will come to play.

There are many open questions related to the gaseous objects:

- Are all of the objects of the same type? We see a large variety of objects, and we have not yet characterized the current population.
- Do some or even all contain a central star? Some source models proposed a central star as source for the gas of G2. While the detection of a drag force makes that model now less attractive, other objects could be of the proposed type.
- On what orbits are they observed? G2 orbits SgrA* in the same plane as the clockwise stellar disk, with a very high eccentricity though.
- What is their origin? Gas clouds should be disrupted on the orbital time scale, if they are on tight orbits, and hence we should be able to see how they form.

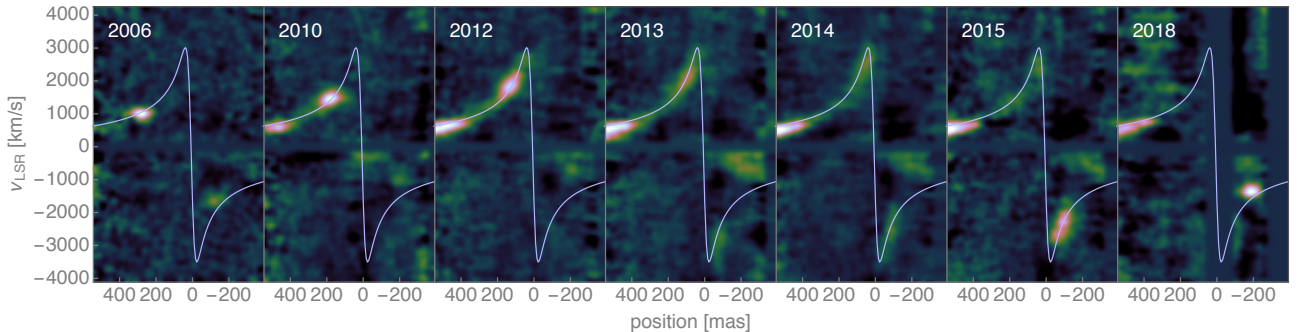


Fig. 10: Series of position-velocity diagrams of G2 obtained with SINFONI at the VLT. One can see how the initially compact gas cloud get stretched ever more as it moves along the orbit (blue line). It starts to swing around the black hole in 2013, in 2014 at nominal pericenter passage roughly equal amounts of gas are on the red- and blue-shifted sides, and in 2015 G2 has completely moved around. In 2018 the cloud appears more compact again, like expected in tidal evolution. Note the deviation from the Keplerian orbit in 2018, showing that the object has slowed down during pericenter passage.

References

- Baganoff et al. 2001, Nature 413, 45
 Clenet et al. 2005, A&A 439, L9
 Dodds-Eden et al. 2009, ApJ 698, 676
 Fritz et al. 2010, ApJ 721, 395
 Genzel et al. 2003, Nature 425, 934
 Genzel, Eisenhauer & Gillessen 2010, RMP 821, 3121
 Ghez et al. 2005, ApJ 620, 744
 Ghez et al. 2008, ApJ 689, 1044
 Gillessen et al. 2009a, ApJ 692, 1075
 Gillessen et al. 2009b, ApJ 707, L114
 Gillessen et al. 2017, ApJ 837, 30
 Gillessen et al. 2019, ApJ 871, 126
 GRAVITY collaboration 2017, A&A 602, 94
 GRAVITY collaboration 2018a, A&A 615, L15
 GRAVITY collaboration 2018b, A&A 618, L10
 GRAVITY collaboration 2019, A&A 625, L10
 Gualandris, Gillessen, Merritt 2010, MNRAS 409, 1146
 Maillard et al. 2004, A&A 423, 155
 Morris 1993, ApJ 408, 496
 Pfuhl et al. 2015, ApJ 798, 111
 Ponti et al. 2017, MNRAS 468, 2447
 Schödel et al. 2002, Nature 419, 694
 Waisberg et al. 2018, MNRAS 476, 3600
 Weinberg, Milosavljevic & Ghez 2005, ApJ 622, 878

3.8 Resolving Individual Stellar photospheres

Pierre Kervella, LESIA/Paris

To date the photospheres of a few very bright nearby stars have been resolved by long-baseline interferometry in the near-infrared. Interferometry has a limited ability to resolve details in a complex image, and so MICADO/SCAO imaging will provide a very important complement to interferometry (e.g. Monnier et al. 2004 ApJ, 605, 436) in revealing intricate details on the surface of nearby stars. This will require observations taken almost simultaneously (within a few nights). An example of what is possible with VLTI/PIONIER is shown by Montargès et al. 2017 (A&A, 605, A108). These data contain information at a resolution of $\sim 1/15$ of the stellar disk. However, it is not possible to reconstruct an image as the (u,v) coverage is too scarce. Including a MICADO/SCAO image (and a bit more VLTI data) this would be different.

Moderately high resolution MICADO spectroscopy of nearby RSG/AGB stars will make it possible to measure the *spatially resolved* velocity fields of their largest convective cells. For Betelgeuse for instance, the angular size of the largest cells is of order the radius of the star (~ 20 mas). It will therefore be possible to confront velocity field predictions of 3D hydro convective simulations to the reality of supergiant star convection (expected in the 10-20 km/s range) in a very straight forward and immediate way.

Contributions:

- Stellar physics with MICADO, by P. Kervella

Stellar physics projects with MICADO

Pierre Kervella

1. Surface and environment of evolved stars

1.1. Convection in extreme conditions

Convection is the most important energy transportation mechanism in physics, and it is simultaneously the most complex and poorly characterized. The ongoing efforts to characterize the convection in stars using massive 3D radiative hydrodynamical codes (e.g., CO5BOLD, Stagger) obtained remarkable successes for the Sun (Caffau et al. [2011SoPh..268..255C](#)) but their reliability in the very low density / low temperature / high opacity regime of evolved stars is still uncertain (Magic et al. [2013A&A...557A..26M](#)). Moreover, convection plays a role in triggering the mass loss of AGB stars and red supergiants (RSGs), but the exact mechanism is still unclear.

The closest evolved stars (Betelgeuse, Antares, R Dor...) exhibit very large angular diameters (~45 to 55 mas) thanks to their extremely large physical sizes (several hundred solar radii). Their surfaces being easily resolved with MICADO, they are the best targets to study the photospheric signatures of convection. Due to the very low density and high opacity, the convective cells are extremely large.

As shown in Figure 1, long-baseline interferometric observations in the near-infrared have resolved a few evolved star photospheres, for instance the RSG Antares (Ohnaka et al. [2017Natur.548..310](#)), the AGB star pi1 Gruis (Paladini et al. [2018Natur.553..310P](#)) and CE Tau (Montargès et al. [2018A&A...614A..12M](#)). In spite of these encouraging results, the performance of long-baseline interferometry on surface feature imaging of evolved stars is limited due to the extended observing time required to obtain the required (u,v) plane coverage. Optical interferometry with a small number of apertures (4 for VLTI) is therefore inefficient both in terms of time coverage and of quality of the reconstructed image, compared to imaging with a large single pupil as ELT-MICADO.

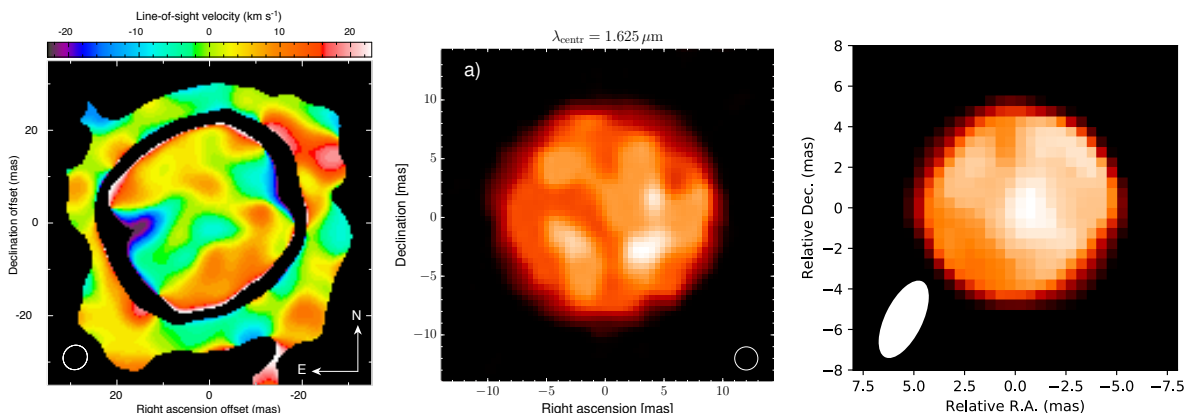


Figure 1. Photospheres of nearby evolved stars resolved by optical interferometry. From left to right: Velocity field at the surface of Antares in the K band (Ohnaka et al. 2017, left), intensity maps in the H band of the AGB stars pi1 Gruis (Paladini et al. 2018, center) and CE Tau (Montargès et al. 2018, right). The angular resolution of these map and images is comparable to that of MICADO in the visible, where the contrast of the convective features is expected to be stronger than in the infrared.

The spatial spectrum of the convective cells is the perfect observable to constrain the convective heat transportation models in the extreme physical conditions of RSGs and AGBs. Thanks to the angular resolution achievable with MICADO, these stars offer the opportunity to probe the innermost layers of the envelope down to the photosphere.

MICADO spectroscopy of the apparent disk of nearby RSG/AGB stars with a spectral resolution of $R=20000$ will make it possible to measure the *spatially resolved* velocity field of their largest convective cells. For Betelgeuse for instance, the angular size of the largest cells is on the order of the radius of the star (~ 20 mas). It will therefore be immediately possible to confront the velocity field predictions of 3D hydro convective simulations to the reality of supergiant star convection (expected in the 10-20 km/s range).

Establishing the behavior of convection in the extremely low density conditions of RSGs / AGB star atmospheres is a key to understanding convection in all types of stars. This will anchor the stellar convection models to both the well known "intermediate density" convection in the solar atmosphere and "very low density" in RSGs /AGB stars

1.2. Mass loss and circumstellar material

Evolved stars are the principal contributors to the enrichment of heavy elements in the interstellar medium and, more generally, to the chemical evolution of the Universe. Within the interface between the photosphere of evolved stars and the interstellar medium, the formation of molecules and the condensation of dust present extraordinary challenges for astrochemistry.

1.2.1. Low and intermediate mass stars (AGB/post-AGB)

Since they are much more numerous than high mass stars, the low and intermediate mass stars ($1-8$ Msun) play a particularly important role. The end product of the evolution of an intermediate mass star is a white dwarf, the difference in mass between the main sequence and the white dwarf is dispersed into space as a planetary nebula (PN).

The origin of bipolar PNe is one of the great classic problems of modern astrophysics. These spectacular objects often present a remarkable axial symmetry, whose origin is often attributed to the presence of a secondary star, but a companion has been detectable only in few cases.

The potential of MICADO to characterize the close environment of AGB stars enshrouded in dust is outstanding, thanks to the high efficiency of light scattering at visible and near-IR wavelengths. The 3D density structure of the envelopes (that include spirals, disks, bipolar outflows...) can be determined with a high degree of fidelity through radiative transfer modeling. The highest priority targets are L2 Puppis (large dust disk with radius ~ 300 mas) and R Dor (photosphere ~ 50 mas + envelope), both shown in Figure 2. Approximately 20 targets have suitable properties for such a study (they are already monitored with ALMA).

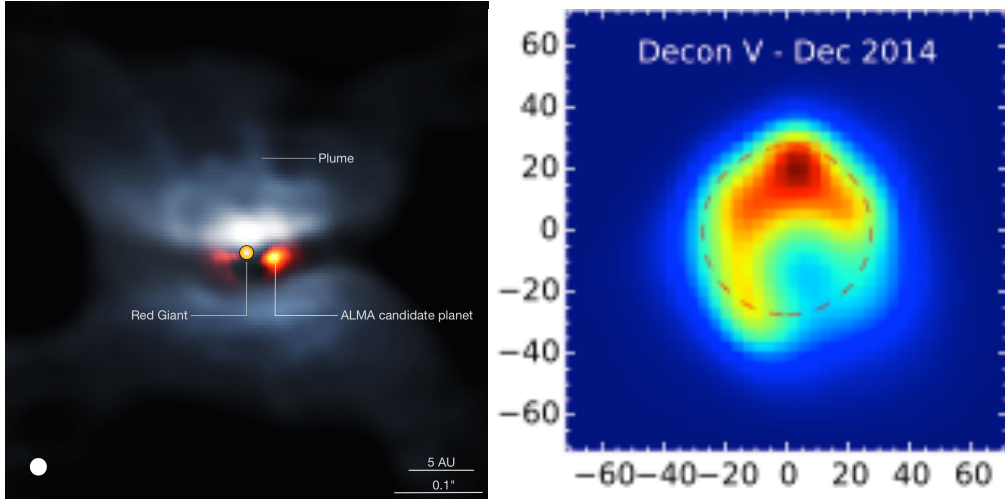


Figure 2. SPHERE/ZIMPOL images at visible wavelengths of the circumstellar disk of the AGB star L2 Puppis (left, Kervella et al. [2016A&A...596A..92K](#)) and of the photosphere of R Doradus (right, Khouri et al. [2016A&A...591A..70K](#)). The angular resolution of MICADO will be several times better than that of these images.

1.2.2. High mass stars (RSGs)

As observed in Betelgeuse and Antares, the environment of RSGs presents complex inhomogeneities. Tracing the molecular gas emission in the envelope of these stars using the numerous molecular lines present in their spectrum is a key to establishing the velocity field.

This type of measurement has been conducted with ALMA in the close-in envelope of Betelgeuse by Kervella et al. ([2018A&A...609A..67K](#)). At millimeter wavelengths, this corresponds to a high altitude over the photosphere (~ 1.5 times the visible radius of the star). The dampening of the convective gas motion seems to occur below this altitude, as the residual velocity field is only ~ 2 km/s. The link between the convective cells at the surface and the circumstellar envelope will therefore require to probe deeper, hence at visible and near-infrared wavelengths, in the atmosphere of Betelgeuse. Thanks to its angular resolution and wavelength coverage, MICADO is perfectly suited for this project. Approximately 10 RSGs have suitable properties for the resolution of their circumstellar material.

End of document